KINEMATIC EVOLUTION OF THE BÜYÜK MENDERES GRABEN IN WESTERN TURKEY INFERRED FROM 2-D SEISMIC INTERPRETATION AND CROSS SECTION RESTORATION

by

OSMAN MEREY

IBRAHIM ÇEMEN, COMMITTEE CHAIR
ANDREW M. GOODLIFFE
BO ZHANG
JAMES W. GRANATH

A THESIS

Submitted in partial fulfillment of the requirements
for the degree of Master of Science
in the Department of Geological Sciences
in the Graduate School of
The University of Alabama

TUSCALOOSA, ALABAMA

2016

ABSTRACT

The Alaşehir and Büyük Menderes Grabens are two major E-W trending grabens that border the central part of the Menderes Metamorphic Core Complex (MMCC) to the north and south, respectively. These two grabens were previously considered to be developed symmetrically under the control of two detachment surfaces; the Alaşehir detachment to the north and the Büyük Menderes detachment to the south, which were initially formed as high angle normal faults and rotated to low angle detachment faults (Gessner et. al., 2001; Seyitoglu et al., 2002 and 2004; Çemen et al., 2006; Çiftci et al., 2009 and 2010; Gessner et al., 2013).

Detailed field mapping and structural interpretation of seismic reflection profiles by previous geological researchers in the Alaşehir Graben suggest the presence of a well-developed rollover structure associated with the fault-bend geometry of the Alaşehir detachment surface (Seyitoglu et al., 2000 and 2002; Çiftci et al., 2009 and 2010).

During this study, eight N-S and six E-W trending seismic reflection profiles in the Büyük Menderes Graben were interpreted to determine the subsurface structural geometry of the graben. Eight N-S cross-sections were restored to determine the original geometry of the normal faults during their initiation in the early Miocene. The cross-section restoration based on seismic reflection profiles reveals that a roll over geometry did not develop on the hanging wall of the south dipping normal fault. Furthermore, the kinematic modeling created by backstripped cross sections and tectonic subsidence rates suggest that the evolution of the Büyük Menderes Graben was controlled by two active boundary faults on its northern and

southern margins. Therefore, this study suggests that the Büyük Menderes Graben differs from the Alaşehir Graben in terms of its structural evolution and may have formed as a rift basin during the early Miocene. This in return indicates that the central part of MMCC has experienced asymmetrical extensional tectonics.

LIST OF ABBREVIATIONS AND SYMBOLS

2-D	Two dimensional
3-D	Three dimensional
AG	Alaşehir Graben
BMG	Büyük Menderes Graben
BSL	Below sea level
CALI	Caliper
CMMCC	Central part of the Menderes Metamorphic Core Complex
RHO	Bulk density correction log
DT	Sonic
GR	Gamma ray
KB	Kelly bushing
km	Kilometer
KTB	Kale-Tavas Basin
m	Meter
m/s	Meter per second
LN	Lycian Nappes
MMCC	Menderes Metamorphic Core Complex
MD	Measured depth
NDBF	North dipping boundary fault

NPHI	Neutron porosity
RHOB	Bulk density
s	Second
SDBF	South dipping boundary fault
SG	Simav Graben
SP	Spontaneous potential
SWASZ	Southwestern Anatolian Shear Zone
TD	Total depth
TS	Tectonic subsidence
TPAO	Turkish Petroleum Corporation
TWT	Two-way travel time
ÖB	Ören Basin

ACKNOWLEDGEMENTS

I could not have completed this research without the help and guidance of my thesis committee, colleagues, friends and family. First and foremost, I would like to thank my advisor, Dr. Ibrahim Çemen, for supporting and guiding me intellectually through the research process and providing helpful feedbacks and invaluable guidance for the earlier drafts of my thesis. I would also like to thank all of my committee members, Dr. Andrew Goodliffe, Dr. Bo Zhang and Dr. James W. Granath for their assistance, mentorship, careful reviews, helpful feedback, invaluable guidance and patience during my thesis research.

This research would not have been possible without the support of my mother. Her belief in me has always helped me remain optimistic about my future and what opportunities lie ahead. I would like to extend special thanks and recognition to my girlfriend Ms. Shelby Cloer, who has always been by my side and who has helped me keep my eyes on the goal. I also express enormous gratitude to all of my friends, fellow graduate students, faculty and staff in the Department of Geological Sciences at The University of Alabama.

Last but not the least, I would like to sincerely thank the Turkish Petroleum Corporation for providing financial support during my Master's degree program and providing the subsurface data set for my thesis research project.

CONTENTS

LIST OF FIGURES

1. INTRODUCTION

The Western Turkey extended terrain is one of the most important regions in the world in terms of active extensional tectonics and has been the focus of considerable geological research for many years. It has experienced the Cenozoic post-collisional extension since the late Oligocene (Dewey and Şengor 1979; Çemen et al., 2006; Jolivet et al., 2013; Gessner et al., 2013; Ersoy et al., 2014). The extensional tectonics in the region are responsible for the exhumation of the Menderes Metamorphic Core Complex (MMCC) and the development of multiple grabens (Figure 1).

The MMCC is divided into northern, central and southern sections by two major east-west trending grabens; the Büyük Menderes Graben to the south and the Alaşehir Graben to the north (Figure 1). These E-W trending grabens are morphologically prominent features and have been considered symmetrical supra-detachment basins that are filled with the Neogene sediments (Gessner et al., 2001; Seyitoğlu et al., 2000,2002 and 2004; Çemen et al., 2006; Çiftçi et al., 2009 and 2010; Gessner et al.,2013). The grabens were considered to develop under the control of two opposite dipping detachment surfaces, which were initially formed as high angle normal faults and rotated to low angle detachment faults (Gessner et al., 2001; Seyitoğlu et al., 2000, 2002 and 2004; Çemen et al., 2006; Gessner et al., 2013). Field oriented geological research, together with subsurface studies based on structural interpretation of 2-D seismic reflection profiles suggest that the Alaşehir Graben contains a well-developed fold-bend roll over structure related to the north dipping detachment fault, which is well exposed along the southern margin of the graben (Seyitoğlu et al., 2000 and 2002; Çiftçi et al., 2009 and 2010; Gessner et al., 2013).

A similar geometry and structural evolution have been proposed for the Büyük Menderes Graben based on surface studies (Seyitoğlu et al., 2000 and 2002; Göğüş, 2004; Çemen et al., 2006; Gessner et al., 2013), which suggest that the graben evolved along the hanging wall of the south dipping low-angle detachment fault located on the northern margin of the graben. Recent studies which interpreted 2-D seismic profiles in the Büyük Menderes Graben suggest that the graben does not contain a fault-bend rollover structure associated with the graben formation (Sert, 2015) as evidenced by the minimal rotation of the internal fault blocks. This indicates that the Büyük Menderes Graben may have developed by planar faults on both margins, and the main graben bounding fault may not become horizontal for a considerable depth in the Earth's crust. Consequently, the structural relationship between the geometry of the hangingwall, active axial surface of the antithetic faults and the sedimentary accumulations in the Büyük Menderes Graben remain in question as well as the deformational process within the basement below the graben. This controversy remains unresolved as to whether the Büyük Menderes Graben developed with a similar structural geometry to the Alaşehir Graben, or it formed with different extensional processes during the Cenozoic extension in western Turkey.

The main purpose of this study is to investigate the kinematic evolution of the Büyük Menderes Graben based on a structural interpretation of available 2-D seismic profiles and a structural restoration. This study will determine the geometry of the normal faults that control the structural evolution of the Büyük Menderes Graben and test the question whether the graben was developed on the hanging wall of the south dipping detachment surface or planar faults along the northern and southern margins of the graben. Consequently, the results of this study will be used to test the hypothesis that the Alaşehir and Büyük Menderes grabens developed with a similar structural geometry, and provide a better understanding for extensional tectonics of the central part of the MMCC.

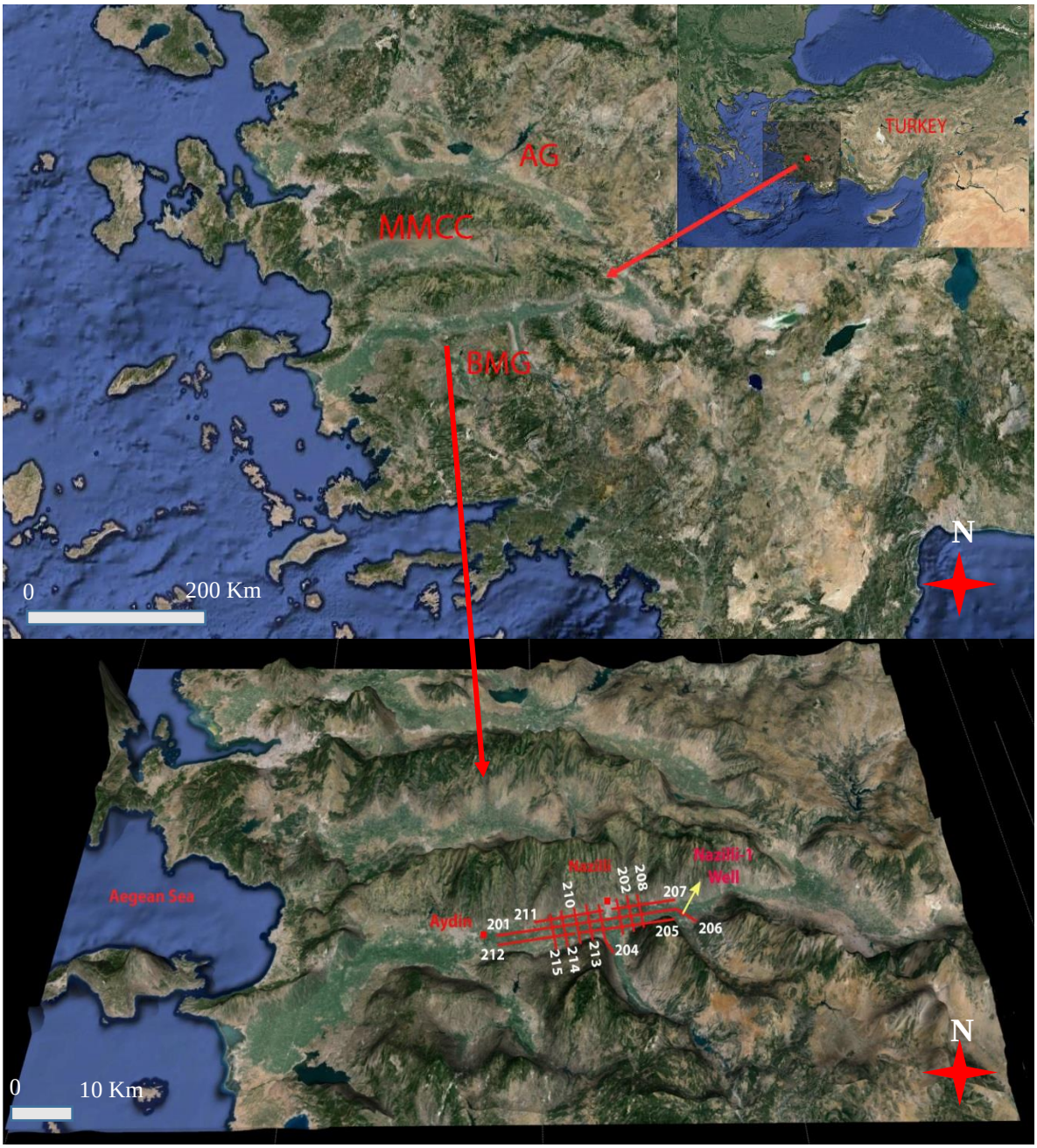

Figure 1- Aerial imagery from Google Earth showing the location of the Menderes Metamorphic Core Complex (MMCC) and the two major E-W trending grabens in western Turkey; the Büyük Menderes and Alaşehir Grabens. The locations of fourteen seismic reflection profiles used in this study are shown by red lines (MUD-99-201-202-203-204-205-206-207-208-210-211-212-213-214-215).The Nazilli-1 well is shown with the yellow arrow. **Abbreviations: AG:** the Alaşehir Graben; **BMG:** the Büyük Menderes Graben; **MMCC:** Menderes Metamorphic Core Complex.

2. GEOLOGIC OVERVIEW

2.1 Regional Geology

The Western Turkey extended terrane is located at the eastern part of the Aegean extensional province. The active tectonics of the region are dominantly constrained by the continental collision of the African and Eurasian plates, Hellenic-Cyprian subduction zone and the Right-Lateral Strike-Sip movement along the North Anatolian Fault zone (NAFZ) (Le Pichon and Angelier, 1979; 1981;Şengor et al., 1985; Meulenkamp et al., 1988; Seyitoğlu and Scott, 1996; Çemen et al.,2006) (Figure 2).

During the last decade, many researchers have proposed explanations for the cause of the initiation of Cenozoic extension in the region. These include: (1) tectonic escape of the Anatolian microplate along the North Anatolian Fault Zone (NAFZ) (Dewey and Şengor, 1979; Şengor, 1979, Şengor and Yılmaz, 1981, Şengor et al., 1985; Çemen et al., 1993, and 1999 b); (2) back-arc extension in response to subduction roll back of the African Plate and migration of the Hellenic-Cyprian Trench system (McKenzie et al., 1978; Le Pichon and Angelier, 1979; 1981; Meulenkamp et al., 1988; Spakman et al., 1988; Jolivet et al., 2013; Göğüş, 2014); (3) orogenic collapse of spreading and thinning of thickened crust as a result of the Paleocene- Eocene Alpine collision (Dewey et al., 1988; Seyitoğlu and Scott, 1996); and (4) a combination of the three mechanisms proposing that extension in the Western Turkey extended terrane was initiated in the late Oligocene as a result of orogenic collapse, and progressively developed in multiple stages following the initiation of a major extensional shear zone named SWASZ (Çemen et al., 2006; Gessner at al., 2013; Ersoy et al ., 2014).

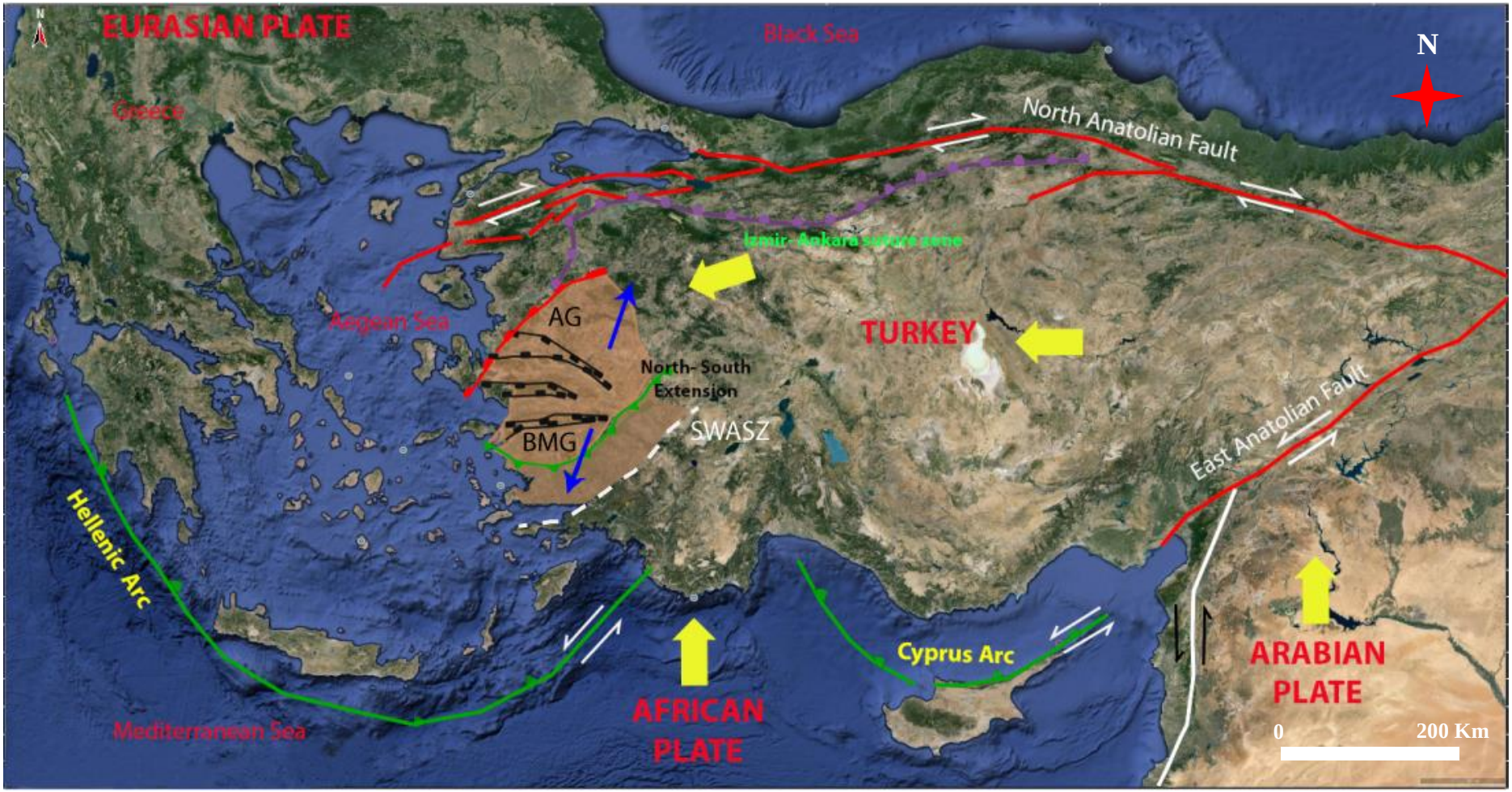

Figure 2- Generalized tectonic map of the Aegean extensional province on a Google Earth image. The block colored with orange shows the Menderes Metamorphic Core Complex experiencing approximately NE-SW extensional deformation. **Abbreviations: SWASZ:** Southwest Anatolian Shear Zone; **BMG**: Büyük Menderes Graben; **AG:** Alaşehir Graben.

2.2 Exhumation of the Menderes Metamorphic Core Complex

The NE-SW directed extension in western Turkey is characterized by the exhumation of Menderes Metamorphic Core Complex (MMCC) and its extensional deformation. The MMCC is bordered by the Izmir-Ankara suture zone to the north and the NE-SW trending Southwest Anatolian Shear Zone (SWASZ) to the south and southeast (Çemen et al., 2006). The MMCC is further divided into northern, central and southern parts by E-W trending horst and graben system (Figure 2). The exhumation mechanism of MMCC during the Cenozoic extension has been discussed in several geological papers in terms of symmetrical/asymmetrical metamorphic core complex development.

Gessner et al., (2001) and Ring et al., (2003) suggested that the MMCC is a symmetrical core complex whose exhumation initiated in the Oligocene between the north dipping Simav detachment and south dipping Lycian detachment surfaces, followed by extension of the central part of the MMCC along the two symmetrical breakaway zones that were initially high angle, the Büyük Menderes detachment to the south and the Alaşehir detachment to the north.

Seyitoğlu et al., (2004); and Çemen et al., (2006) proposed that the MMCC exhumed asymmetrically along a main breakaway zone that extends form the Datça fault located in the Gulf of Gökova to the south extending northeastward to the Kale basin. Çemen et al., (2006) observed that the Datça- Kale Breakaway zone extends northeastward and constitutes the southern boundary between the Western Turkey extended terrane and the western Taurids. They named this structure the Southwestern Anatolian Shear Zone (SWASZ), which comprises the Datça, Kale-Tavas, and Acıgöl fault segments (Figure 3). The southwestern segment of this shear zone, the Datça fault, was interpreted by Kurt et al., 1999 based on a seismic reflection profile along the Gulf of Gökova. On the seismic section, the fault shows a listric geometry with a large rollover structure and associated antithetic faults (Kurt et al.,

1999 see figure 4). Based on the seismic line from the southern segment of the SWASZ, Çemen et al., (2006) proposed that the late Oligocene basins of the Southern Menderes Massif formed on the hanging wall of the SWASZ. Thus, they suggested that the SWASZ is a large listric detachment surface and initiated as a primary breakaway on the southern part of western Turkey. Finally, they suggested that ongoing extension along the SWASZ associated tectonic uplift caused the exhumation of the MMCC and development of the symmetrical the Alaşehir and Büyük Menderes grabens on the central part of the MMCC in the early Miocene (Çemen et. al., 2006 see figure 3).

Gessner et al., (2013) proposed that asthenospheric flow resulting from the subduction roll-back of the African slab caused the dome shaped evolution of the Central Menderes Metamorphic Core Complex (CMMCC) on the SWASZ, and the extension created two symmetrical detachment systems that bordered the CMMCC. Also, Biryol et al., (2011) constructed a P- wave tomography study for the subduction of the African plate related to the Aegean extension. They founded a slab tear between the Hellenic and Cyprus arcs. They proposed that hot materials coming from the tear triggered the extension beneath the Menderes Metamorphic Core Complex. Recently, Mahatsente et al., (in press) conducted a satellite based gravity modeling study in western Turkey and the Aegean region. They found out that the crustal thickness ranges from 24-29 km beneath western Turkey and the shallowest part is located around the Denizli region where the Büyük Menderes and Alaşehir grabens join in the eastern part of the CMMCC. They concluded that the crustal thinning in the region might be related to thermal erosion caused by the emplacement of hot asthenospheric material as a result of lateral tear of the subducting African slab.

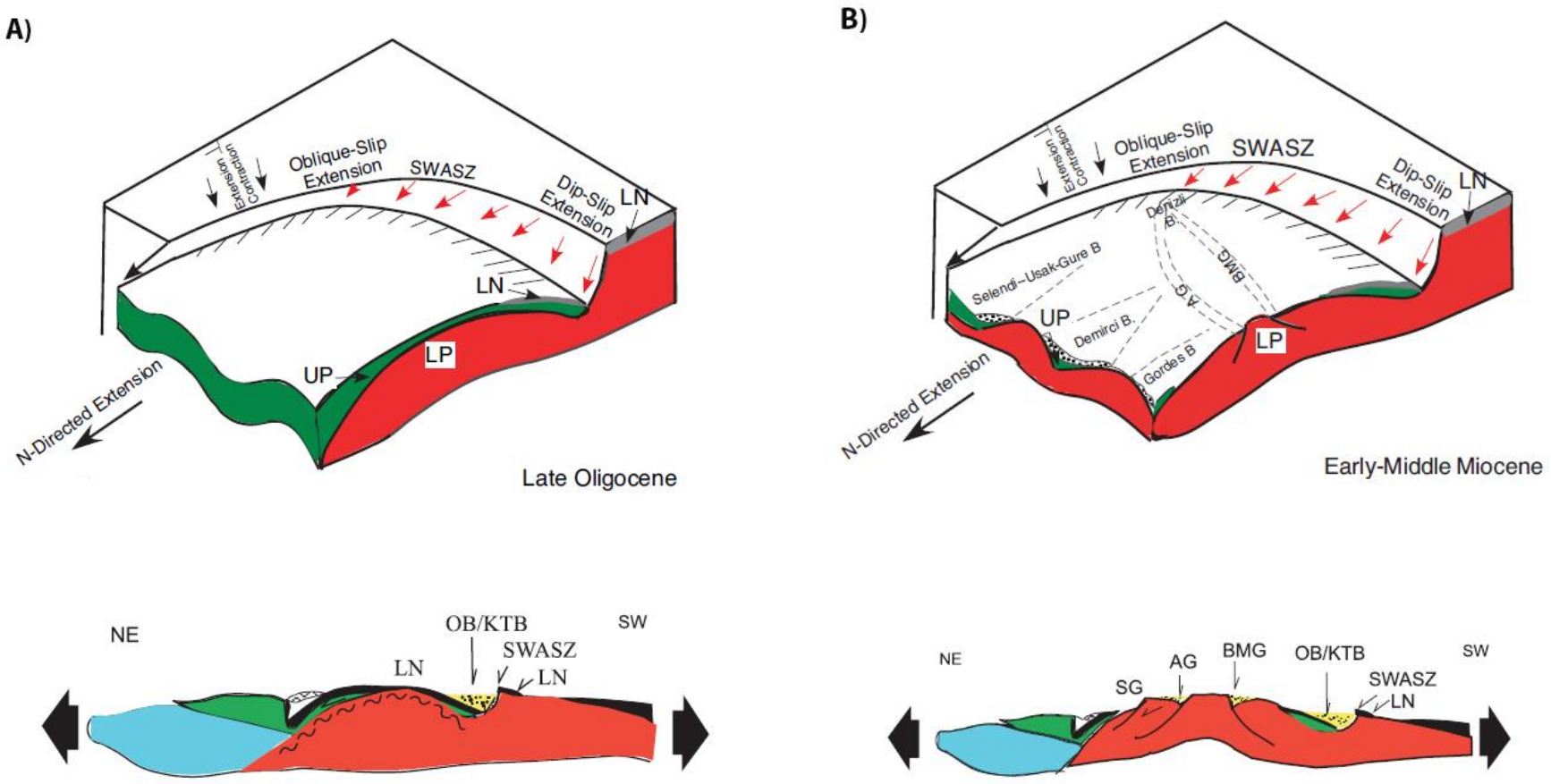

Figure 3- 3D cartoons and cross- sections showing the Cenozoic extensional evolution of western Turkey (from Seyitoğlu et al., 2004 and Çemen et al., 2006). (A)The late Oligocene extension on the SWASZ; (B) The early- to mid-Miocene extension that causes the development of the E-W and N-S trending grabens**. Abbreviations: AG:** Alaşehir graben; **BMG:** Büyük Menderes graben; **KTB**: Kale-Tavas Basin; **LN:** Lycian Nappes; **ÖB:** Ören Basin; **SG:** Simav Graben; **SWASZ:** Southwest Anatolian Shear Zone.

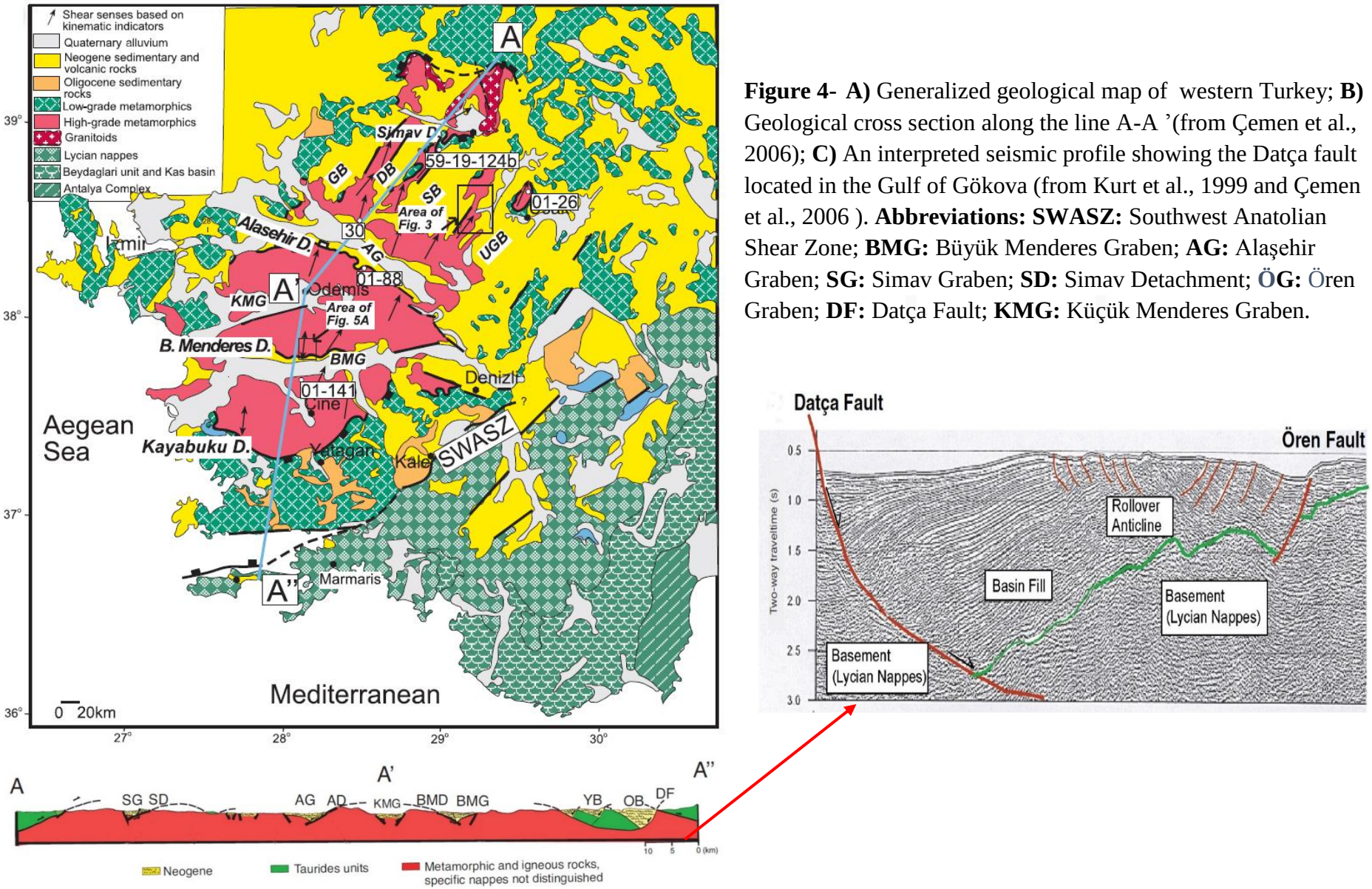

Figure 4- A) Generalized geological map of western Turkey; **B)** Geological cross section along the line A-A ’(from Çemen et al., 2006); **C)** An interpreted seismic profile showing the Datça fault located in the Gulf of Gökova (from Kurt et al., 1999 and Çemen et al., 2006). **Abbreviations: SWASZ:** Southwest Anatolian Shear Zone; **BMG:** Büyük Menderes Graben; **AG:** Alaşehir Graben; **SG:** Simav Graben; **SD:** Simav Detachment; **ÖG:** Ören Graben; **DF:** Datça Fault; **KMG:** Küçük Menderes Graben.

2.3. Stratigraphy and Structural Overview of the Büyük Menderes Graben

Sedimentary rock units of the Büyük Menderes Graben are either adjacent to the well-developed normal faults along the graben or are disconformably overlying the Pre-Neogene metamorphic basement rocks (Cohen et al., 1995; Emre and Sözbilir, 1997; Bozkurt 2000; Göğüş, 2004; Çemen et al., 2006; Şen and Seyitoğlu, 2009; Kazancı et al., 2009).

2.3.1 Pre-Neogene Metamorphic Basement Rocks

The Pre-Neogene metamorphic basement rocks of the graben consists of metamorphic rocks of the Menderes Metamorphic Core Complex (MMCC), which was exhumed as a result of extensional tectonics in the region (Gessner et al., 2001; Seyitoğlu et al., 2002; Çemen et al., 2006; Gessner et al., 2013; Ersoy et al., 2014). This investigation is concerned with the Neogene sedimentary units of the Büyük Menderes Graben. Therefore, the reader is referred to other publications for detailed descriptions of the metamorphic basement rocks in the graben (e.g., Şengör et al., 1984; Konak et al., 1987; Candan et al., 2011).

2.3.2 Sedimentary Rocks

Sedimentary rocks of the Büyük Menderes Graben are mainly composed of the lacustrine, fluvial Neogene sediments and Quaternary alluvium (Sözbilir and Emre, 1991; Göğüş, 2004; Çemen et al., 2006; Şen and Seyitoğlu, 2009). The Neogene sedimentary successions that overlie the metamorphic basement consist of the early to middle Miocene Bascayir, late Miocene Aydin and the Pliocene Huseyinciler formations. These units are overlain by the Quaternary Hamzali Formation (Kazancı et al., 2009; see Figure 6).

2.3.2.1 Bascayir Formation

The Bascayir Formation represents the oldest sequence (early-middle Miocene) related to extensional tectonics and overlies the metamorphic basement in the graben (Göğüş, 2004). The basal unit of this formation is composed of coarse-grained conglomerate, which is overlain by a shale-dominated sequence that is laterally filled with alluvial fan delta and lacustrine deposits (Sözbilir and Emre 1991; Cohen et al., 1995). The cross-bedding and the growth faulting in this formation suggest that the deposition of the Bascayir Formation is syn-extensional (Göğüş, 2004; Çiftci et al., 2010).

2.3.2.2 Aydin Formation

The late Miocene Aydin Formation is composed of coarse-grained conglomerate with interbedded layers of sandstone, mudstone and claystone (Sözbilir and Emre 1991; Bozkurt 2000; Şen and Seyitoğlu, 2009). Clastic sediments in the formation were derived from the underlying metamorphic basement and the early- middle Miocene Bascayir Formation. The thickness change in the formation is also controlled by the E-W trending growth faults.

2.3.2.3 Huseyinciler Formation

The Huseyinciler Formation consists of lateral alluvial clastic sediments that are massive to moderately-bedded, poorly-compacted boulder conglomerates with interbedded layers of sandstones and mudstones (Emre and Sözbilir 1997; Çemen et al., 2006; Şen and Seyitoğlu, 2009; Çiftci et. al., 2010). This late Pliocene age formation unconformably overlies the Aydin Formation (Ünay et al., 1995).

2.3.2.4 Quaternary Alluvium (Hamzali Formation)

The Quaternary Hamzali Formation consists of basin floor clastic sediments and alluvium deposited from lateral alluvial fans that are sourced from N-S directed streams perpendicular to the axis of the Büyük Menderes River (Kazancı et al., 2009, Çiftci et al., 2010).

2.4 Structural Geology

The Büyük Menderes Graben is the largest E-W trending graben in western Turkey (Figures 1 and 2). The graben is 8–12 km in width and about 200 km in length. It borders the central part of the MMCC to the south (Figure 2). It has been characterized by an extensional fault system that controls the graben architecture and sedimentary deposition (Yılmaz et al., 2000; Göğüş, 2004; Çemen et al., 2006; Şen and Seyitoğlu, 2009). The south dipping low angle fault on the northern flank of the graben was interpreted as a detachment fault that separates the Neogene sedimentary rocks from the exhumed metamorphic basement rocks (Seyitoğlu et al., 2000; Gessner et al., 2001; Göğüş, 2004; Çemen at al., 2006; Gessner et al., 2013). Based on kinematic indicators of the brittle deformation of the south dipping detachment fault, this fault was proposed to have southward movement along the graben with ~20° to 25° dip angles in the Kaplan valley in the Büyük Menderes Graben (Göğüş, 2004; see Figure 5).

Structural interpretation of the seismic reflection profiles along the eastern part of the graben shows that the Neogene sedimentary units get thicker towards the central part of the graben, and they gradually get thinner towards edges of the graben to the north and south. This suggests that the graben has experienced a syn-extensional deformation controlled by synthetic growth faulting (Çiftci et al 2011; Sert, 2015).

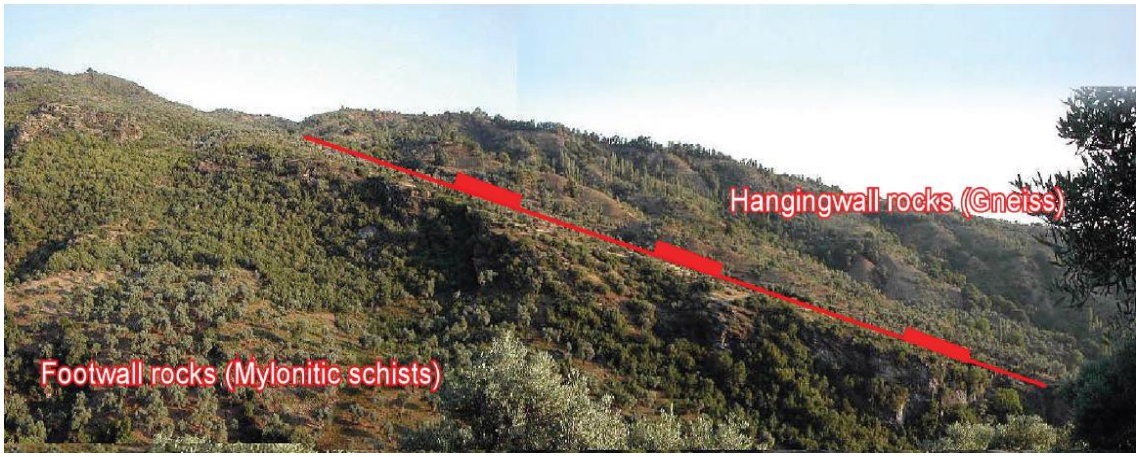

Figure 5 - Approximate location of the Büyük Menderes detachment surface along the Kaplan valley (from Göğüş, 2004).

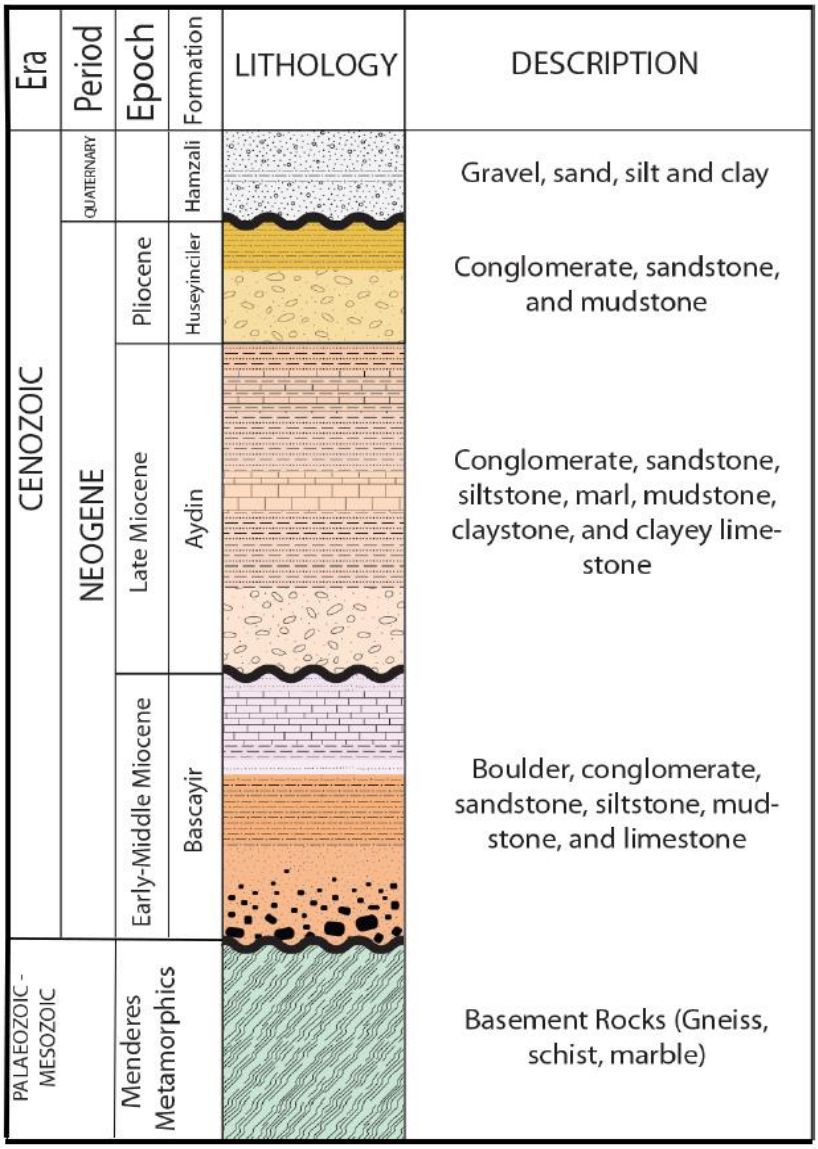

Figure 6 -Generalized stratigraphic column of the Büyük Menderes Graben. (Modified form Yılmaz et al., (2000); Yazman et al, (2004); Kazancı et al., (2009); and Sert, 2015).

3. DATA AND METHODOLOGY

3.1 Data Set

The Turkish Petroleum Corporation (TPAO) made available fourteen 2-D seismic reflection profiles with a 5 second TWT record length and a 50 m shot point interval along the Büyük Menderes Graben. The seismic data were acquired in 1999 and consist of five E-W trending seismic profiles: MUD- 99-201, MUD- 99-205, MUD- 99-207, MUD- 99-211, MUD- 99-212, and eight N-S trending seismic profiles : MUD- 99-208, MUD- 99-202, MUD- 99-204, MUD- 99-203, MUD- 99-213, MUD- 99-210, MUD- 99-214, MUD- 99-215, and a NW-SE trending MUD- 99- 206 seismic profile on which the Nazilli -1 wildcat well is located (Figure 7a).

The Nazilli-1well was drilled in the study area by TPAO and completed as a dry well in 2003. The well is located at X: 627 486.865 and Y: 4 196 431.839 UTM 35 coordinates on the NW-SE trending seismic profile, MUD-99-206. The well initiated at the Quaternary Hamzali Formation at the surface and penetrated the Pliocene Huseyinciler Formation (240 m), the late Miocene Aydin formation (225 m), and the early Miocene Bascayir Formation (320 m) before reaching the metamorphic basement at 965 m below the surface (Figure 7b). The Nazillli-1 database provided for this study consists of SP, gamma-ray, caliper, resistivity, density, neutron porosity and sonic logs. The resistivity, density and neutron porosity logs are available only for the lower part of the Aydin and Bascayir formations within the 560-965 m interval (Figure 7b).

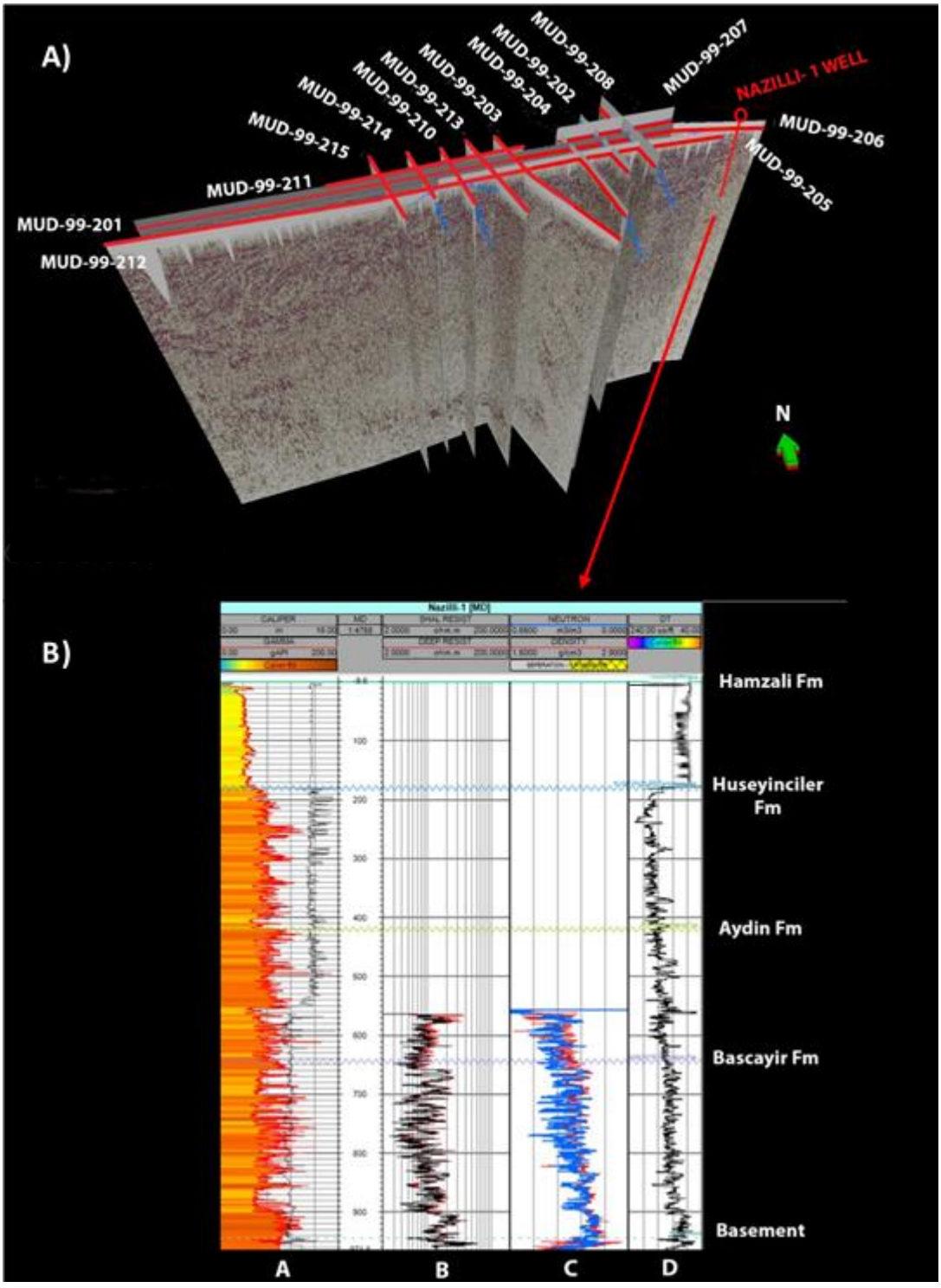

Figure 7- A) 3D view of the fourteen seismic lines from the PETREL project in the time domain. The red lines are seismic lines MUD-99-201, 202, 204, 205, 206, 207, 208, 203, 210, 211,212, 213, 214, and 215. **B)** Geophysical logs from the Nazilli-1 well demonstrating gamma ray and caliper logs (A); shallow and deep resistivity logs (B); neutron porosity and bulk density logs (C); and sonic log (D). The data base of the well does not include resistivity, density and neutron porosity logs above 560 m.

3.2 Methodology

In this study, three main methods were used to provide a better insight into the structural evolution of the Büyük Menderes Graben. The methods are: 1) Interpretation of 2-D seismic reflection profiles; 2) Structural cross -section restoration of depth converted 2-D seismic profiles; and 3) 3-D kinematic modeling.

Seismic interpretation comprises a two-step process to delineate the subsurface geology of the Büyük Menderes Graben. The first step is the generation of a synthetic seismogram for the well to seismic tie resulting in a preliminary horizon and fault interpretation in the time domain. The second step is the creation of a velocity model and structural interpretation in the depth domain.

The structural restoration process was used to construct admissible structural cross sections from the depth converted seismic reflection profiles. This method was used to facilitate validation of horizon and fault interpretation, and trace the main fault trajectory at depth where it is not clearly seen on the seismic reflection profiles.

From the restored cross sections, a 3-D kinematic model was created to reveal the structural development of the Büyük Menderes Graben in the early Miocene, late Miocene and Pliocene geologic epochs to have a better understanding of the structural evolution of the graben. Finally, a backstripping technique was used to determine tectonic subsidence rates for each formations during their time of deposition.

3.2.1 Seismic Interpretation

Fourteen seismic reflection profiles and available wireline well logs from the Nazilli-1 well were used to interpret the structural geometry of the Büyük Menderes Graben in the study area (Figure 7). The formation tops in the Nazilli-1 well were correlated to the seismic line MUD-99-206 by creating a synthetic seismogram. This provided a seismic tie to determine formation tops and interpreted structural geometry in the time domain. Finally, a velocity model was created and, a time to depth conversion was constructed to determine an accurate subsurface seismic interpretation.

3.2.1.1 Well to Seismic Tie

A well to seismic tie allows for correlations to the lithology observed along the well in depth domain with specific reflections on the seismic profiles (Cunningham and Droxler, 2000; Yılmaz, 2001). Time-depth correlations for the well to seismic tie are generated using a synthetic seismogram, which is a convolution of reflection coefficient (RI) and a wavelet extracted from seismic data (Yılmaz, 2001). Three steps are required for this process. The first step is the calculation of the reflection coefficient (R) which is an expression of acoustic impedance (AI) contrast at a boundary between two layers. AI is calculated by multiplying density and velocity values obtained form well logs. The formula below is used to determine reflection coefficient (R).

$$R = (AI_{n+1} - AI_n)/(AI_{n+1} + AI_n)$$

The second step is the convolution of derived reflectivity series with a wavelet extracted from the seismic data to create a synthetic trace. The third step is to match the synthetic trace with the seismic trace by aligning seismic reflections to determine formation tops. As a result of these steps, a synthetic seismogram allows correlations of formation tops

with seismic traces to define beds and delineate the structural geometry on the seismic profiles (Cunningham and Droxler, 2000).

Since Nazilli-1 well does not have density (RHOB) values down to 560 m, which corresponds to Huseyinciler Formation, Hamzali Formation and the upper part of the Aydin Formation, density values of the upper part of the well section were calculated from the sonic log using the Gardner's equation to obtain an accurate synthetic seismogram (Figure 8).

$$P = 0.23V_p^{-0.25}$$

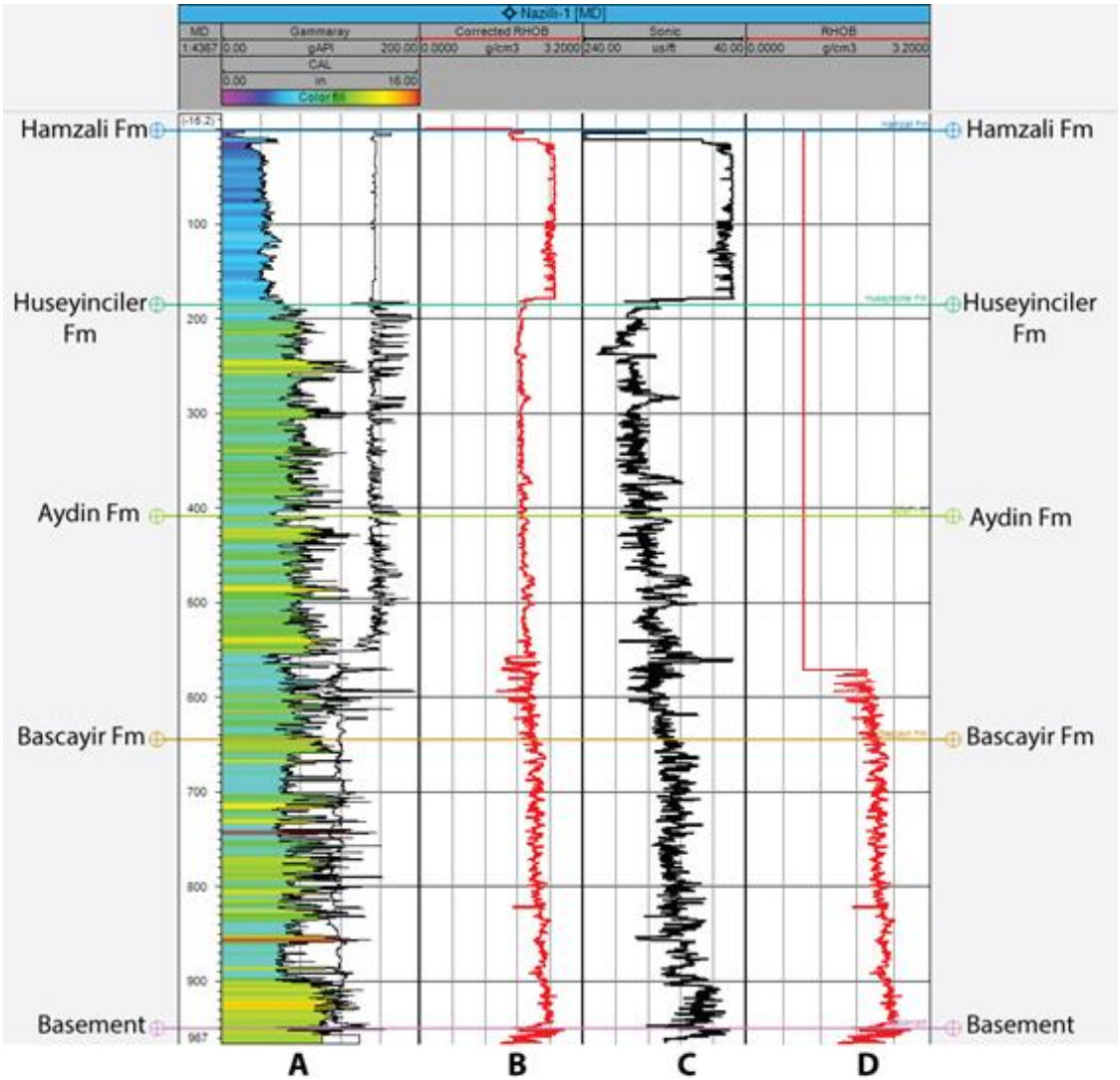

Figure 8- Geophysical well log from the Nazilli- 1 well displaying corrected density (RHOB) values using the Gardner's equation. **A)** Gamma ray and caliper logs; **B)** Corrected density log from sonic log using the Gardner's equation; **C)** Sonic log; **D)** Original density log.

After correction of the density log, the acoustic impedance (AI) was calculated by multiplying bulk density (RHOB) and velocity values (Figure 8). Then, the reflection coefficient (R) obtained from the AI was convolved with a statistic wavelet extracted from seismic line MUD-99-206 to create the synthetic seismogram. This allowed us to determine the top of the Huseyinciler, Aydin, and Bascayir formations and the metamorphic basement in the study area accurately (Figure 9).

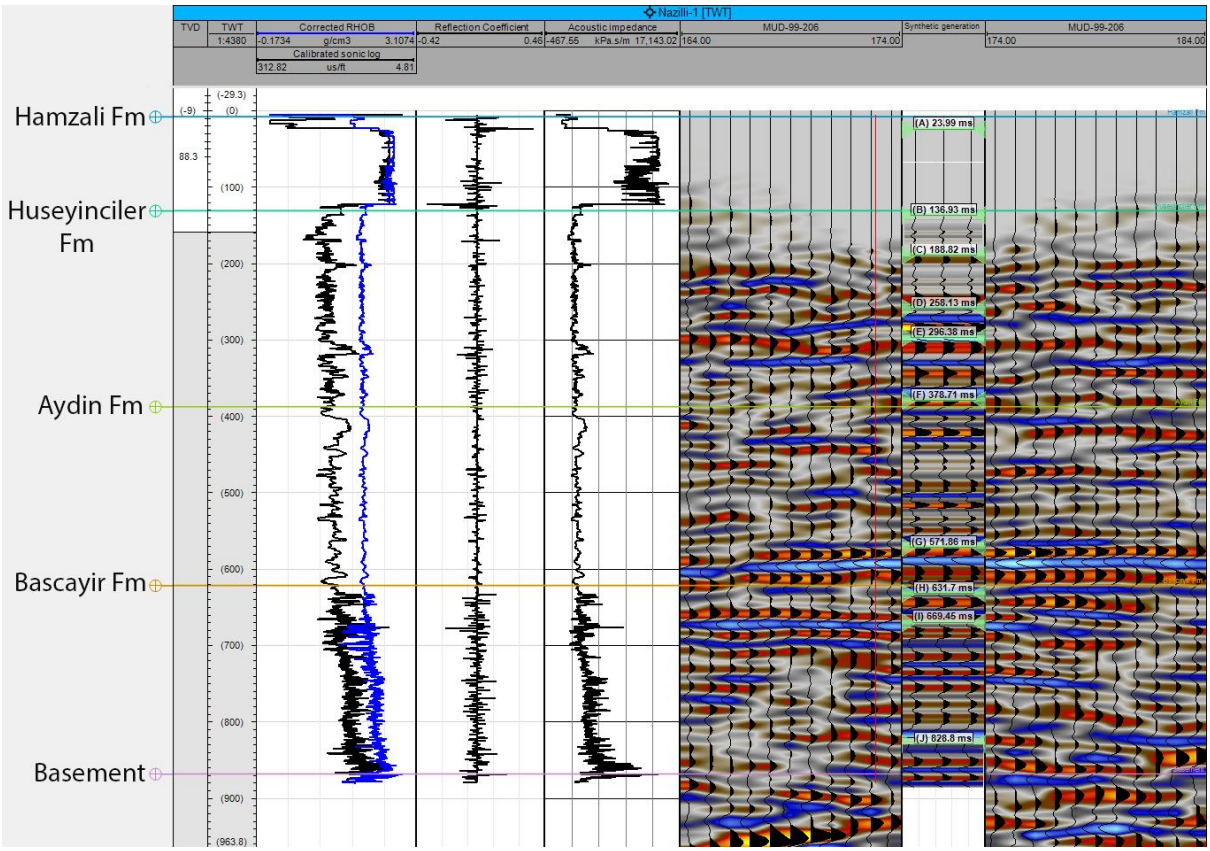

Figure 9- Synthetic seismogram generation. The synthetic is shown with the calibrated sonic log, corrected density log (blue), acoustic impedance, reflection coefficient, and seismic image of the MUD-99-206 where the Nazilli well is located.

3.2.1.2 Time to Depth Conversion

Interpreting geological structures from the seismic profiles in the time domain can lead to an inaccurate interpretation of the subsurface structures, because even simple geology such as dipping beds can produce false highs in the time domain (Yılmaz, 2001; Robein, 2003). Thus, time to depth conversion is required to remove the structural ambiguity in the time domain (TWT) to verify structural features (Yılmaz, 2001; Robein, 2003). Depth conversion is accomplished using a velocity model that is generated by defining a mathematical function for each geological formation after a complete horizon interpretation in the time domain (Yılmaz, 2001; Robein, 2003).

After horizon and preliminary fault interpretations were completed in the time domain using interval velocities calculated for each formation from calibrated sonic log (DT), a velocity equation (Adlinvel equation) was used for depth conversion.

$$V=Vo+k\ (Z-Zo)$$

Where, V = velocity (m/s),

V_o = velocity at the top of the zone (m/s),

$Z-Z_o$ = distance between the point and the top of the zone (m) and

k = velocity factor (constant).

Surfaces created for the tops of all formations in the study area were input into the velocity model to describe zone intervals. The formations are from youngest to oldest: Hamzali, Huseyinciler, Aydin, Bascayir sedimentary units and the metamorphic basement. Each formation in the velocity model was defined with specific interval velocities. The first and highest interval is the 180 m of the Hamzali formation, which was mostly alluvial. The interval was defined with 1700 m/s interval velocity. The second interval is the 244 m of the Huseyinciler formation, which was mainly composed of poorly sorted sediments. It was

defined with 1880 m/s velocity. The third and fourth intervals, 224 m of the Aydin and 324 m of the Bascayir formations, composed mainly coarse-grained sediments were defined as 2010 and 2177 m/s velocity intervals, respectively. A constant velocity of 3200 m/s was assigned for depth conversion in the metamorphic basement below the sedimentary section (Figure 10). This velocity model was applied to all seismic reflection lines including horizons and fault interpretations in the time domain. Consequently, position of the horizons and fault orientations were checked in the depth domain to correct the velocity model that was defined in the time domain (Figure 10).

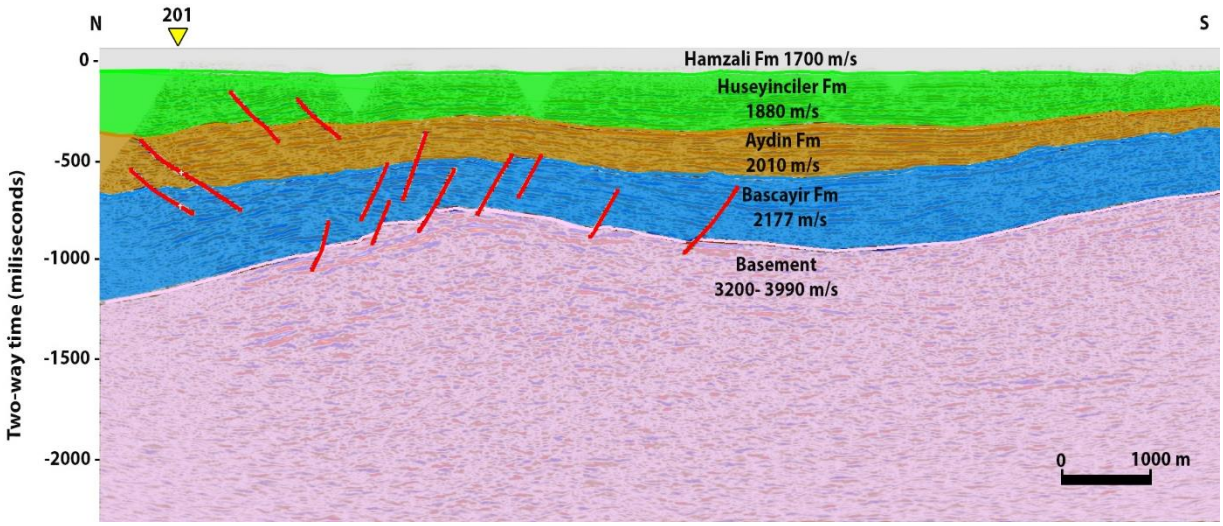

Figure 10- Velocity values used for the velocity model for each formation on the seismic reflection profile, MUD-99-206.

3.2.2 Structural Cross-Section Restoration

Structural restoration is a useful tool to construct admissible structural cross sections to observe the point where deformation initiates from its undeformed state (Bland et al., 2006). Since the seismic profiles in this study have a limited resolution at depth, tracing the trajectory of the main graben boundary faults is difficult. Hence, sedimentary rock accumulations related to the main graben boundary fault geometry and associated basin development are controversial.

Structural restoration of the depth converted seismic profiles plays an important role in determining the subsurface structural geometry in the study area. In this study, a restoration workflow in the 2D MOVE software was used (Figure 11) to construct restored cross sections from the depth converted seismic reflection profiles. Three restoration steps were applied to the depth converted seismic reflection profiles. They are move-on-fault, unfold to horizon, and decompaction. Each step shown in the restoration workflow was repeated for each geological cross section until a structurally valid model was obtained.

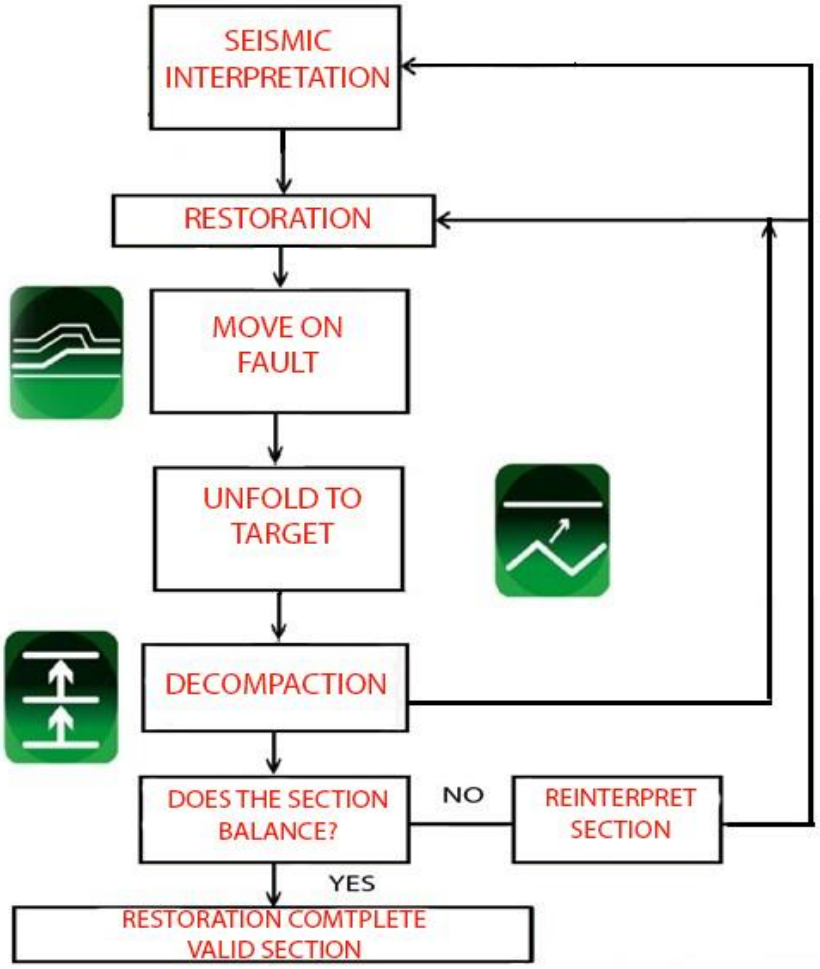

Figure 11- The work flow of structural cross section restoration in the 2D Move software (modified form the 2D Move Manual, 2012).

The restoration process starts with digitizing interpreted seismic reflection profiles to form polygons for each point. Then, each point in the hanging wall is moved the same horizontal distance following a path parallel to the fault (Figure 12). During this process, overlays and mismatching on the hanging wall of the faults due to misinterpretation are fixed. This process validates the interpretation by correcting the relationship between fault orientation and depositional geometry during restoration.

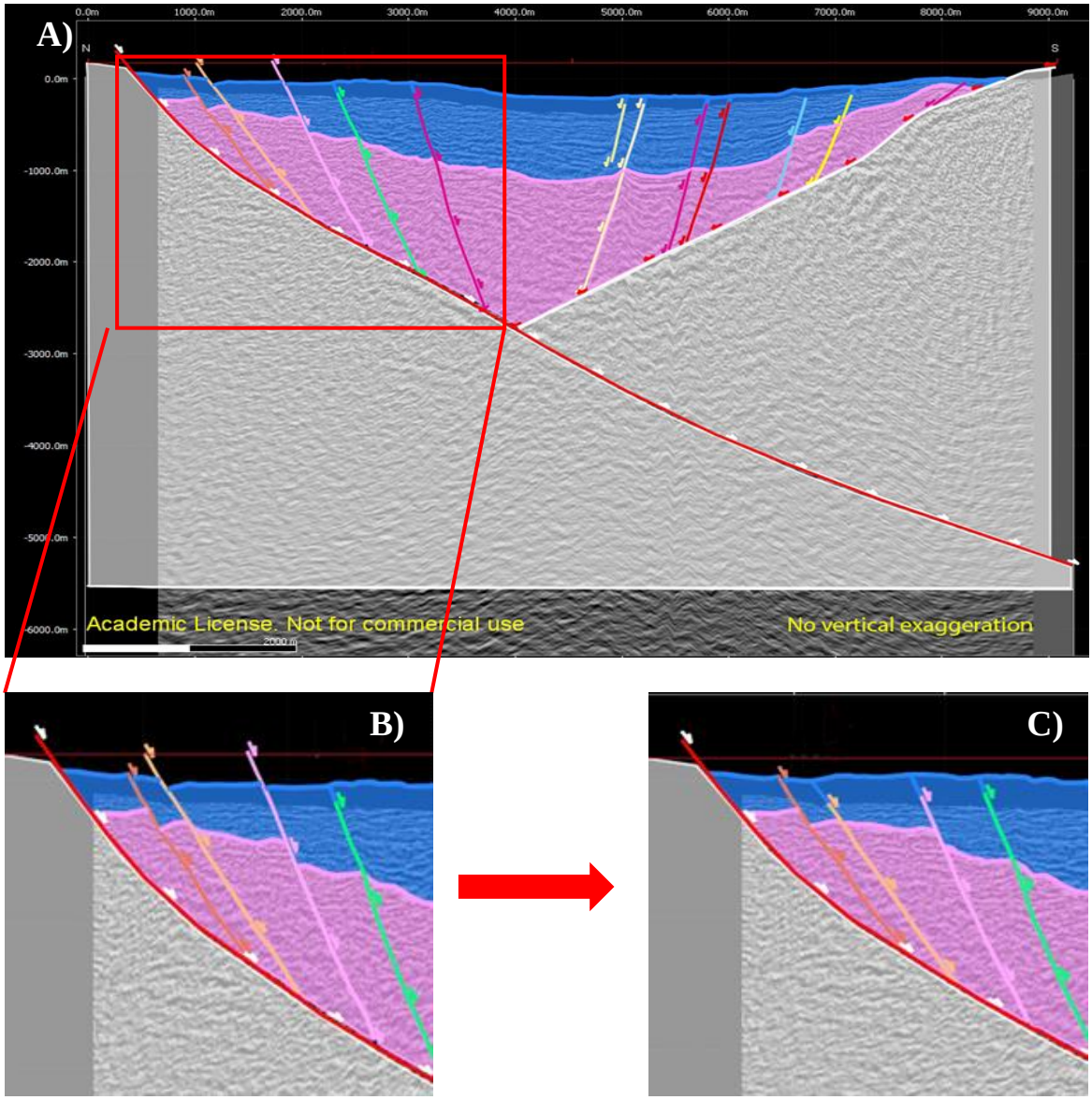

Figure 12- Restoration steps in the 2D Move software showing **A)** polygon creation for the seismic profile, MUD-99-202, **B)** moving horizons on the hangingwall of the faults, and **C)** balanced horizon (blue) without any overlays and mismatches.

Horizons moved along the faults are unfolded to remove deformation in the surface during deposition and fixed horizons are decompacted by assuming that the basin was uplifted due to Airy isostasy (Figure 13). Decompaction of the restored unit allows us to delineate the geometry of the basin at the time when each formation was deposited (Allen and Allen 2013). Each step in this process is repeated for each geological time period until a valid section is obtained (the 2D Move Manual, 2012).

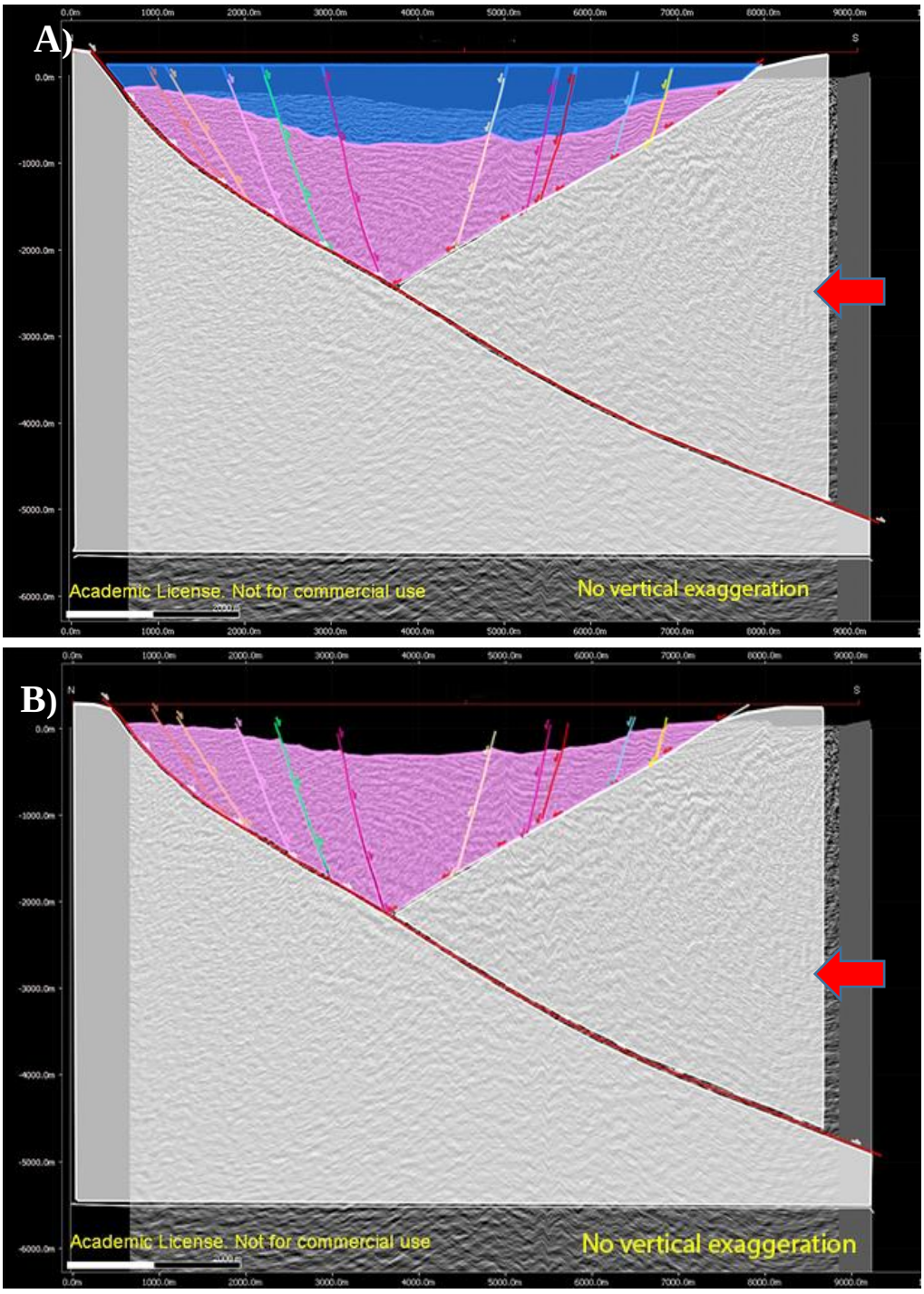

Figure 13-A) Unfolding of balanced horizons to remove the deformation of a surface during deposition. **B)** Decompaction of the unfolded horizon (blue).

3.2.3 3D Kinematic Modeling and Tectonic Subsidence

Backstripping is a process of analyzing sedimentary basin evolution by calculating tectonic subsidence rates through time (Watts, 2001). Backstripping technique relies on decompaction of the sediment column and reconstruction of its original thickness at the time of deposition and the correction of paleobathymetric and eustatic variations (Allen and Allen, 2013).

Decompaction allows for calculation of the effects of each sediment volume change due to porosity loss related to depth during deposition (Sclater and Christie, 1980). A porosity-depth relationship can be constructed from values measured in well logs, or from a theoretical porosity-depth curve calculated from the deformation tests (Sclater and Christie, 1980). In this study, the porosity depth relationship was created using calculated porosity values from the density log of the Nazilli-1 well.

From the porosity-depth curves, the decompacted thickness (S^*) and average density (P_S) of a particular sediment layer at a certain geologic time can be obtained by using the formula below (Sclater and Christie, 1980).

$$S^* = S\frac{1-\emptyset_s}{1-\emptyset_s}$$

$$P_s = p_w\emptyset_s^* + p_g(1-\emptyset_s^*)$$

Where;

S = present day formation thicknesses,

(ϕ_s) = porosity of the compacted and decompacted layers

(ϕ_s^*)= porosity of decompacted layers

Ps= Average density

p_w and p_g are water and sediment densities.

Since sedimentary basins have more than one sedimentary unit, decompaction of all units according to their thicknesses and porosities at the time of deposition must be considered (Steckler and Watts, 1978). To obtain tectonic subsidence rates during basin evolution, the average density of the restored layers are summed and divided by the total thickness (Steckler and Watts, 1978).

$$P_s = \frac{\sum_{i=1}^{n}\left[p_w \emptyset_{si}^{*} + p_g i(1-\emptyset_{si}^{*})\right] S_i^{*}}{S^{*}}$$

Where i is the i^{th} layer and n is the total number of stratigraphic layers.

The backstripping process removes the effects of sediment loading and allows for density calculations of sediments through time (Watts, 2001). Assuming water depth and sea-level changes have no effect, tectonic subsidence (TS) can be calculated using density (p_s) and decompacted thickness (S^{*}) of the sediments (Figure 14).

$$TS = S^{*}\left(\frac{P_m - P_s}{P_m - P_w}\right)$$

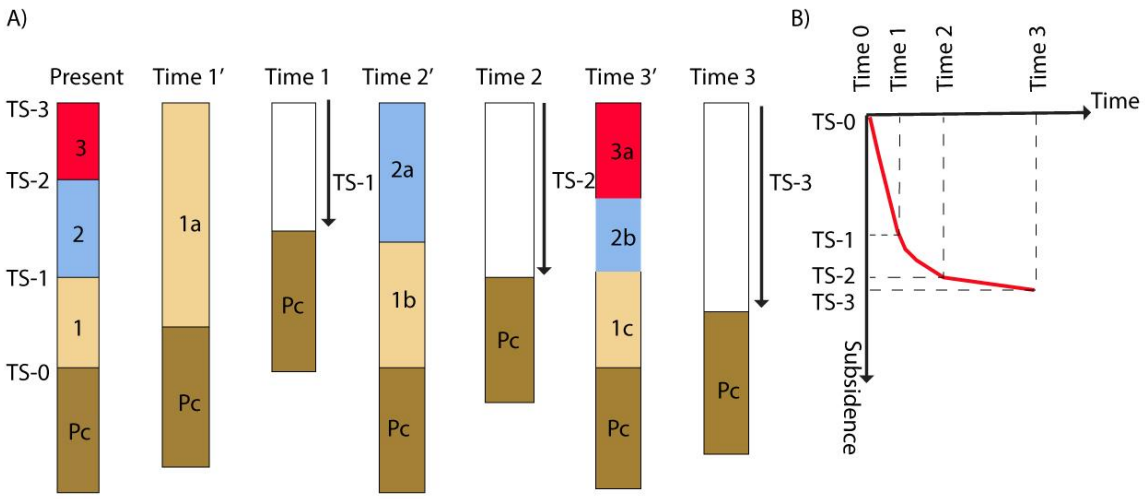

Figure 14- A) An example of 1-D backstripping' steps. The first column shows the present day sedimentary rock units. The second column represents decompaction of unit 1 to its original thickness and density at time 1'. The third column shows the tectonic subsidence of the second column at time 1. The fourth column shows the calculated tectonic subsidence of the decompacted unit at time 2'. The initial thickness of units 1 and unit 2, according to their new depth are decompacted, then new tectonic subsidence rate at that time is calculated based on decompacted unit 1. In column five, this process is repeated for time 3'.**B)** Tectonic subsidence rates through the time of deposition of the units in times 1, 2 and 3 (Modified from Bond and Kominz 1984; Cunha, 2008).

Finally, a 3-D kinematic model was created using the balanced structural cross sections and tectonic subsidence rates calculated from the backstripping technique in order to understand evolution of the Büyük Menderes Graben. The model allowed us to delineate the geometry of the boundary faults on both margins associated with their synthetic splays and syn-extensional deposition rate of sedimentary rocks through geological time (Figure 15).

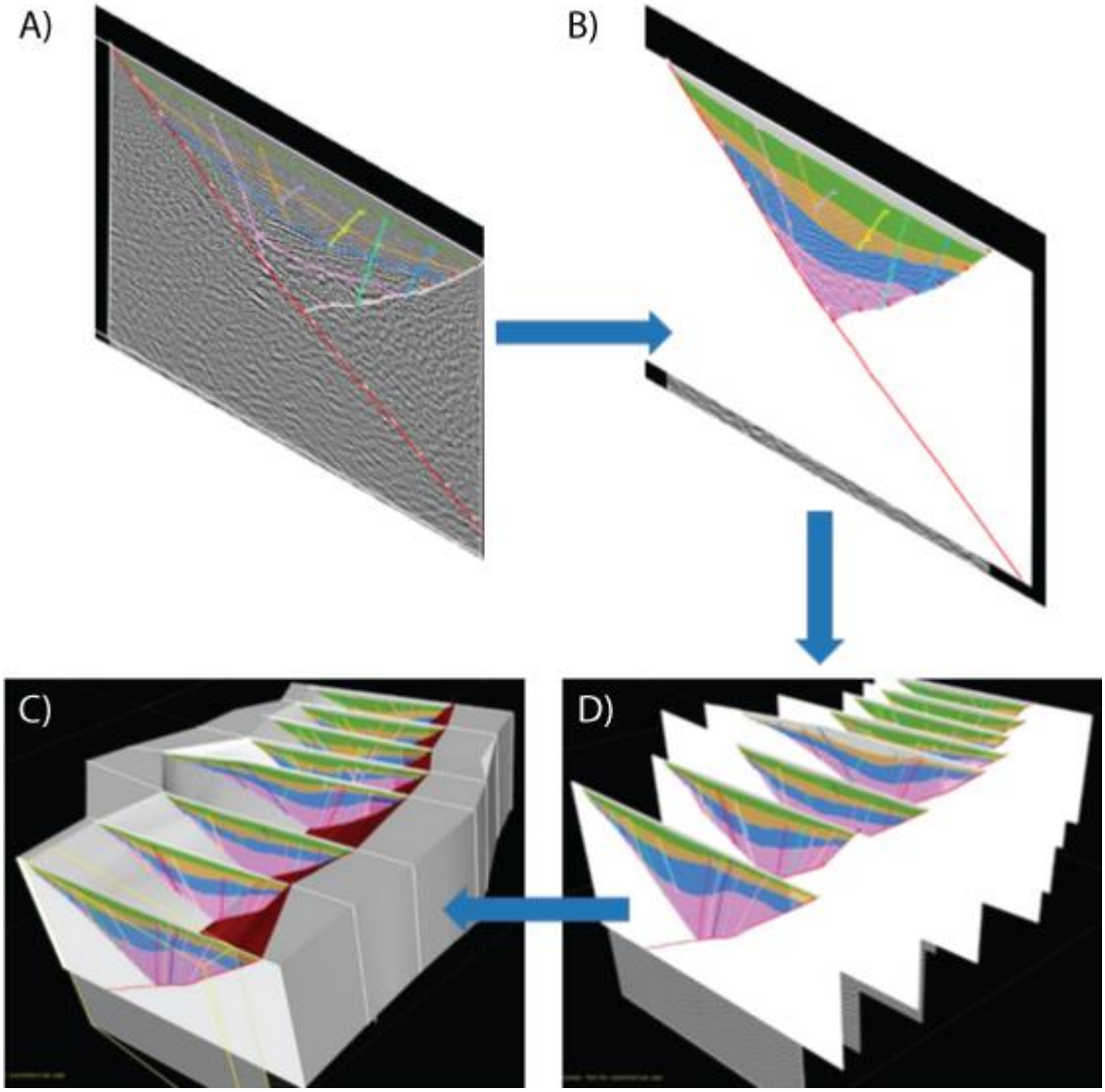

Figure 15- 3D kinematic modeling created from the balanced 2-D depth converted seismic profiles (present time). The figure shows the steps of creation of the model; **A)** Structurally balanced depth converted seismic line; **B)** Digitized balanced seismic cross section, and **C) and D**) the series of cross sections created for the 3D modeling that is ready for backstripping.

4. CROSS SECTION RESTORATION AND SEISMIC INTERPRETATION

4.1 Cross Section Restoration

Based on field oriented studies, it was proposed that the Büyük Menderes graben was developed along a low angle south dipping detachment fault (Seyitoğlu et al., 2004; Göğüş, 2004; Çemen et al., 2006; Çiftçi et al., 2010). However, structural interpretation of the available seismic reflection profiles indicates that sedimentary rocks on the hanging wall of the south-dipping normal fault along the northern margin of the graben do not contain a rollover structure related to detachment faulting (Figure 16). This geometry contradicts the presence of a south dipping low angle detachment surface, which is supposed to cause formation of a rollover structure in the sedimentary rock units above the basement (Xiao and Suppe, 1992).

In the seismic profiles, the south and north dipping boundary faults located on the northern and southern margins of the graben can only be traced to about 2500 m below sea level (Figure 16). Tracing fault plane trajectory below ~ 2500 m is very difficult because of poor resolution of the seismic reflections. This uncertainty could result either from juxtaposition of metamorphic rocks or from seismic processing. Therefore, testing boundary fault geometry on both margins of the graben using the cross-section restoration techniques plays an important role in determining the boundary fault geometry and its role in the evolution of the graben.

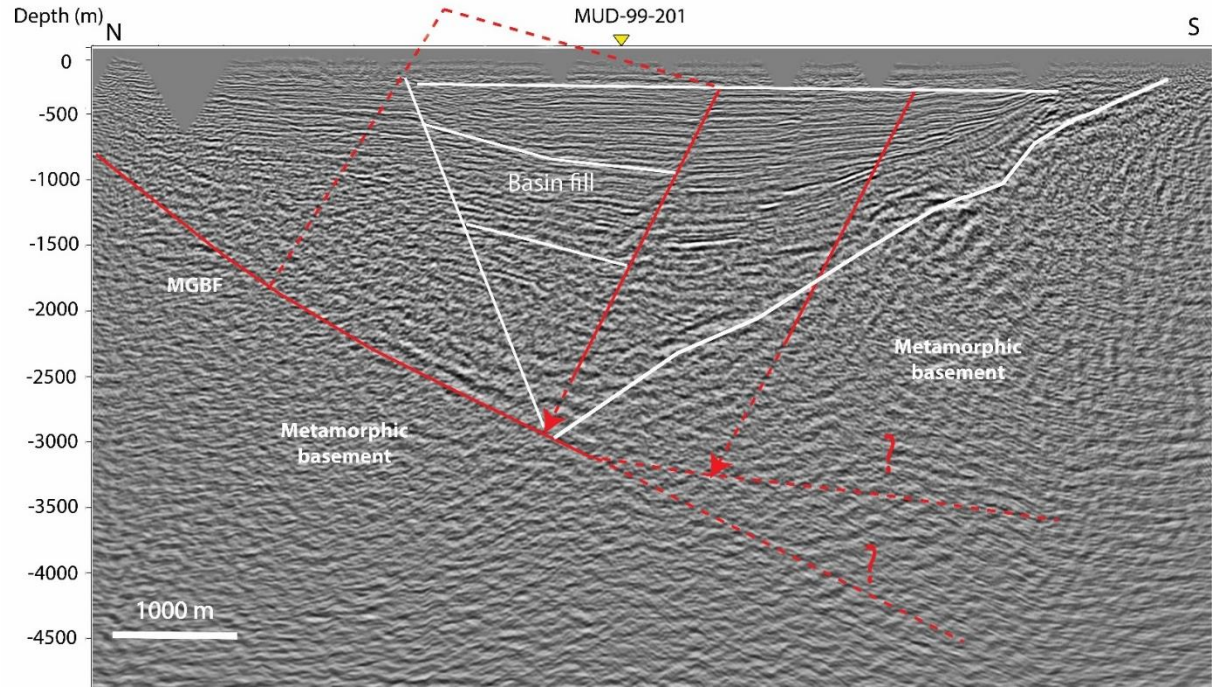

Figure 16- Seismic profile MUD-99-202 illustrating two possible geomertries of the main graben baundary fault shown in red and deposition trend (white) of the basin fill, which is bending towards the southern margin of the graben.

To verify the boundary fault interpretation, the main fault geometry at depth including listric shape was modeled by changing the fault dip angle until a balanced section was obtained. One representative cross section was constructed from the depth converted seismic reflection profile of MUD-99-202 to exemplify the restoration technique used in this study for validation seismic interpretation and solve uncertainty in the interpretation of graben bounding structures. First, the profile was restored assuming a listric geometry to test whether the sediment orientation on the hanging wall of the south dipping fault is matched with the interpreted subsurface geometry (Figure 17).

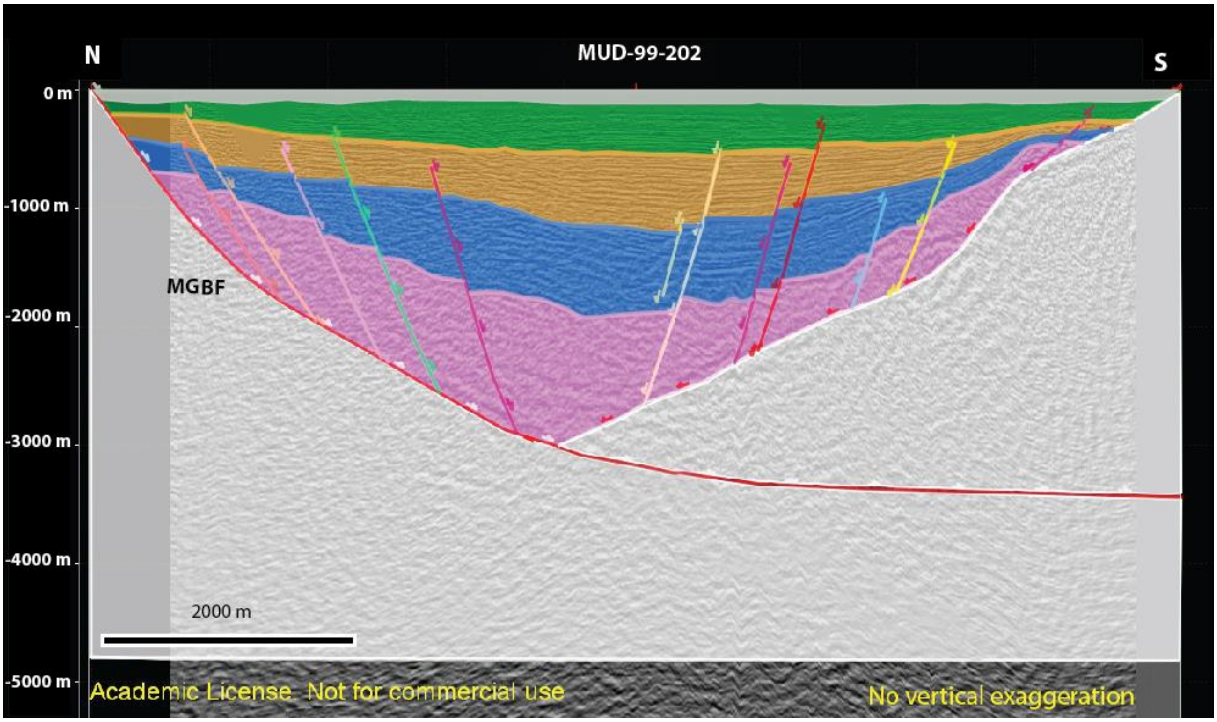

Figure 17- Restoration of the seismic profile MUD-99-202 considering the main graben bounding fault is listric and becomes horizotal at depth.

During the restoration process, first the Quaternary and Pliocene formations were decompacted because it is not seen any faulting in these formations (Figure 18). Then, the late Miocene Aydin Formation was restored assuming the hanging wall of each fault block was deformed by simple shear. Calculating the shear angle of each fault along both synthetic and antithetic faults, each point in the hanging wall was moved the same horizontal distance following a path parallel to the fault using a fault algorithm in the 2-D Move software (Figure 18).

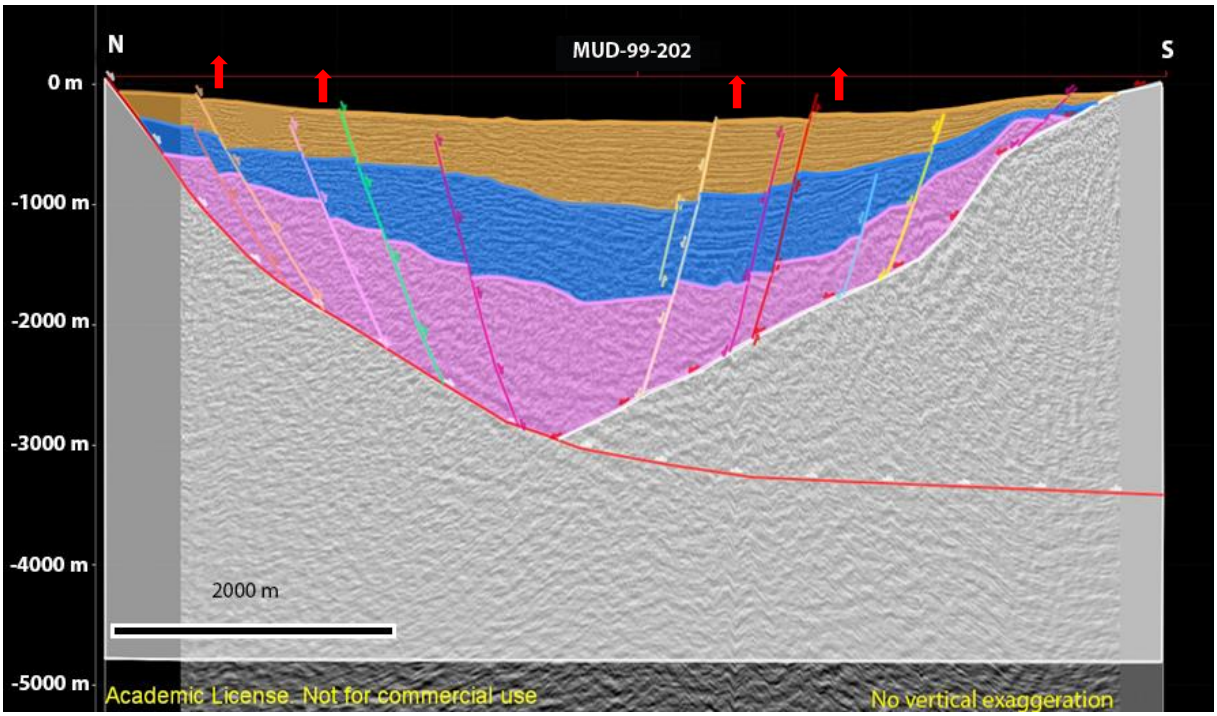

Figure 18- Decompaction of the Quaternary and Pliocene units and balancing of fault displacement in the Aydin Formation (orange unit) by moving faults up along the hanging wall.

However, when the late Miocene Aydin Formation was unfolded and the boundary faults along both sides were rotated, the listric geometry of the graben was not balanced, because the rotated hanging wall block overlays the basement and the south dipping boundary fault does not fill the gap due to its geometry (Figure 19). This suggests that the lower part of the south dipping fault should be steeper at depth and the graben floor should have more space for the basement unit at the intersection point of the boundary faults (Figure 19).

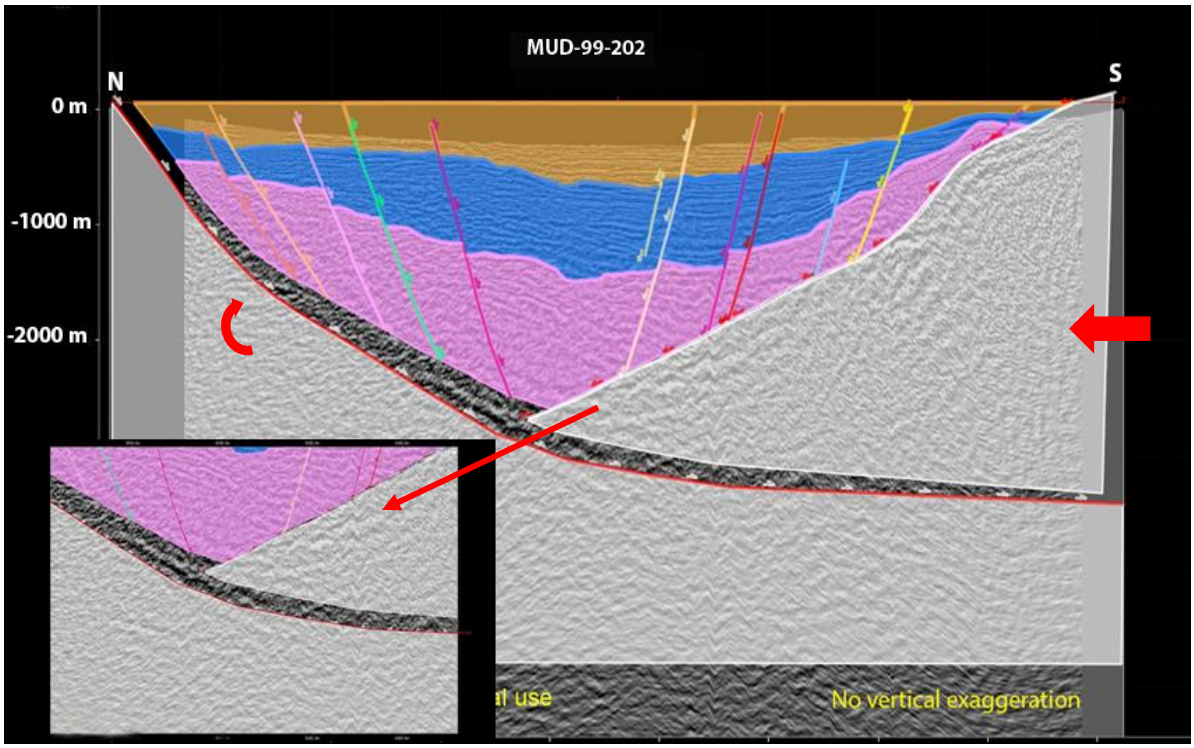

Figure 19- Unfolding of the restored late Miocene Aydin Formation (orange unit) together with rotation of the blocks, assuming a listric fault geometry. Small screen shot shows discordance at the basement if the main fault is considered as becoming horizontal at depth.

Since the listric fault geometry did not produce a balanced structural section, the fault dip was rotated at 5° increments until the graben geometry was balanced in order to properly restore the section without gaps and overlaps (Figure 20). As a result of this process, the south dipping fault with 42 to ~35° dip angle was found as the best fit to balance the cross section (Figure 20).

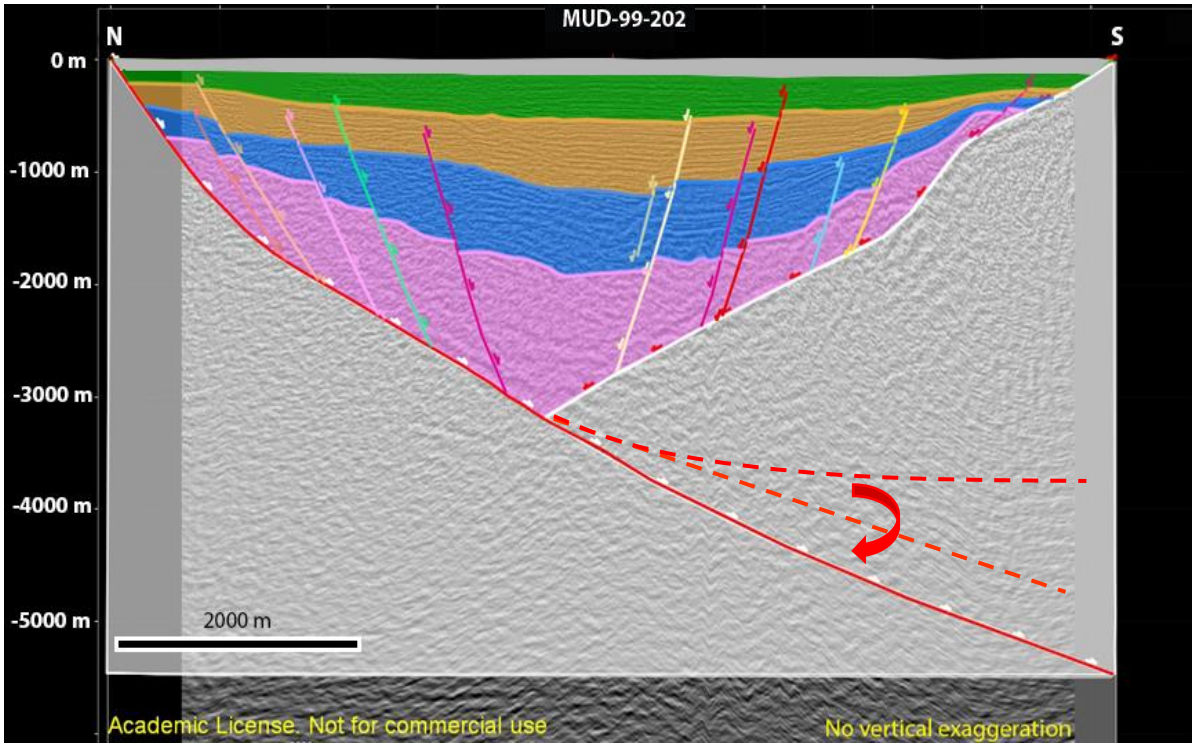

Figure 20- The position of the south dipping boundary fault that produces a balanced cross-section without any gaps and overlaps in the section.

Figure 21 shows the restoration steps of the balanced section along the seismic section MUD-99-202 with the best fit dip angle of the south dipping fault at depth. The figure demonstrates that there is no gap, or overlap on the section when horizons on the synthetic and antithetic faults are restored. Therefore, the Aydin Formation (orange unit) can be unfolded to the surface rotating hanging wall and footwall blocks (Figure 21 a and b).

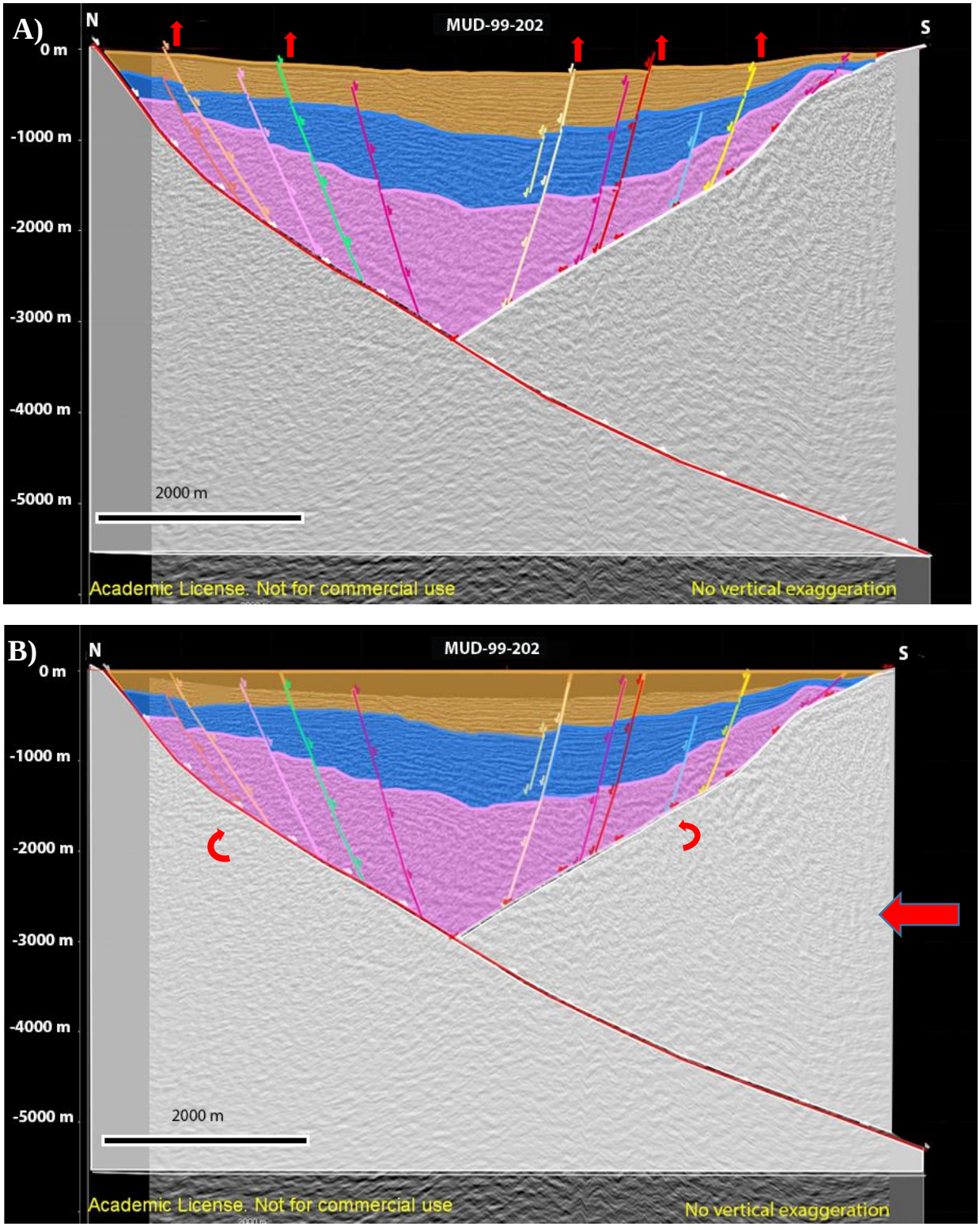

Figure 21- A**)** Restoration of the late Miocene Aydin Formation (orange unit), moving the horizons on the faults. **B)** Balanced section after moving horizons on the fault rotating hanging wall and footwall blocks, and unfolding the formation.

After decompaction of the restored the late Miocene Aydin Formation, the same steps were applied for the middle Miocene Bascayir Formation (blue unit) to finalize the restoration. As shown in figure 22, movement of the horizons on the hanging wall of the faults and rotation of the boundary fault at both margins show the same geometric consistency during the restoration of the Bascayir Formation. The balanced structural cross section (Figure 22) demonstrates that the south dipping boundary fault is not becoming horizontal at depth. On the contrary, the fault maintains its dip angle until the reliable depth of the seismic section (~5 km). This process not only allowed for validation of the geometry of the south dipping boundary fault, but also helped to understand the role of the north dipping boundary fault and its antithetic and synthetic splays during the Miocene extension, which will be discussed later in the kinematic evolution section.

Consequently, validating the graben geometry resulting from the restoration process applied to the seismic profile MUD-99-202 enabled the same steps to be taken for the whole N-S directed seismic reflection profiles to delineate the graben geometry from the early Miocene to the present in 3-D.

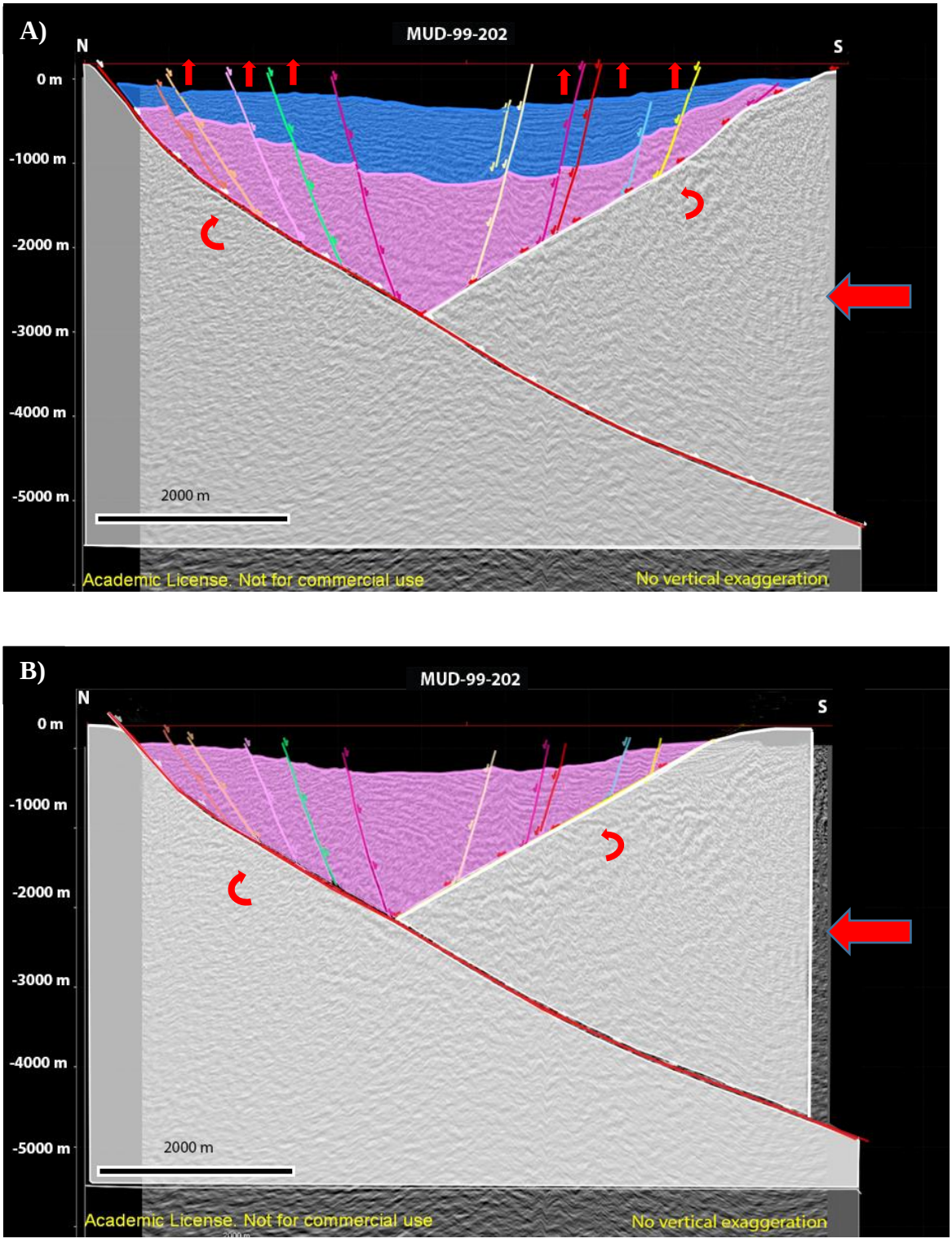

Figure 22- A) Restoration of the middle Miocene Bascayir Formation (blue unit) showing rotation of the synthetic and antithetic faults and moving horizons. **B)** Position of the metamorphic basement (pink unit) after decompaction of the Bascayir Formation.

4.2 Structural and Stratigraphic Interpretation of the Büyük Menderes Graben

During this study, the Cenozoic stratigraphy and subsurface structural geometry of the Büyük Menderes Graben were analyzed based on the depth converted 2D seismic reflection profiles that were structurally balanced. Structural and stratigraphic interpretations of the eight N-S and five E-W trending 2-D seismic reflection profiles are used to explain sedimentary rock accumulations and their thickness changes along the graben from east to the west in addition to the structural geometry related to the Cenozoic extensional tectonics in western Turkey.

4.2.1 Stratigraphic Interpretation

The Neogene sedimentary sequences and metamorphic basement in the Büyük Menderes Graben were interpreted from the correlation of seismic profile MUD-99-206 and the synthetic seismic created from the Nazilli-1 well's sonic and density logs. The four Neogene formations, which were mapped on the surface by previous researchers, are identified in the well logs of the Nazilli-1 well and interpreted on the seismic reflection profiles. These formations are from oldest to youngest: 1) The early Miocene Bascayir Formation, 2) the late Miocene Aydin Formation, 3) the Pliocene Huseyinciler Formation and 4) the Quaternary Hamzali Formation.

Envelope attribute analysis, which is also useful in highlighting main sequence boundaries, was used to contribute to seismic stratigraphic interpretation (Figure 23). Envelope attribute analysis shows that the metamorphic basement can be observed around 860 ms with strong high amplitude reflections (Figure 23). The early Miocene Bascayir and the late Miocene Aydin formations above the basement rocks are mainly composed of coarse-grained sediments that are characterized by strong lens-shaped reflection geometry on the seismic line, while the Pliocene Huseyinciler Formation that overlies the Miocene units

documents relatively weak seismic reflection due to its poorly sorted clastic rock composition as well as the youngest Quaternary Hamzali Formation that represents alluvial deposits of the modern Büyük Menderes River.

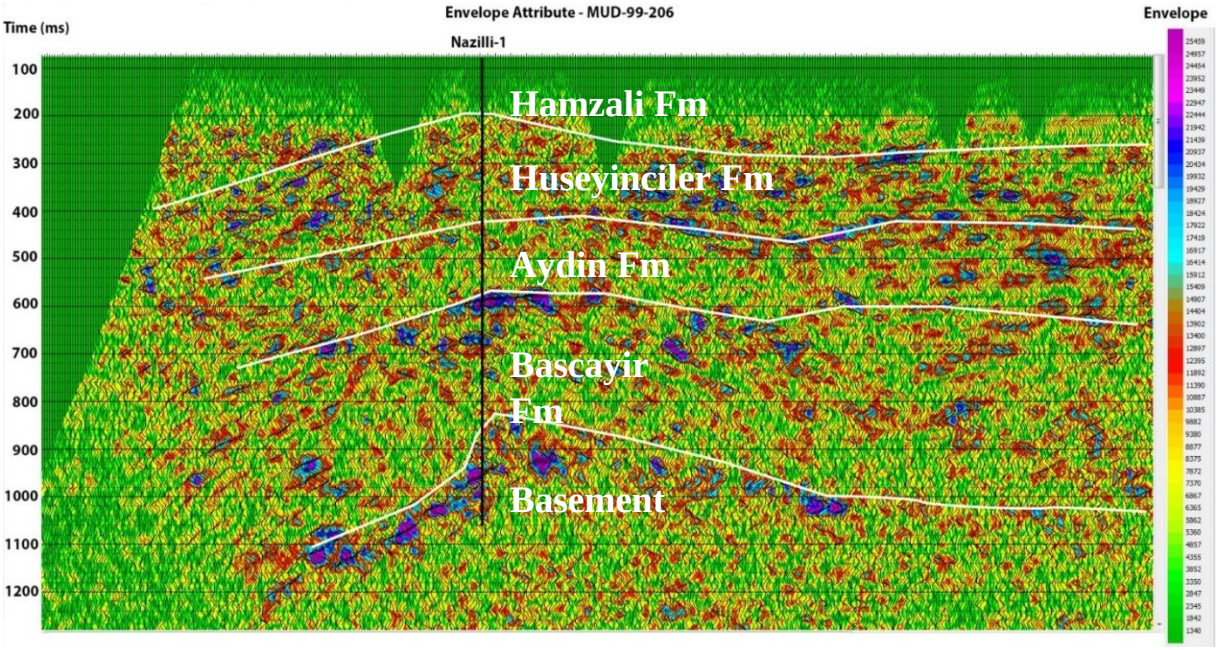

Figure 23- Envelope attribute analysis of the seismic section MUD-99-206 showing high amplitude anomalies of stratigraphic boundaries and metamorphic basement.

4.2.2 Structural Interpretation

4.2.2.1 N-S Trending Seismic Profiles

Along the eight N-S trending seismic profiles, the Büyük Menderes Graben has a slightly symmetrical geometry bounded by two major south and north dipping normal faults. Along the northern flank of the graben, the south dipping boundary fault propagates almost a planar normal fault geometry with ~38° to 45°dip angles without flatting out at depth along the graben from east to the west (Figures 24 to 39). This fault becomes steeper towards the western part of the study area.

The north dipping boundary fault dips ~35° along the southern flank of the graben and joins to the south dipping boundary fault around 3500 meters below sea level (BSL) in the eastern part (Figure 24, seismic profile MUD-99- 208) and at about 2300 meters BSL (Figure 38, seismic profile MUD-99-215) in the western part of the study area (Figures 24 to 39). This indicates that exhumation of the metamorphic basement rock decreases towards the west since the graben floor becomes shallower.

The 2-D seismic reflection profiles show that the graben fill is offset by the synthetic and antithetic normal faults traced with a displacement on the hanging wall units. They merges into the boundary faults at ~ 3400 m BSL at the eastern part and at about 2000 m BSL at the western part of the study area (Figures 24 to 39). The pattern of the synthetic and antithetic normal faults also suggests growth faulting and syn-extensional deposition geometry due to sedimentary packages thickening on the downthrown side of these normal faults.

The fault orientation of the synthetic and antithetic normal faults shows that in the center of the graben the normal faults on the hanging wall of the two boundary faults dip with high angles (65°-78°), while those that are located on the edges have shallower dip angles

(50°-60°) along the graben from east to the west within the study area (Figures 24 to 39). This suggests that the faults located on both flanks of the graben developed first and experienced fault rotation due to continuous extension and footwall uplift.

The seismic profiles show that there is more sedimentary rock deposition on the northern margin than the southern margin of the graben in the southern part of the study area, while this thickness difference becomes more balanced towards the west. The Neogene succession thickens towards the center of the graben and gets thinner and progressively higher in elevation towards the northern and southern margins of the graben (Figures 24 to 39). This suggests that the margins of the graben have experienced basement uplift preferentially to the center, which caused sediment accumulation from the northern and southern margins to the center of the basin due to ongoing Cenozoic extension. The thickness change also suggests that the extension might have initiated along the northern margin of the graben with initiation of the south dipping boundary fault and created more accommodation space for sedimentary rock deposition on the northern margin of the graben. Then, the graben experienced a polarity change towards the west due to the north dipping boundary fault activity on the southern margin of the graben. Therefore, it can be suggested based on the geometry observed in the cross sections (Figures 24 to 39) that the pattern of sediment deposition shifted to the north dipping boundary fault along the southern margin of the graben after considerable sedimentation along the northern margin. This geometry suggests that both boundary faults were active at different times and disagrees with the idea that Büyük Menderes Graben is a supradetachment basin mainly controlled by the movement and rotation along the south dipping boundary fault along its northern margin.

The statement above is evidenced by the fault rotation along the seismic profiles from the eastern to the western part of the study area. For instance, in the seismic profiles MUD-99- 208-202 and 204, the synthetic and antithetic faults located on the northern margin of the

graben dip shallower than the southern flank (Figures 24 to 28). The same normal faults rotate more in the western part of the graben along the seismic profiles MUD-99-210,213,214 and 215 located along the southern margin of the graben (Figures 29 to 39). This in turn, suggests that the graben was initiated in the eastern part of the study area under the control of the south dipping boundary fault most likely during the deposition of the early Miocene Bascayir Formation. Then, the north dipping fault became more dominant during the late Miocene Aydin Formation deposition.

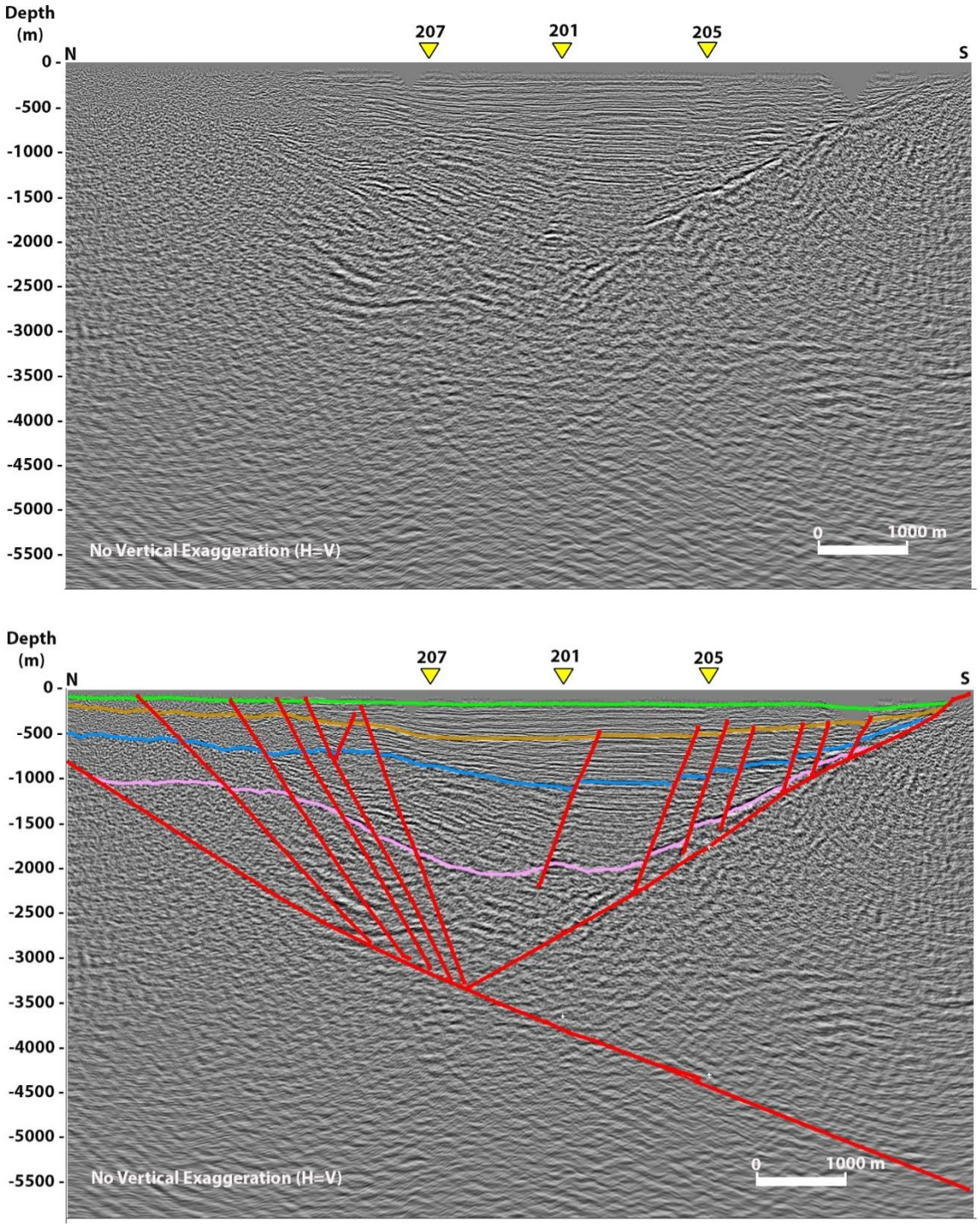

Figure 24- Depth converted uninterpreted and interpreted N-S trending seismic reflection profile, MUD-99-208. The yellow triangles represent cross lines MUD-99-207, 201, and 205. Color codes indicates formation tops (Surface = Hamzali Formation, green = Huseyinciler Formation, orange = Aydin Formation, blue = Bascayir Formation, pink = Basement, red = Normal faults).

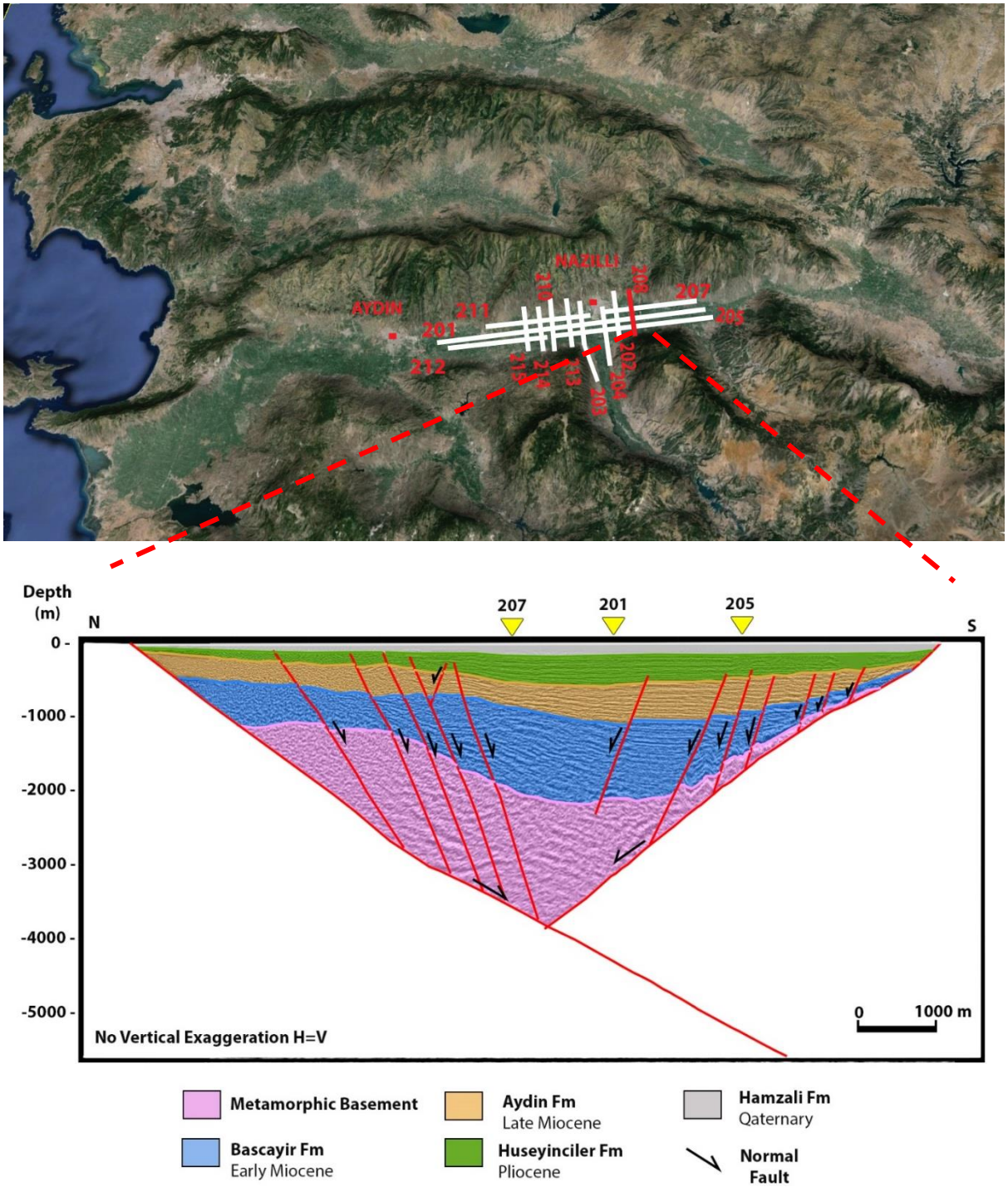

Figure 25- Balanced structural cross-section along the N-S oriented MUD-99-208 seismic reflection profile showing the main boundary faults and their synthetic splays. The yellow triangles represent cross lines MUD-99-207, 201, and 205.

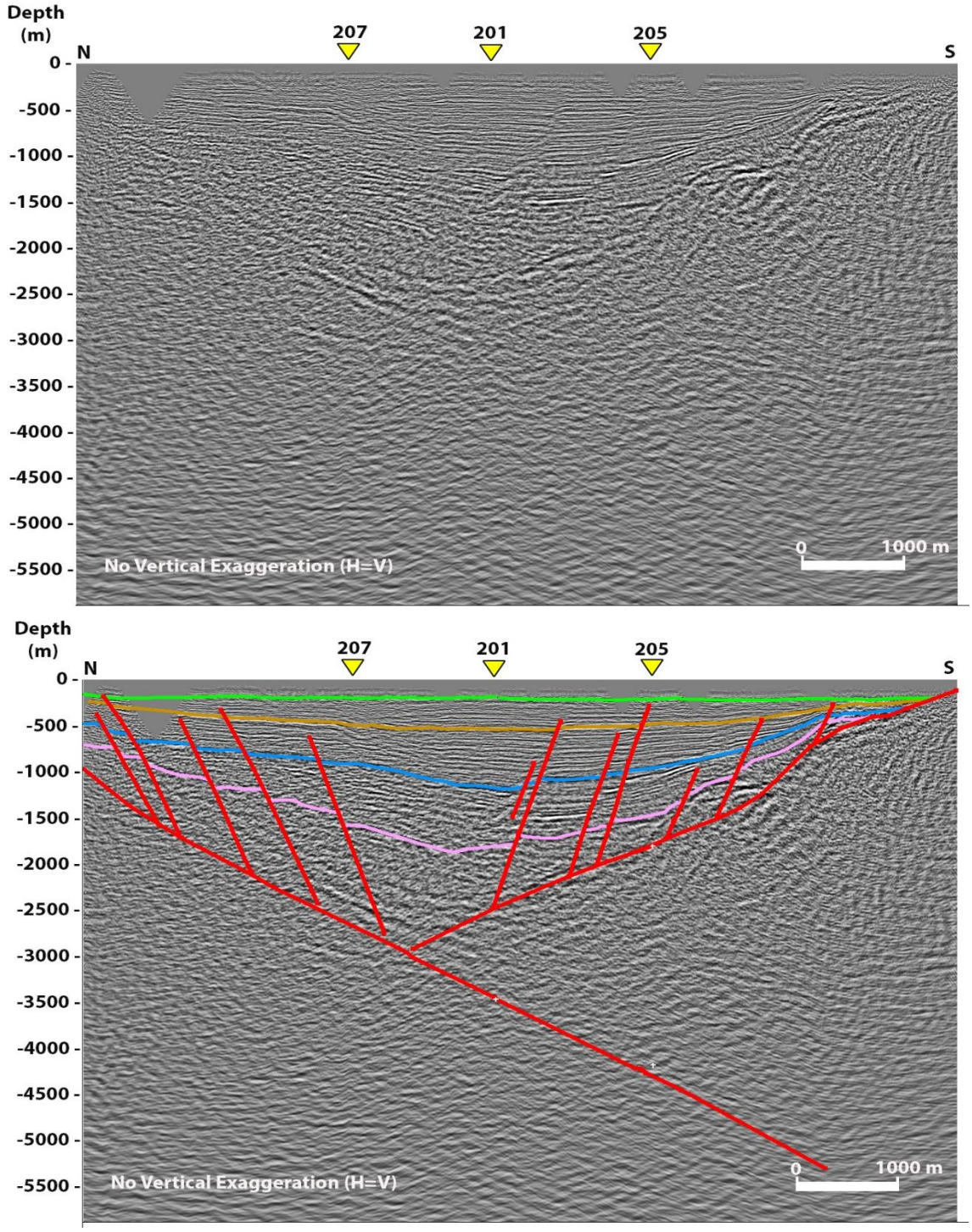

Figure 26- Depth converted uninterpreted and interpreted N-S trending seismic reflection profile, MUD-99-202. The yellow triangles represent cross lines MUD-99-207, 201, and 205. Color codes indicates formation tops (Surface = Hamzali Formation, green = Huseyinciler Formation, orange = Aydin Formation, blue =Bascayir Formation, pink = Basement, red = Normal faults).

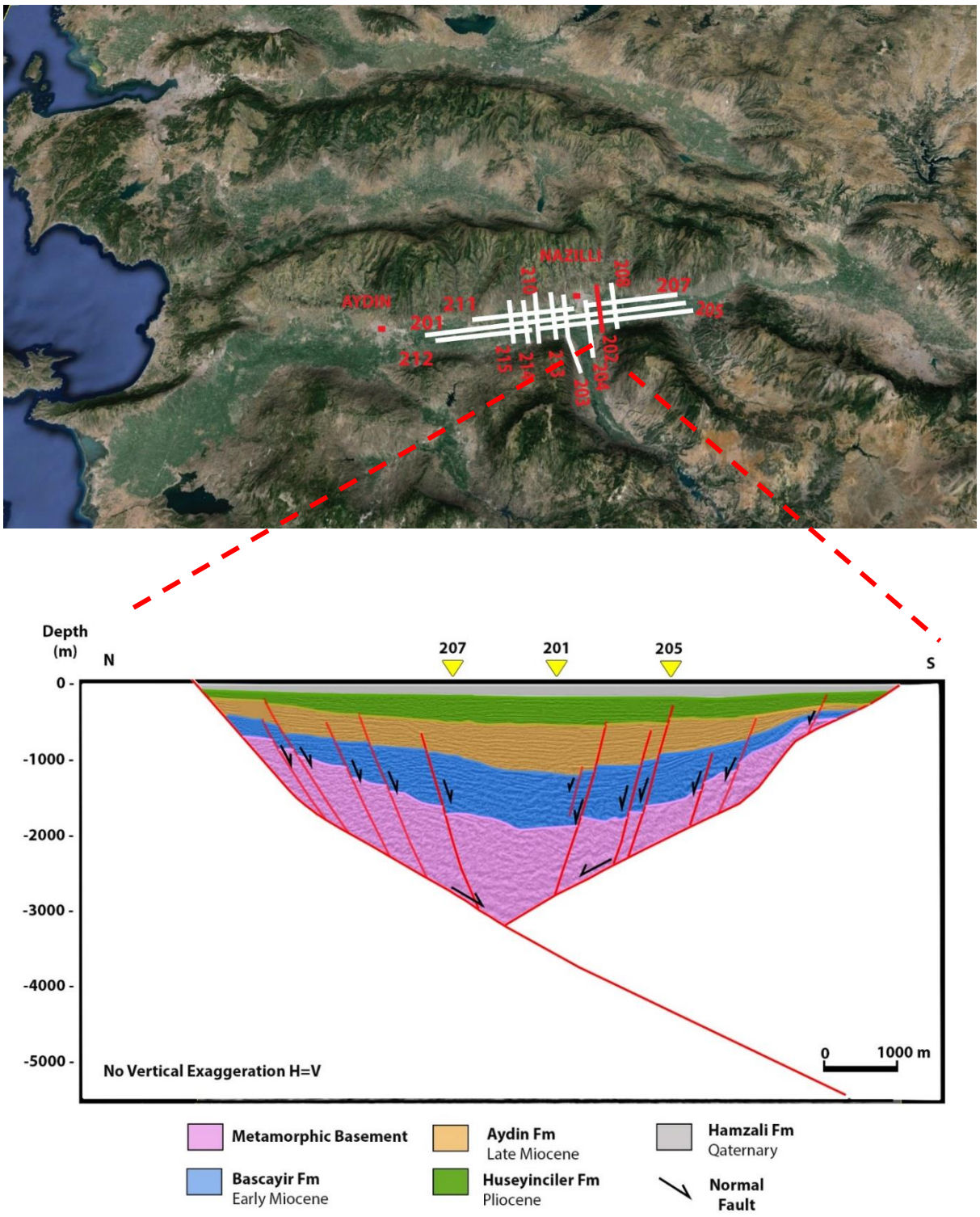

Figure 27- Balanced structural cross-section along the N-S oriented MUD-99-202 seismic reflection profile showing main boundary faults and their synthetic splays. The yellow triangles represent cross lines MUD-99-207,201, and 205.

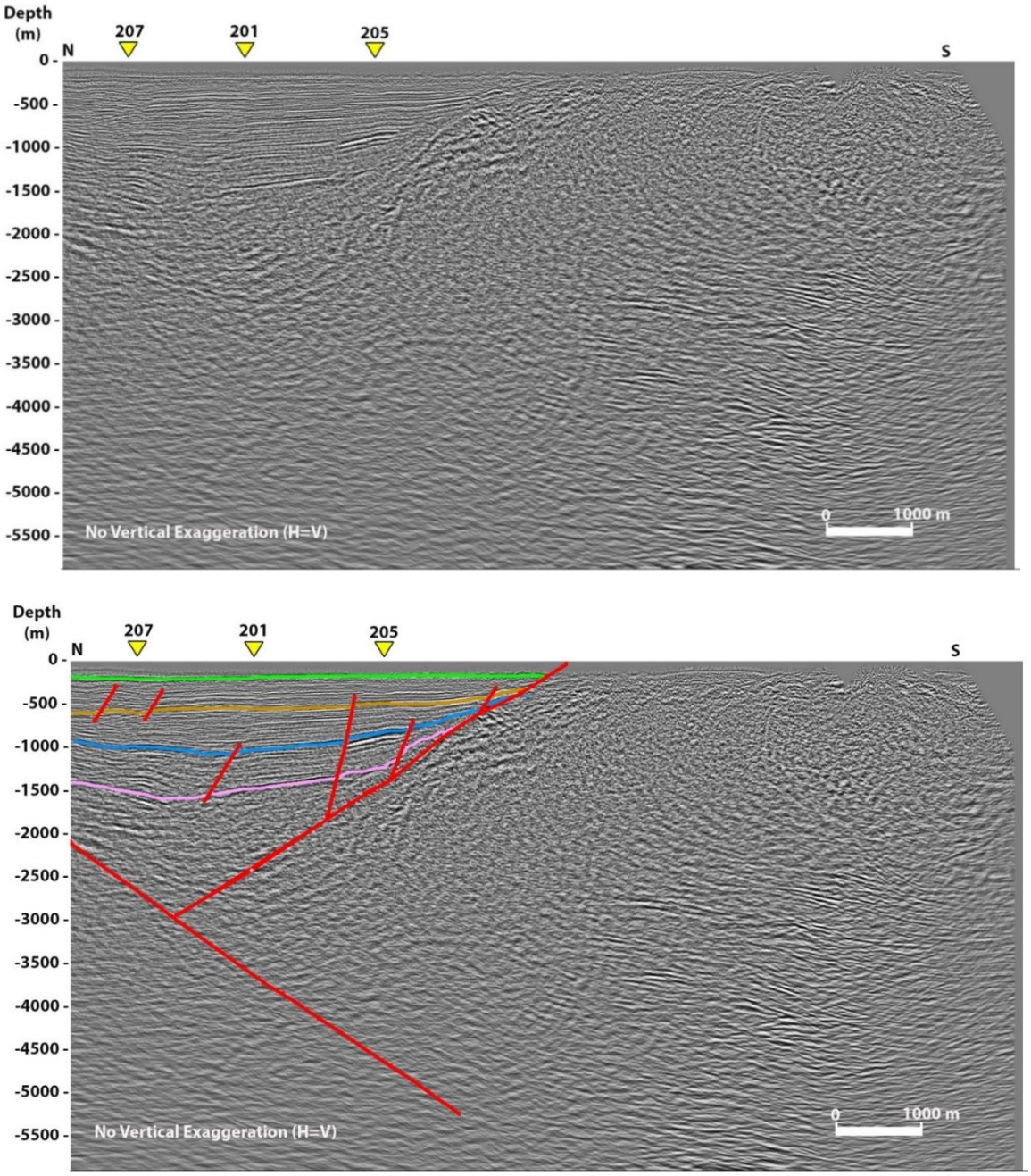

Figure 28- Depth converted uninterpreted and interpreted N-S trending seismic reflection profile, MUD-99-204. The yellow triangles represent cross lines MUD-99-207,201, and 205. Color codes indicates formation tops (Surface = Hamzali Formation, green = Huseyinciler Formation, orange = Aydin Formation, blue =Bascayir Formation, pink = Basement, red = Normal faults).

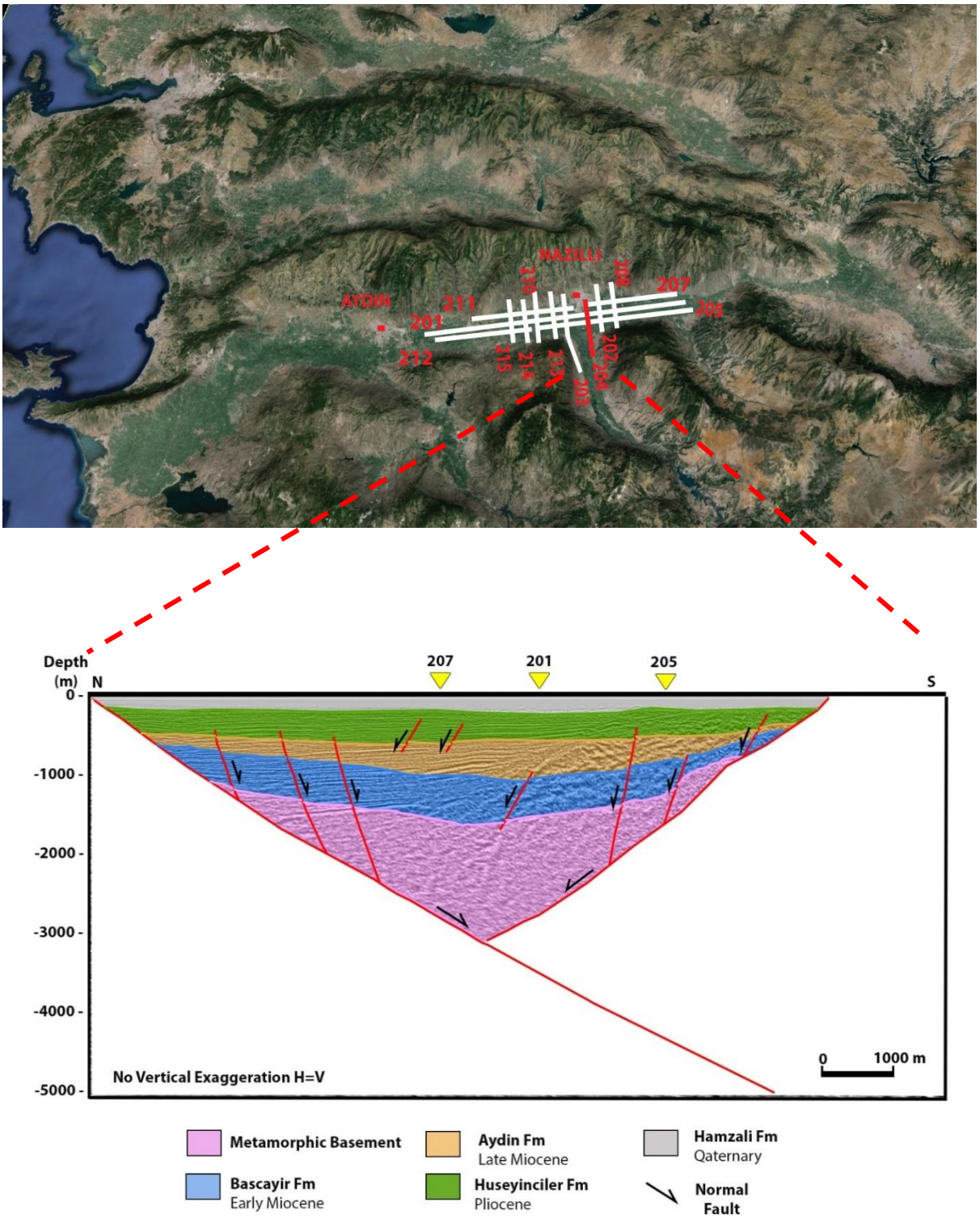

Figure 29- Balanced structural cross-section along the N-S oriented MUD-99-204 seismic reflection profile showing main boundary faults and their synthetic splays. The yellow triangles represent cross lines MUD-99-207,201, and 205.

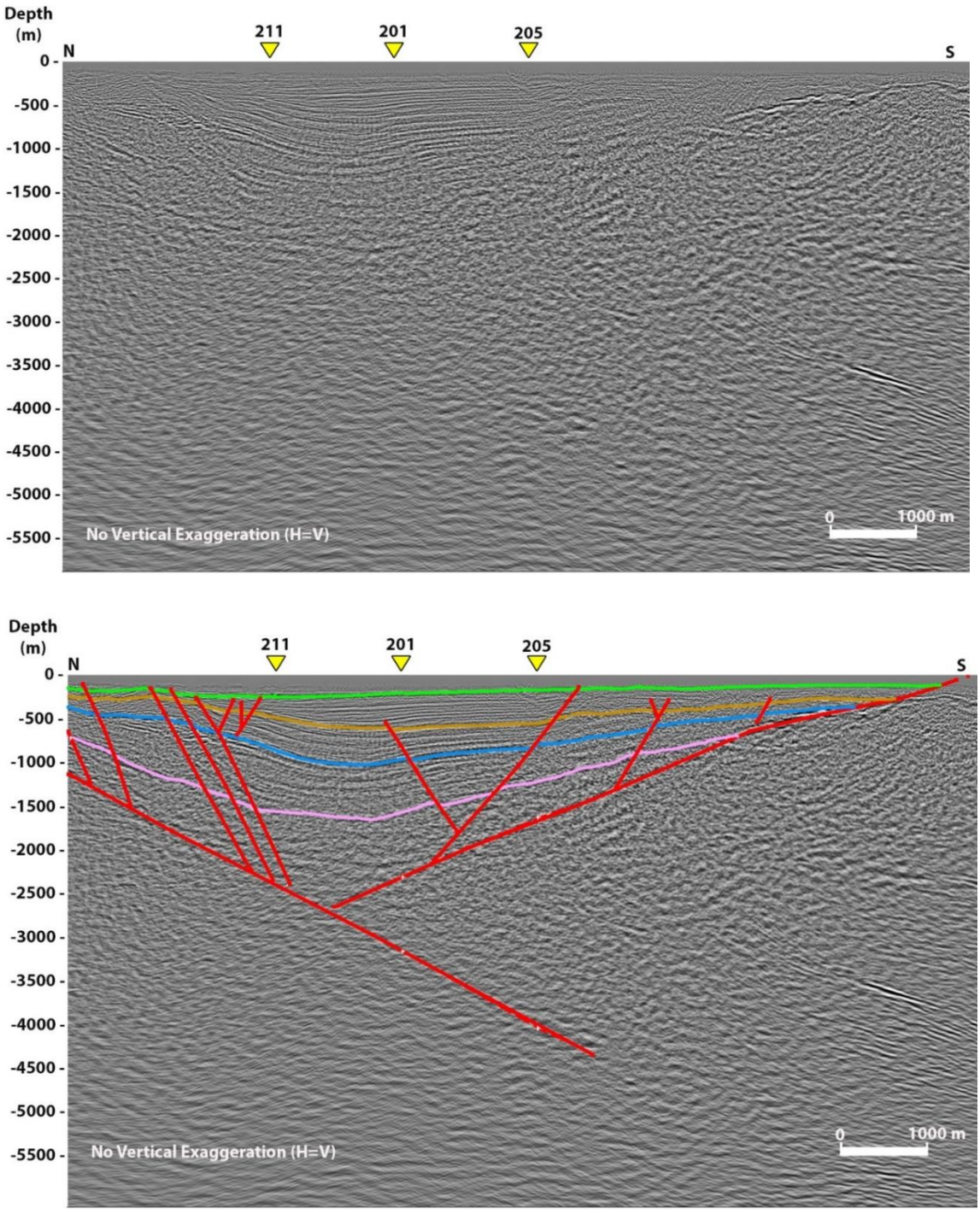

Figure 30- Depth converted uninterpreted and interpreted N-S trending seismic reflection profile, MUD-99-203. The yellow triangles represent cross lines MUD-99-211,201, and 205. Color codes indicates formation tops (Surface = Hamzali Formation, green = Huseyinciler Formation, orange = Aydin Formation, blue = Bascayir Formation, pink = Basement, red = Normal faults).

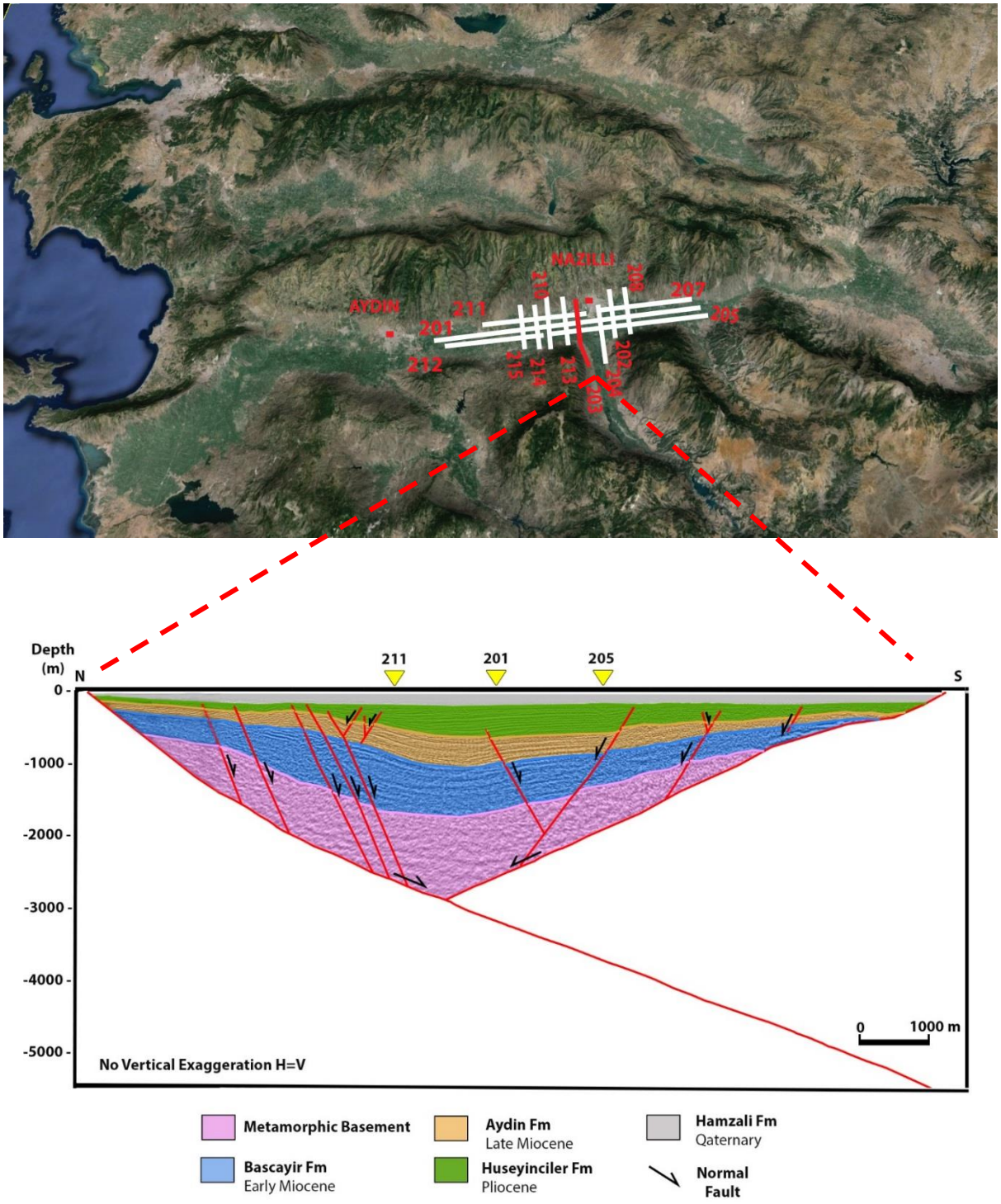

Figure 31- Balanced structural cross-section along the N-S oriented MUD-99-203 seismic reflection profile showing main boundary faults and their synthetic splays. The yellow triangles represent cross lines MUD-99-211,201, and 205.

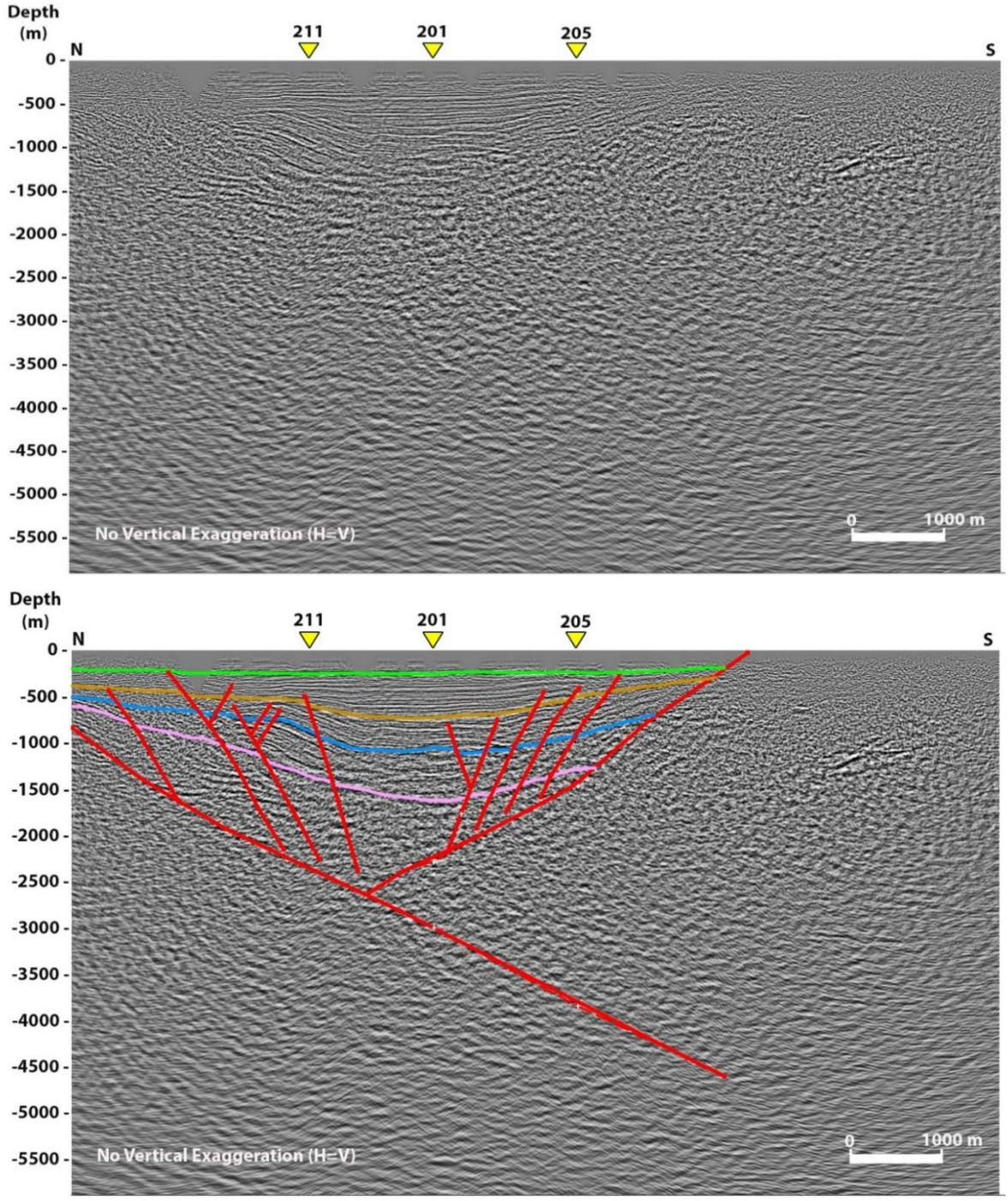

Figure 32- Depth converted uninterpreted and interpreted N-S trending seismic reflection profile, MUD-99-213. The yellow triangles represent cross lines MUD-99-211,201, and 205. Color codes indicates formation tops (Surface= Hamzali Formation, green = Huseyinciler Formation, orange = Aydin Formation, blue = Bascayir Formation, pink = Basement, red = Normal faults).

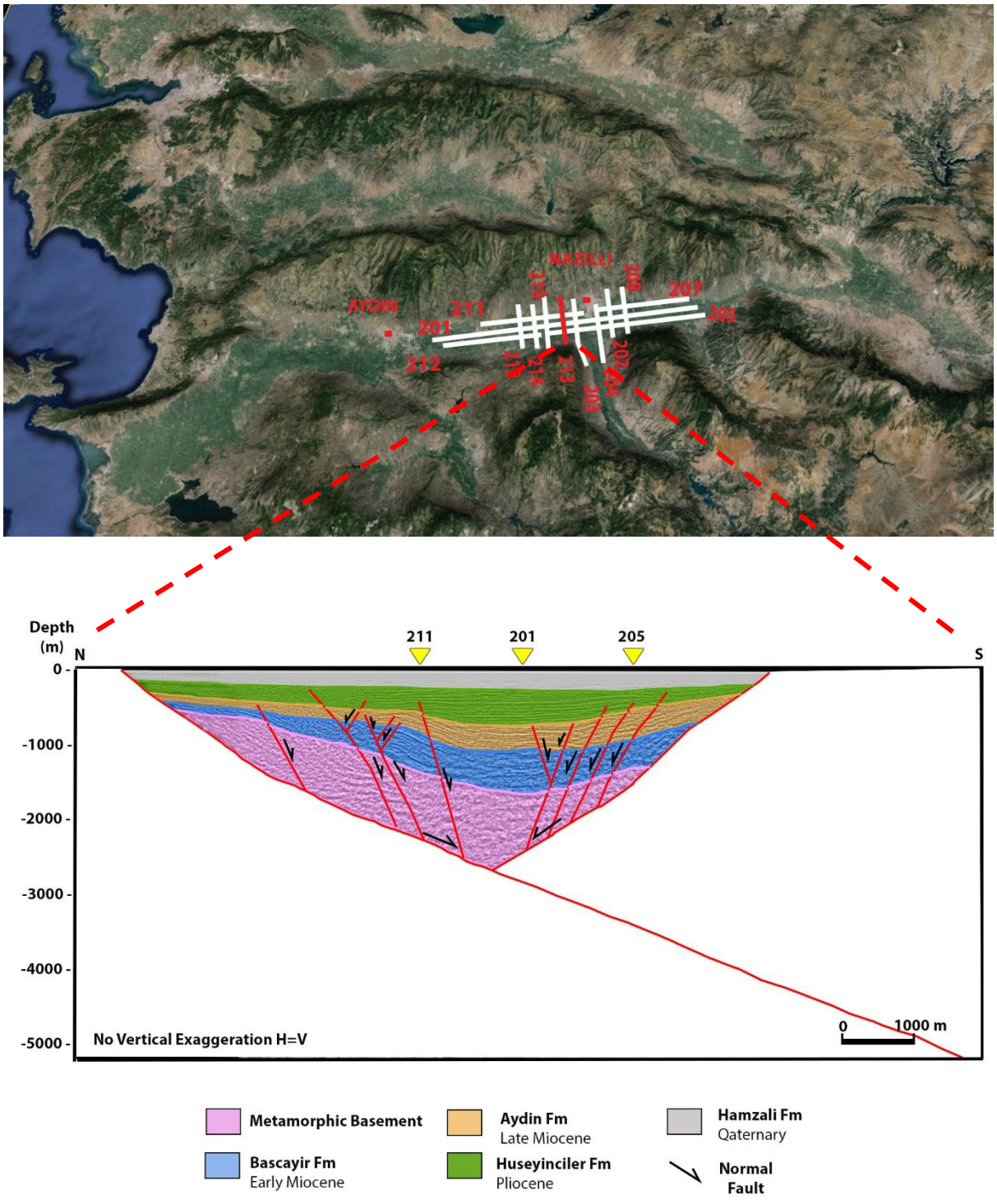

Figure 33- Balanced structural cross-section along the N-S oriented MUD-99-213 seismic reflection profile showing main boundary faults and their synthetic splays. The yellow triangles represent cross lines MUD-99-211,201, and 205.

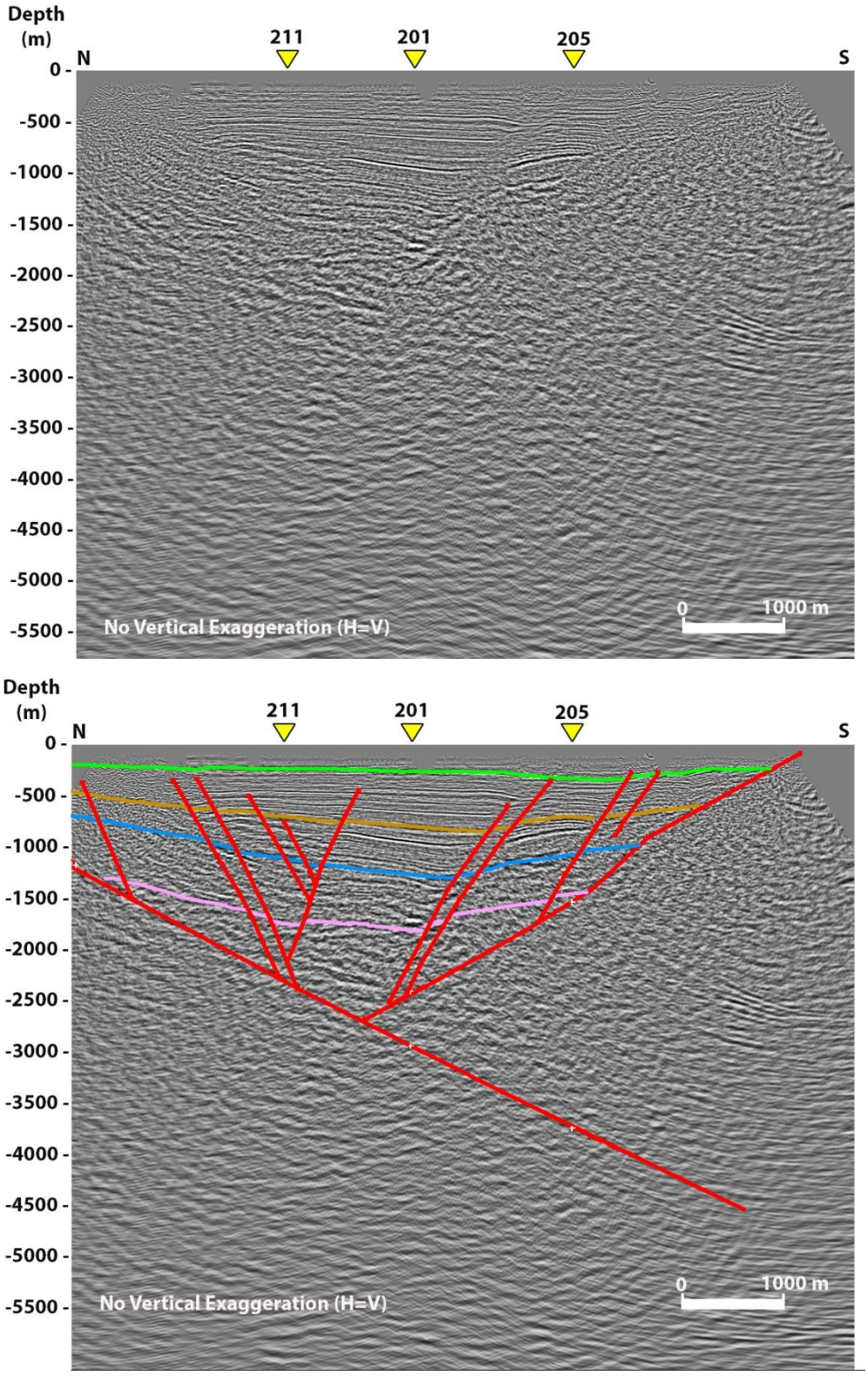

Figure 34- Depth converted uninterpreted and interpreted N-S trending seismic reflection profile, MUD-99-210. The yellow triangles represent cross lines MUD-99-211,201, and 205. Color codes indicates formation tops (Surface= Hamzali Formation, green = Huseyinciler Formation, orange = Aydin Formation, blue = Bascayir Formation, pink = Basement, red = Normal faults).

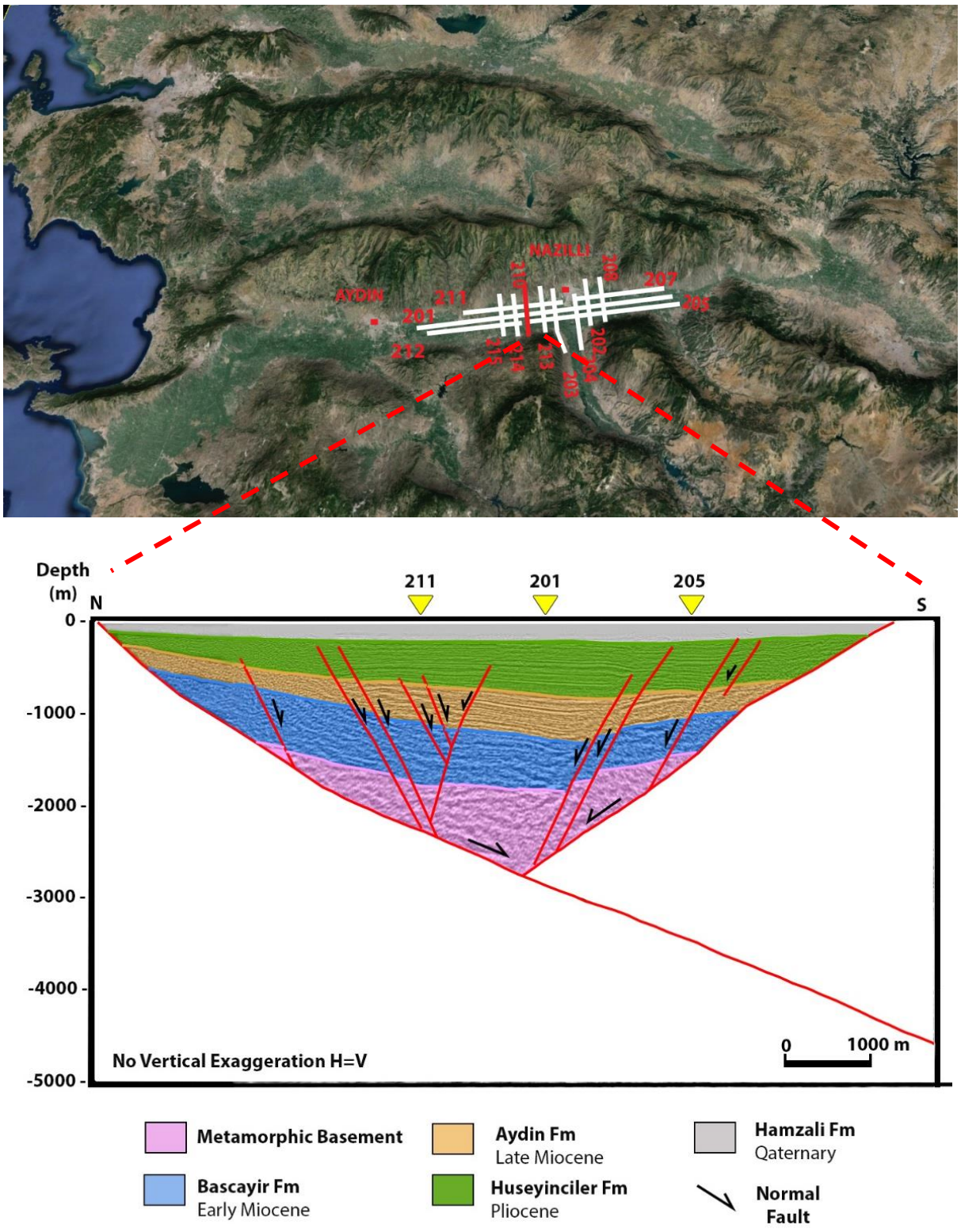

Figure 35- Balanced structural cross-section along the N-S oriented MUD-99-210 seismic reflection profile showing main boundary faults and their synthetic splays. The yellow triangles represent cross lines MUD-99-211,201, and 205.

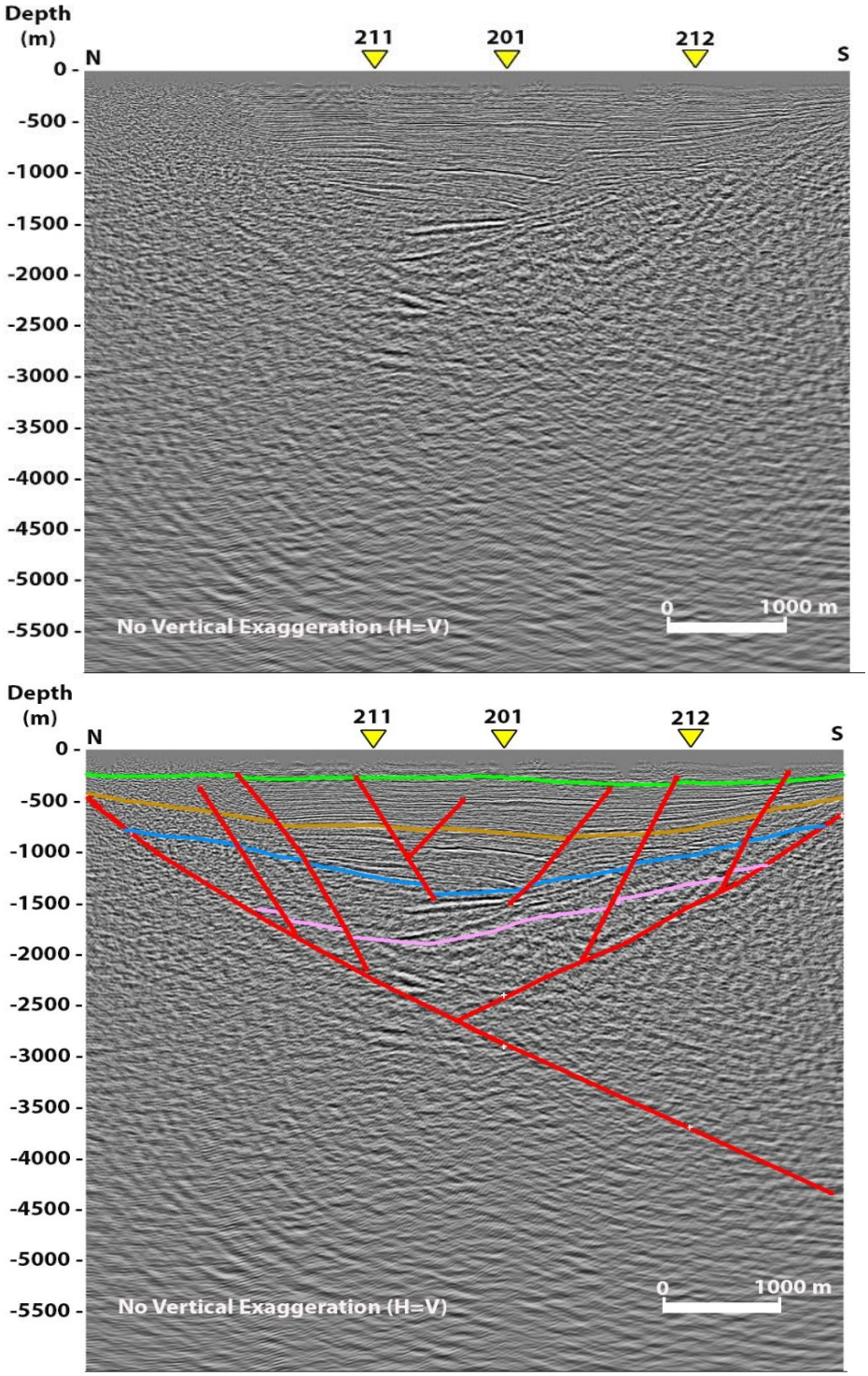

Figure 36- Depth converted uninterpreted and interpreted N-S trending seismic reflection profile, MUD-99-214. The yellow triangles represent cross lines MUD-99-211,201, and 212. Color codes indicates formation tops (Surface = Hamzali Formation, green = Huseyinciler Formation, orange = Aydin Fm, blue = Bascayir Formation, pink = Basement, red = Normal faults).

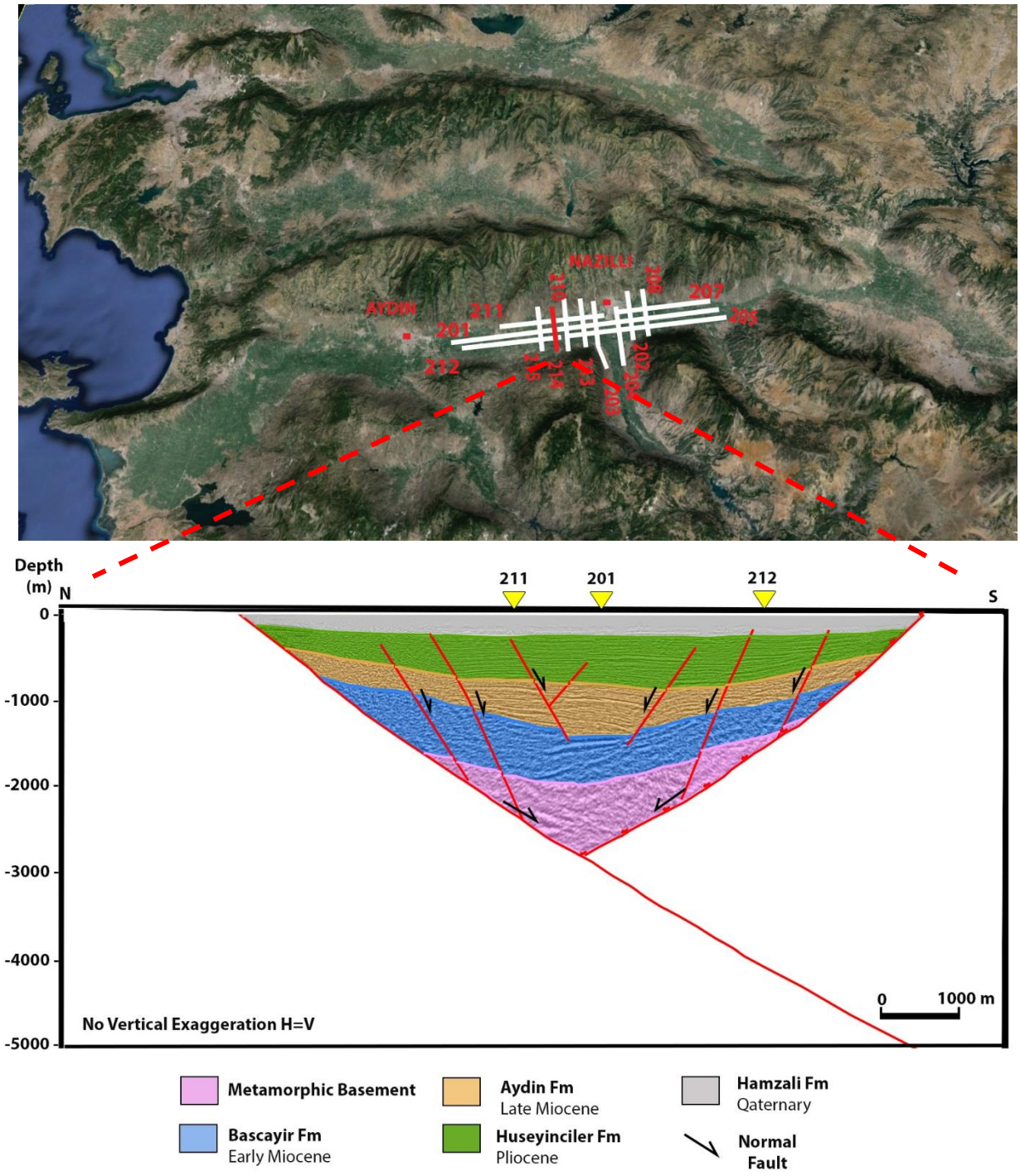

Figure 37- Balanced structural cross-section along the N-S oriented MUD-99-214 seismic reflection profile showing the main boundary faults and their synthetic splays. The yellow triangles represent cross lines MUD-99-211,201, and 212.

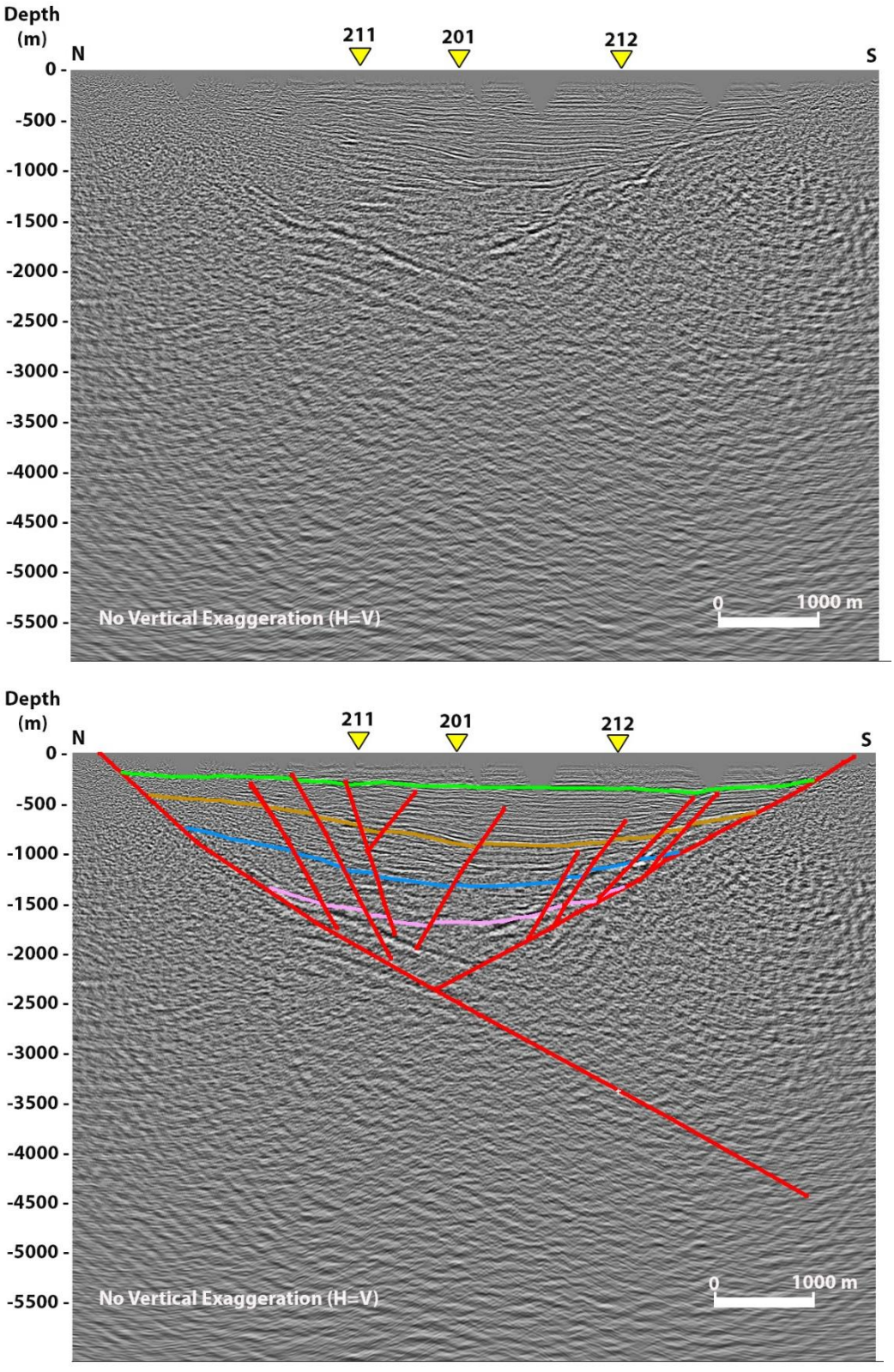

Figure 38- Depth converted uninterpreted and interpreted N-S trending seismic reflection profile, MUD-99-215. The yellow triangles represent cross lines MUD-99-211,201, and 212. Color codes indicates formation tops (Surface = Hamzali Formation, green = Huseyinciler Formation, orange = Aydin Formation, blue = Bascayir Formation, pink = Basement, red = Normal faults).

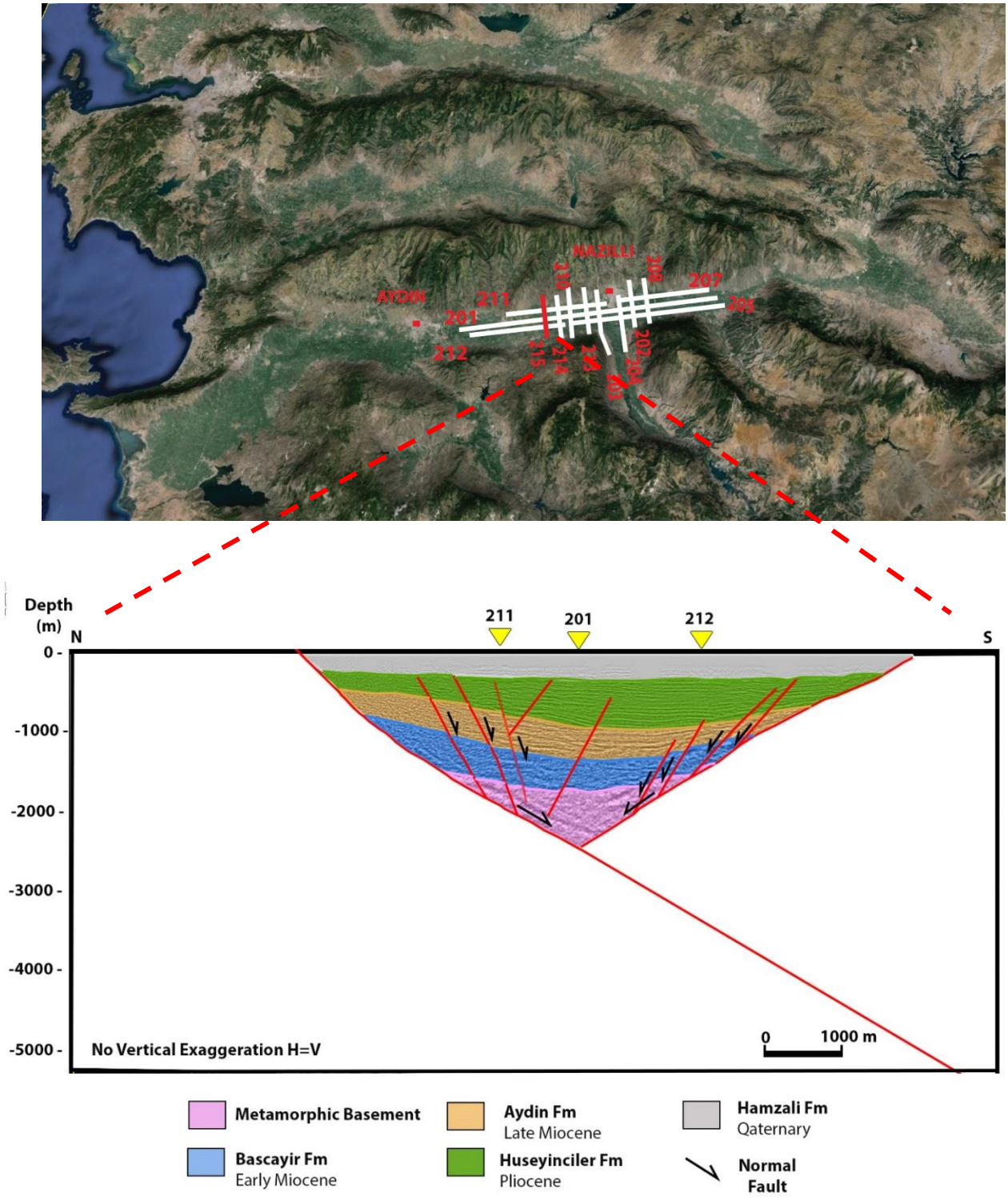

Figure 39- Balanced structural cross-section along the N-S oriented MUD-99-215 seismic reflection profile showing the main boundary faults and their synthetic splays. The yellow triangles represent cross lines MUD-99-211,201, and 212.

The isochore maps created from depth converted seismic lines also back the interpretation above. They illustrate that thickness of the Neogene sedimentary units vary along the graben. The isochore map (Figure 40) showing the distribution of the Miocene sediments (the Aydin and Bascayir formations) along the graben indicates that the thickness of the Miocene sedimentary units reach a maximum of about 1500 meters in the eastern part of the graben and becomes thinner along the northern and southern margins of the graben.

The Miocene thickness decreases gradually to the west along the graben and reaches about 1000 meters, which may indicate that the graben has become shallower towards the west. The westward stratigraphic thinning might also suggests that the period of deposition of the Miocene sediments may be shorter towards the west because the opening of the Büyük Menderes Graben was initiated from the eastern part.

The present time isochore map shown in Figure 41 indicates that the sedimentary thickness is decreasing slightly towards the western part of the study area, except between the seismic profiles MUD-99-203 and MUD-99-204 where the N-S trending Bozdogan Graben is located. The slight thickness change suggests that the graben has had more uniform thickness distribution in the Plio-Pleistocene (post Miocene) time compared to the Miocene time. The post Miocene thickness distribution also suggests that the graben has experienced more Pliocene sedimentation and Quaternary alluvial deposition towards the western part of the study area. This might be caused by the polarity change to the west due to the activity along the north dipping boundary fault at the southern margin of the graben.

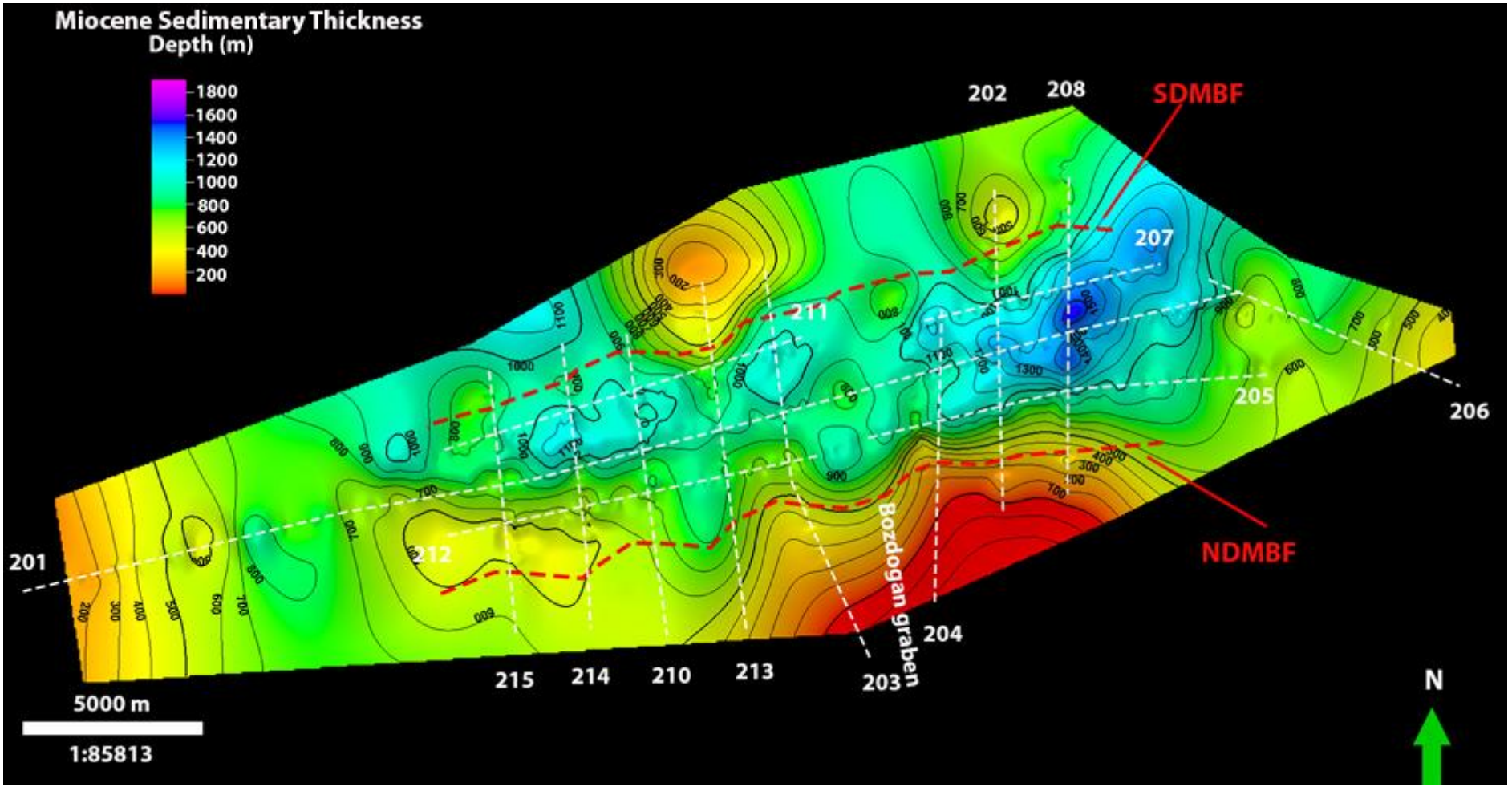

Figure 40- Isochore map showing the Miocene sedimentary (Aydin and Bascayir formations) thickness variation along the Büyük Menderes Graben within the study area. It shows that sediment thickness decreases towards the western part of the study area during the Miocene time. **Abbreviations: SDMBF:** The south dipping main boundary fault**; NDMBF:** The north dipping main boundary fault.

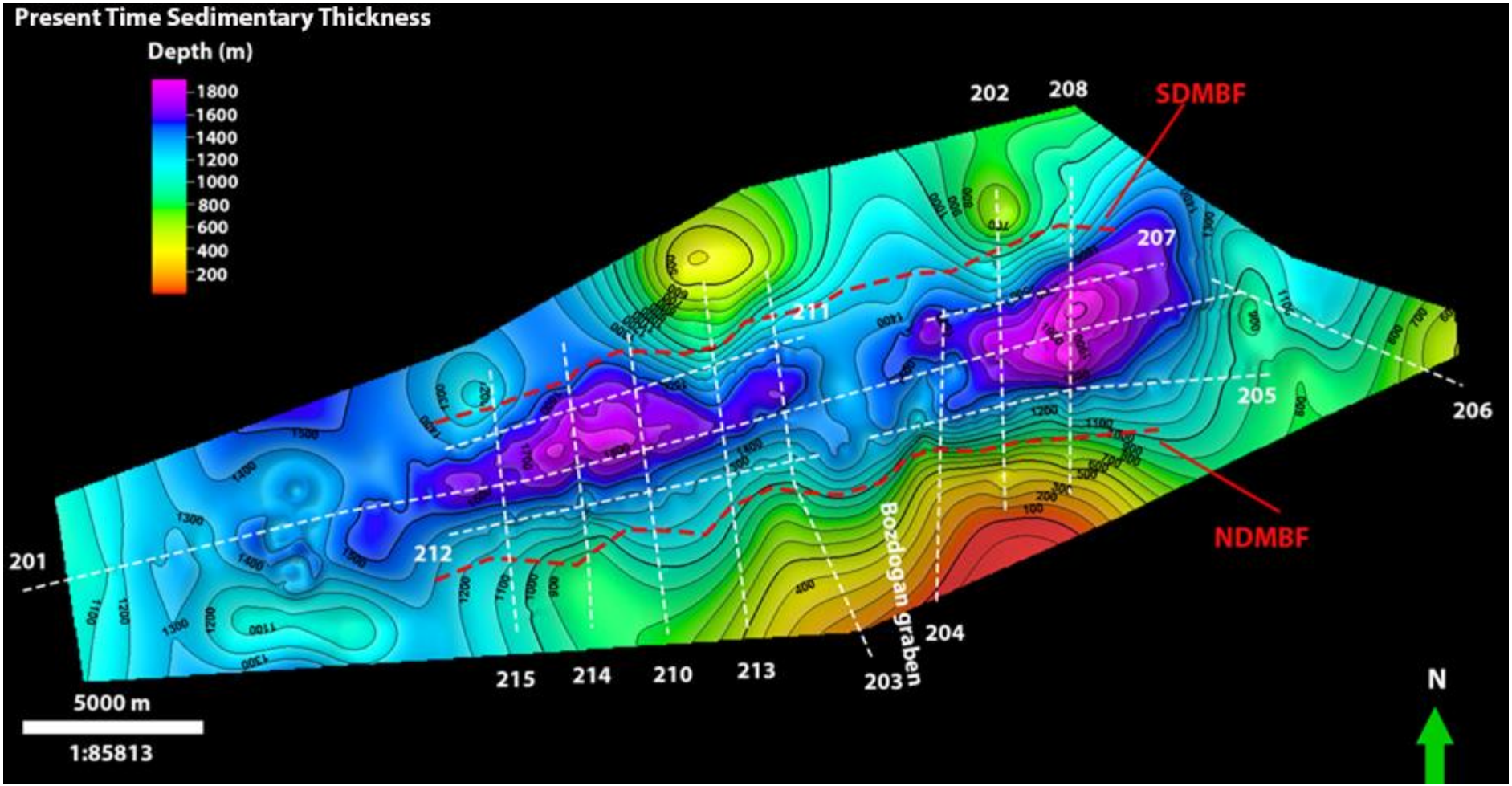

Figure 41- Isochore map showing present time sedimentary thickness variation along the graben. It shows that the sediment thickness distribution is almost symmetrical along the graben within the study area after the Miocene time. **Abbreviations: SDMBF:** The south dipping main boundary fault**; NDMBF:** The north dipping main boundary fault.

4.2.2.2 E-W Trending Seismic Profiles

The seismic reflection profiles MUD-99-201, 205, 207, 211 and 212 trend approximately E-W perpendicular to the extension direction in the region. The profile MUD-99-201 is the longest E-W trending profile (~21 km) that intersects all of the N-S trending profiles and proceeds along the central part of the graben within the study area. Interpretation of the depth converted MUD-99-201 (Figures 42 and 43) illustrates the thickness variation of the Neogene sedimentary units over the basement rocks from east to the west. The profile also shows that the base of the Neogene sedimentary units becomes deeper in the eastern part (until the profile MUD-99-204) where the Neogene sedimentary units reach maximum thickness of ~2000 meters along the seismic profile MUD-99-208. This thickness decreases towards the profile MUD-99-203 and reaches to ~1500 meters where an intrabasinal high is located and again reaches ~1800 meters to the west of the intrabasinal high (Figures 42 and 43).

The seismic profile MUD-99-201 shows that the intrabasinal high between the N-S trending profiles MUD-99-203 and 204 separates the graben into two depocentres where the Neogene sedimentary thickness variations occur. Between the seismic profiles MUD-99-213 and 204, the Neogene sedimentary units reach their minimum thickness of approximately 1200 meters, and sedimentary section shows anticlinal and synclinal geometries that are deformed by normal faults. Towards the western part of the study area (profile MUD-99-215), the Neogene sedimentary thickness increases to ~1800 meters with onlapping on the basement rocks (Figures 42 and 43). The profile MUD-99-201 shows that the Miocene sediments (the Bascayir and Aydin formations) have non-uniform thickness variation from east to the west while thickness of the Plio-Pleistocene sediments (the Pliocene Huseyinciler and Quaternary Hamzali formations) have a consistent thickness variation with gradual increase towards the west (Figures 42 and 43).

Along the seismic profiles MUD-99-207, 211, 205, and 212 (Figures 44 to 51) located at the northernmost and southernmost parts of the graben, the lateral Neogene sedimentary thickness distribution shows similarity with the center of the graben along the seismic line MUD-99-201 (Figures 42 and 43). However, it has been observed that the sedimentary rocks are thicker in the northern part of the graben than the southern part as shown in the isochore map, probably because the northern margin of the graben may have developed earlier than southern margin.

Along the seismic profiles MUD-99-205 and 212 (Figures 48 to 51), the north dipping boundary fault intersects the Neogene sedimentary rocks and the basement rocks at depths ranging from 1100 to 2000 meters and deepens towards the west due to deepening of the base of the Neogene sedimentary rocks along the southern margin of the graben (Figures 48 to 51). The south dipping boundary fault along these seismic lines reaches ~4000 meters at the eastern part, getting shallower towards the west with ~3500 meters. Also, the same geometry for the south dipping boundary fault can be seen at the southern margin of the graben along the seismic profiles MUD-99-207 and 211 (Figures 44 to 47).

The geometry explained above suggests that the graben may have rotated towards southwest along the southern margin of the graben possibly due to counterclockwise rotation of western Turkey. This rotation might have caused the activation of the north dipping boundary fault during the deposition of the late Miocene Aydin Formation.

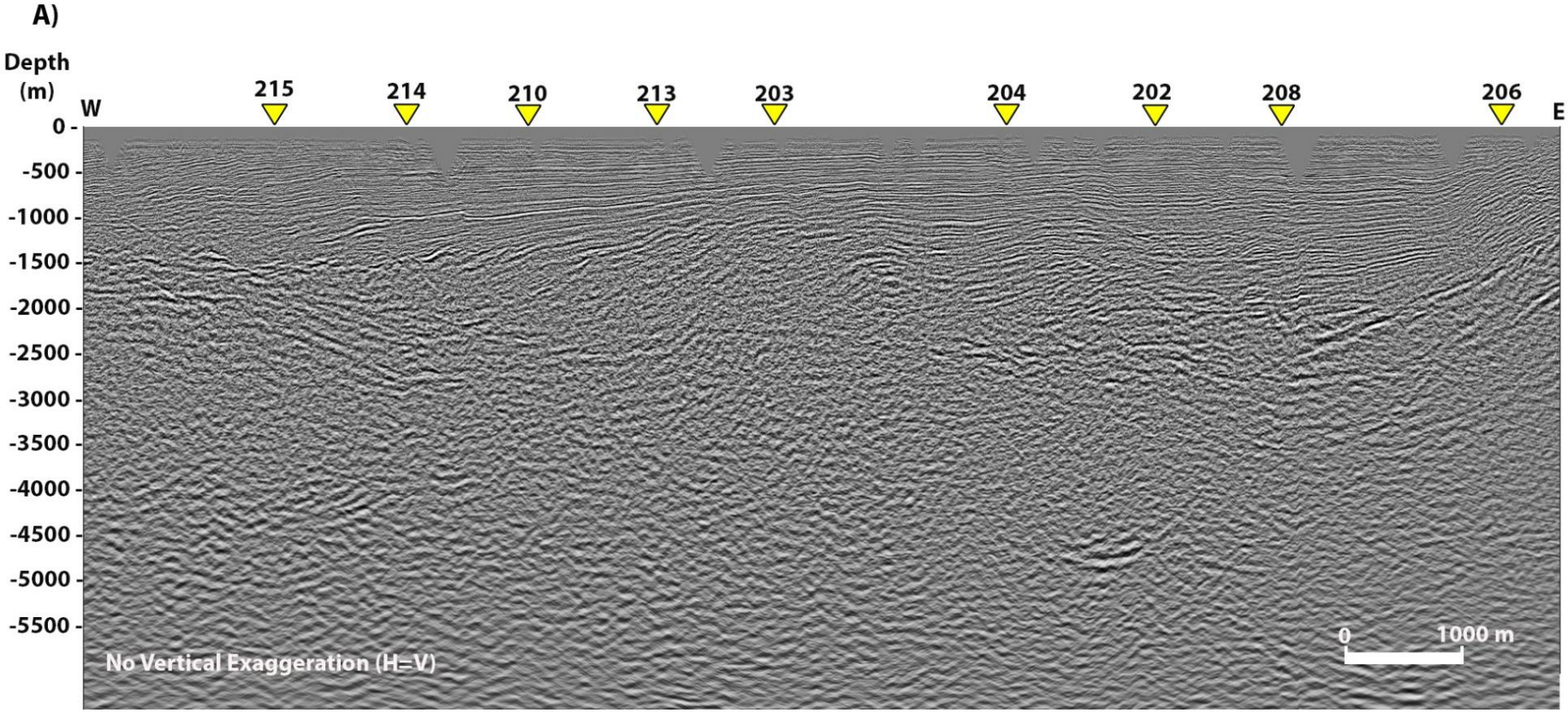
A)
Depth
(m)
W
215
214
210
213
203
204
202
208
206
E
0
-500
-1000
-1500
-2000
-2500
-3000
-3500
-4000
-4500
-5000
-5500
No Vertical Exaggeration (H=V)
0
1000 m

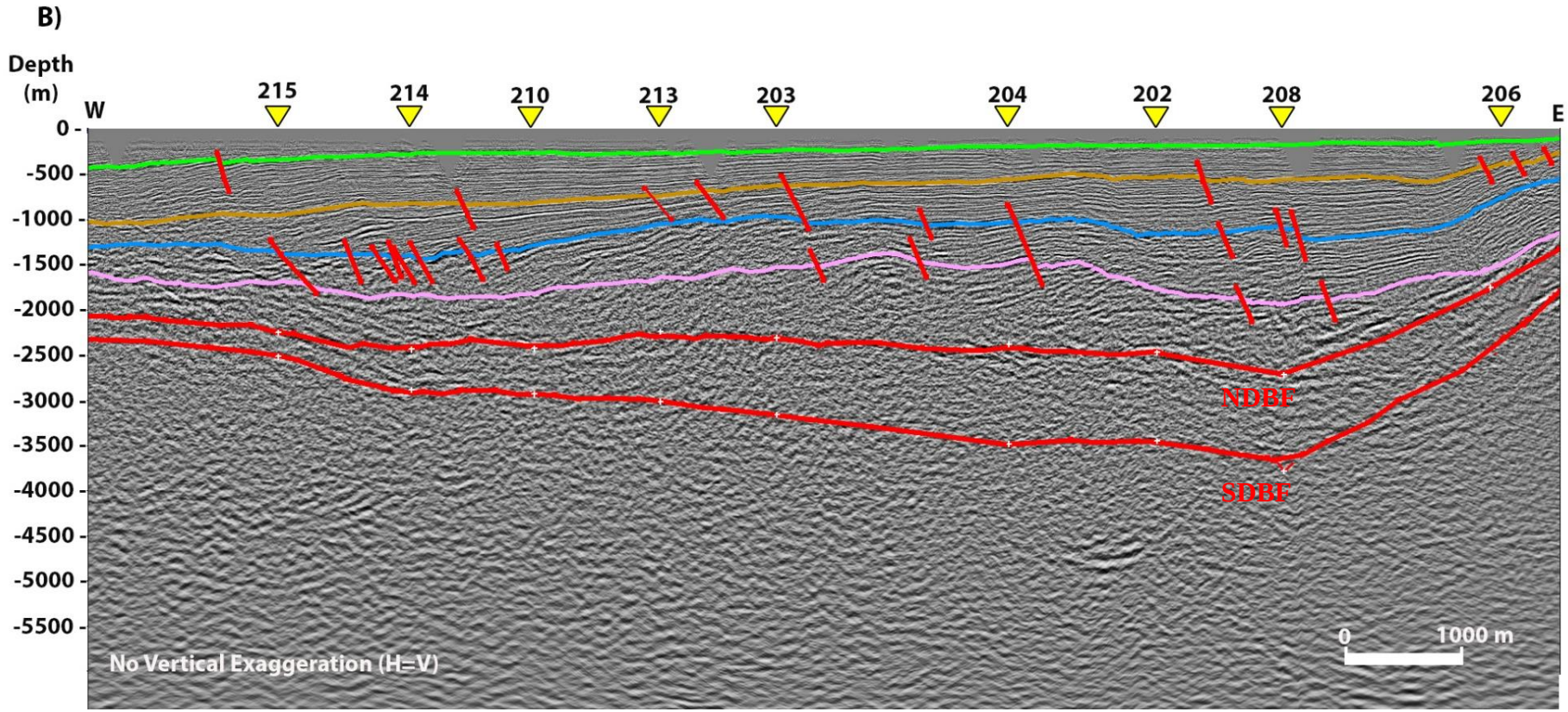

Figure 42- Depth converted uninterpreted **(A)** and interpreted **(B)** E-W trending seismic reflection profile, MUD-99-201.The yellow triangles represent cross lines MUD-99-215,214,210,213,203,204,202 and 208. Color codes indicates formation tops (Surface= Hamzali Formation, green= Huseyinciler Formation, orange = Aydin Formation, blue = Bascayir Formation, pink =Basement, red = Normal faults, NDBF: North Dipping Boundary Fault, SDBF: South Dipping Boundary Fault).

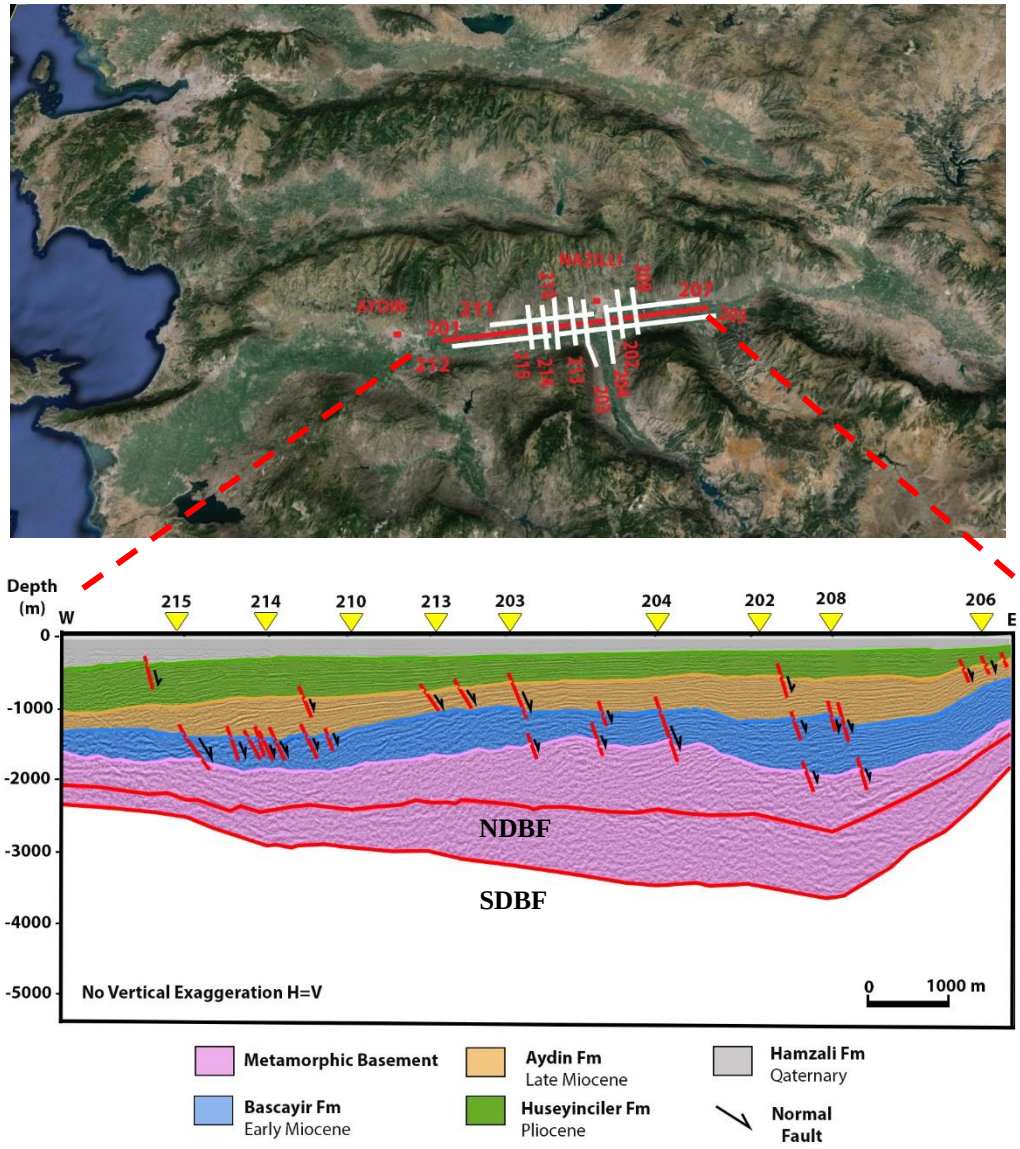

Figure 43- Structural cross-section along the E-W oriented MUD-99-201 seismic reflection profile showing lateral thickness variation and orientation of normal faults. The yellow triangles represent cross lines MUD-99-215,214,210,213,203,204,202 and 208 (NDBF: North Dipping Boundary Fault, SDBF: South Dipping Boundary Fault).

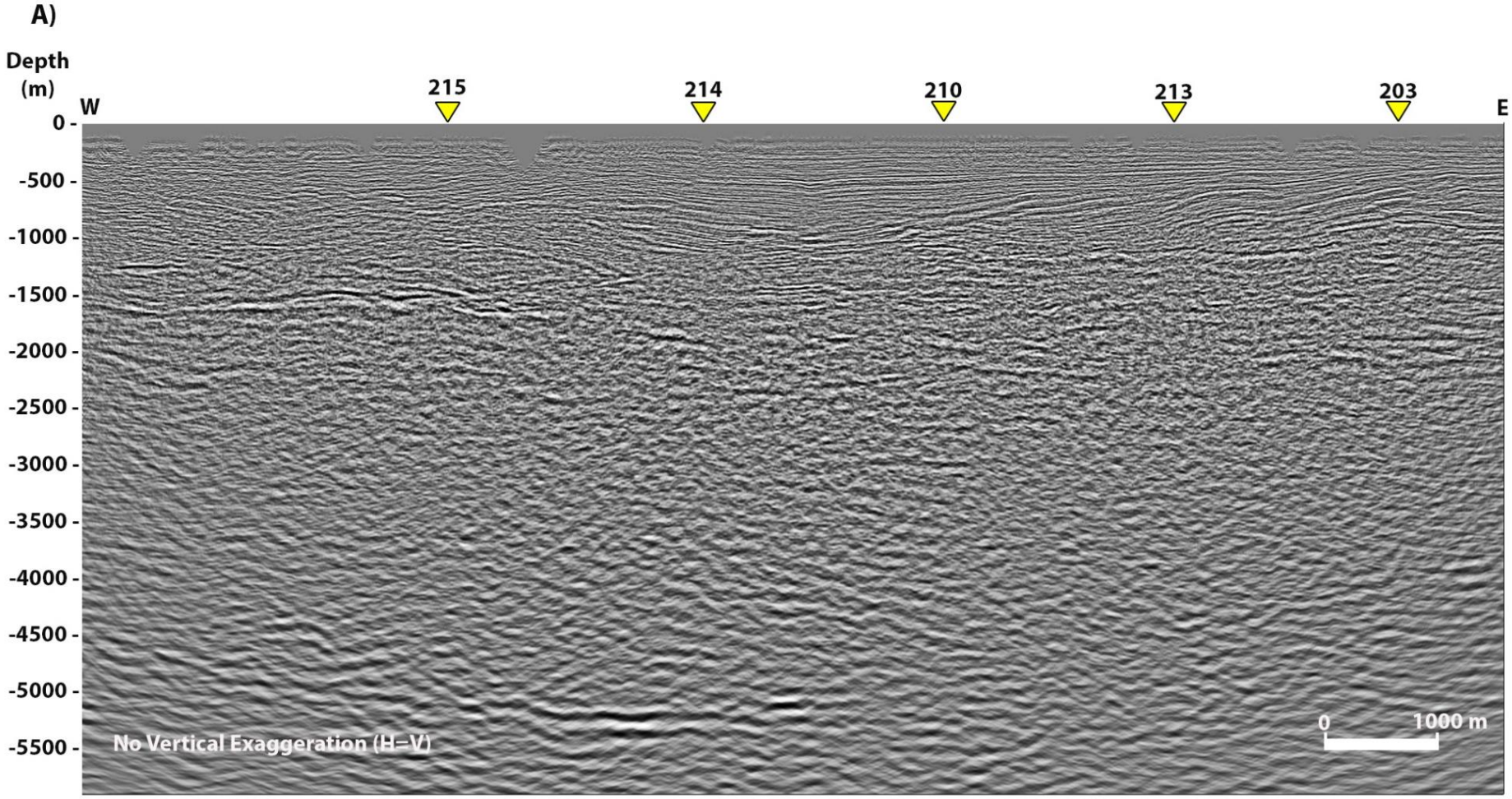
A)
Depth
(m)
W
215
214
210
213
203
E
0 -
-500 -
-1000 -
-1500 -
-2000 -
-2500 -
-3000 -
-3500 -
-4000 -
-4500 -
-5000 -
-5500 -
No Vertical Exaggeration (H=V)
0
1000 m

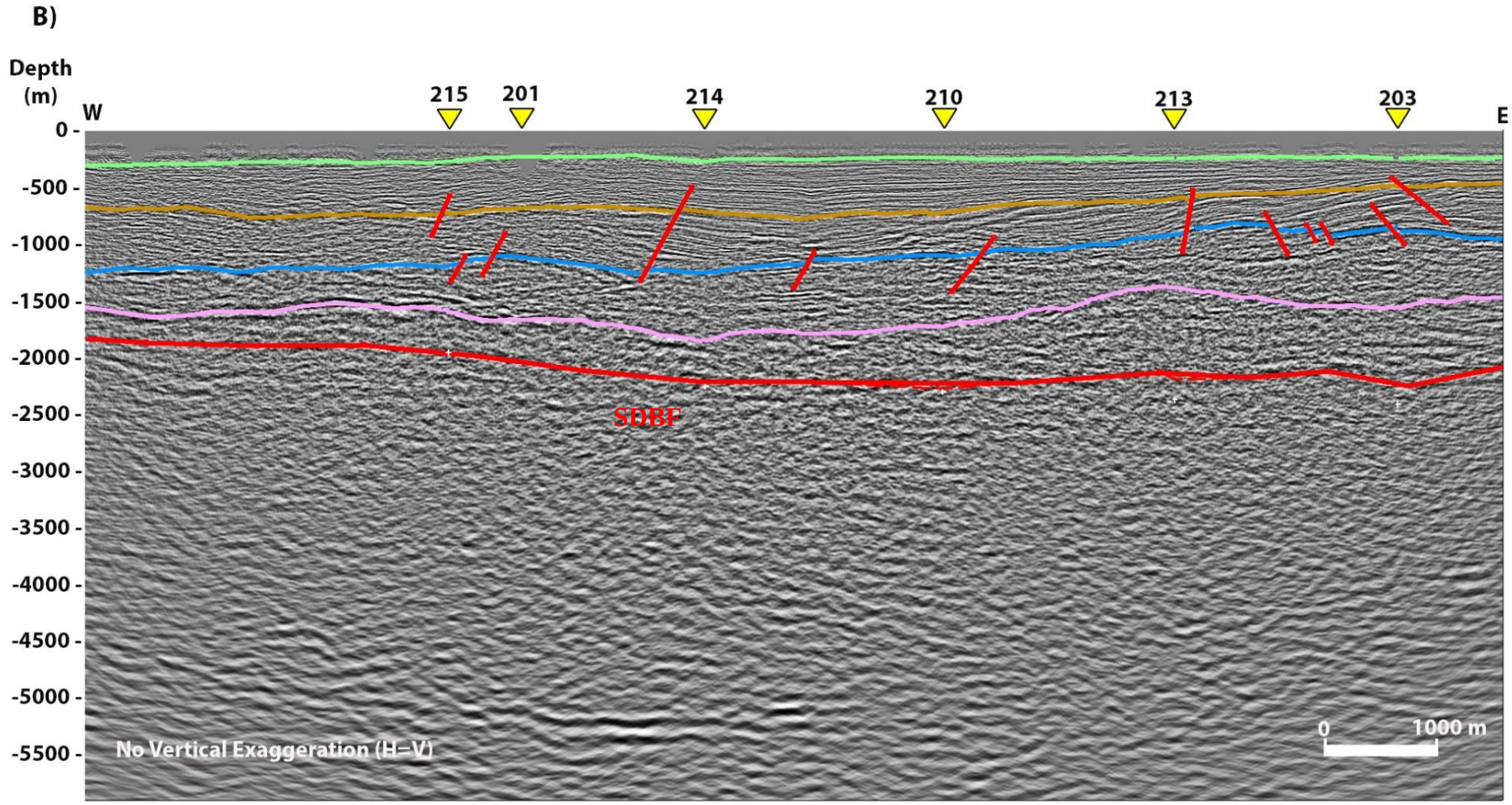

Figure 44- Depth converted uninterpreted **(A)** and interpreted **(B)** E-W trending seismic reflection profile, MUD-99-211. The yellow triangles represent cross lines MUD-99-215,214,210,213,203,204,202 and 208. Color codes indicates formation tops (Surface= Hamzali Formation, green = Huseyinciler Formation, orange = Aydin Formation, blue = Bascayir Formation, pink = Basement, red = Normal faults, SDBF: South Dipping Boundary Fault).

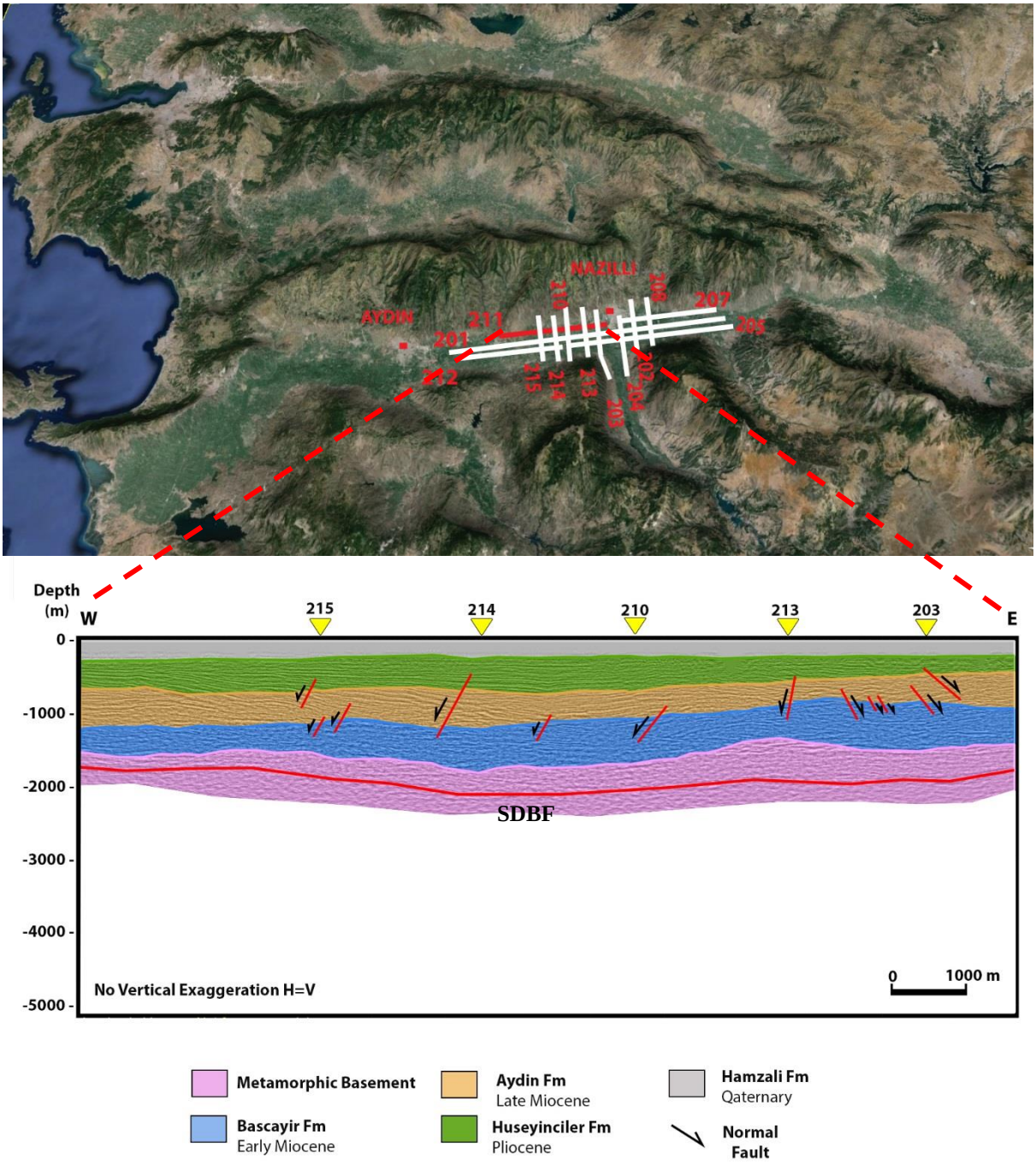

Figure 45- Structural cross-section along E-W oriented MUD-99-211 seismic reflection profile. The yellow triangles represent cross lines MUD-99-215,214,210,213,203,204,202 and 208 (SDBF: South Dipping Boundary Fault).

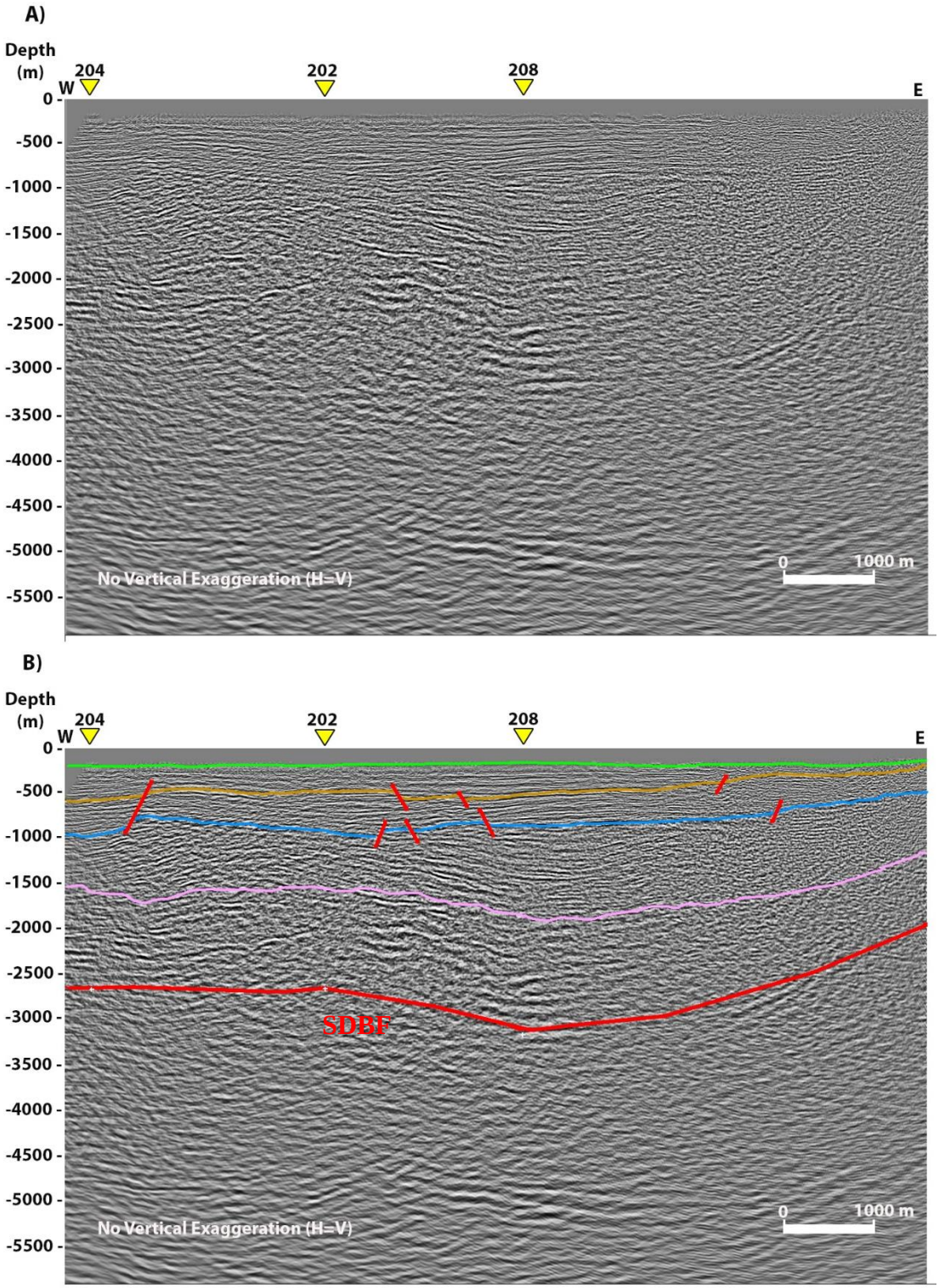

Figure 46- Depth converted uninterpreted and interpreted E-W trending seismic reflection profile, MUD-99-207. The yellow triangles represent cross lines MUD-99-204,202 and 208. Color codes indicates formation tops (Surface = Hamzali Formation, green = Huseyinciler Formation, orange = Aydin Fm, blue = Bascayir Formation, pink = Basement, red = Normal faults, SDBF: South Dipping Boundary Fault).

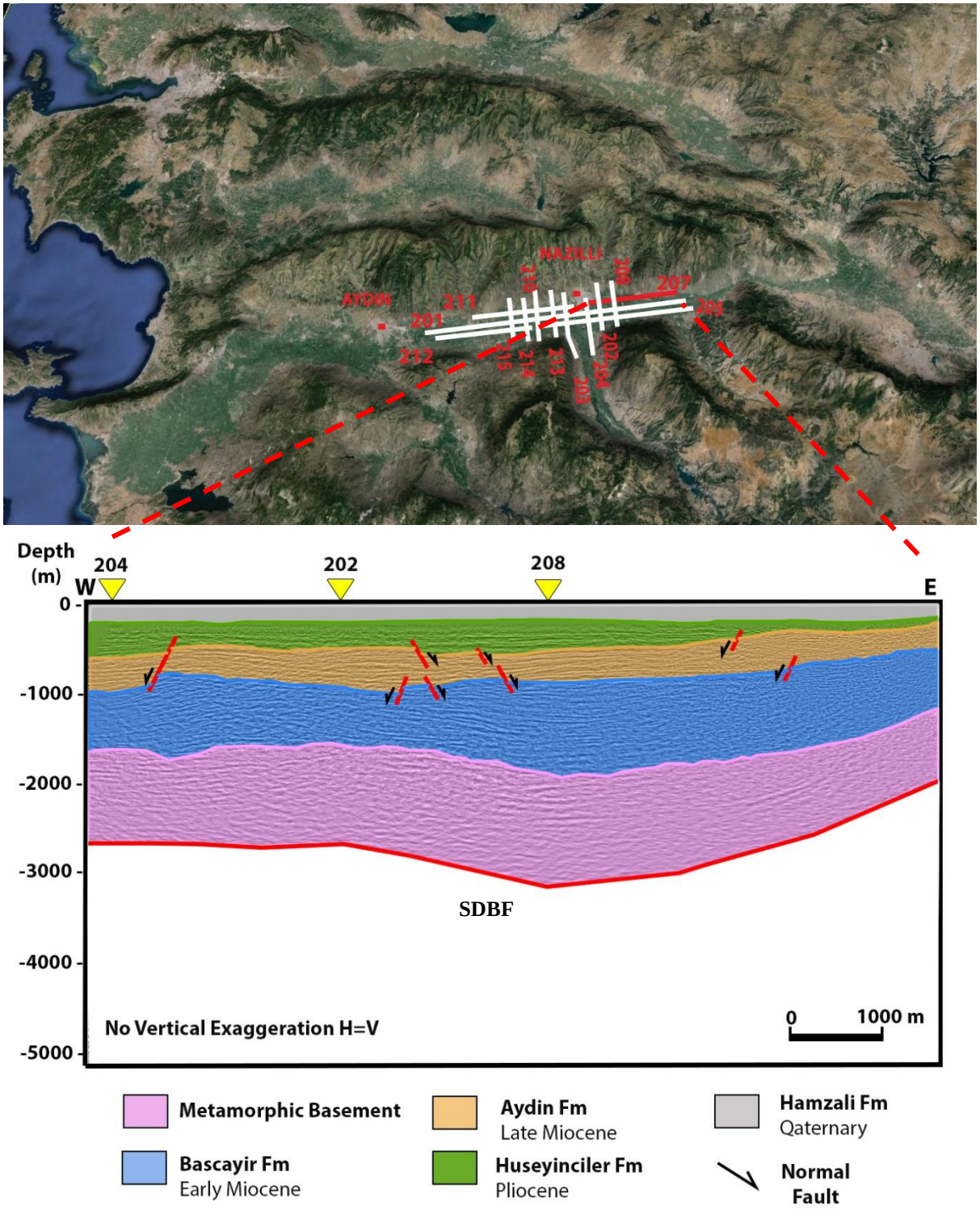

Figure 47- Structural cross-section along E-W oriented MUD-99-207 seismic reflection profile. The yellow triangles represent cross lines MUD-99-204,202 and 208 (SDBF: South Dipping Boundary Fault).

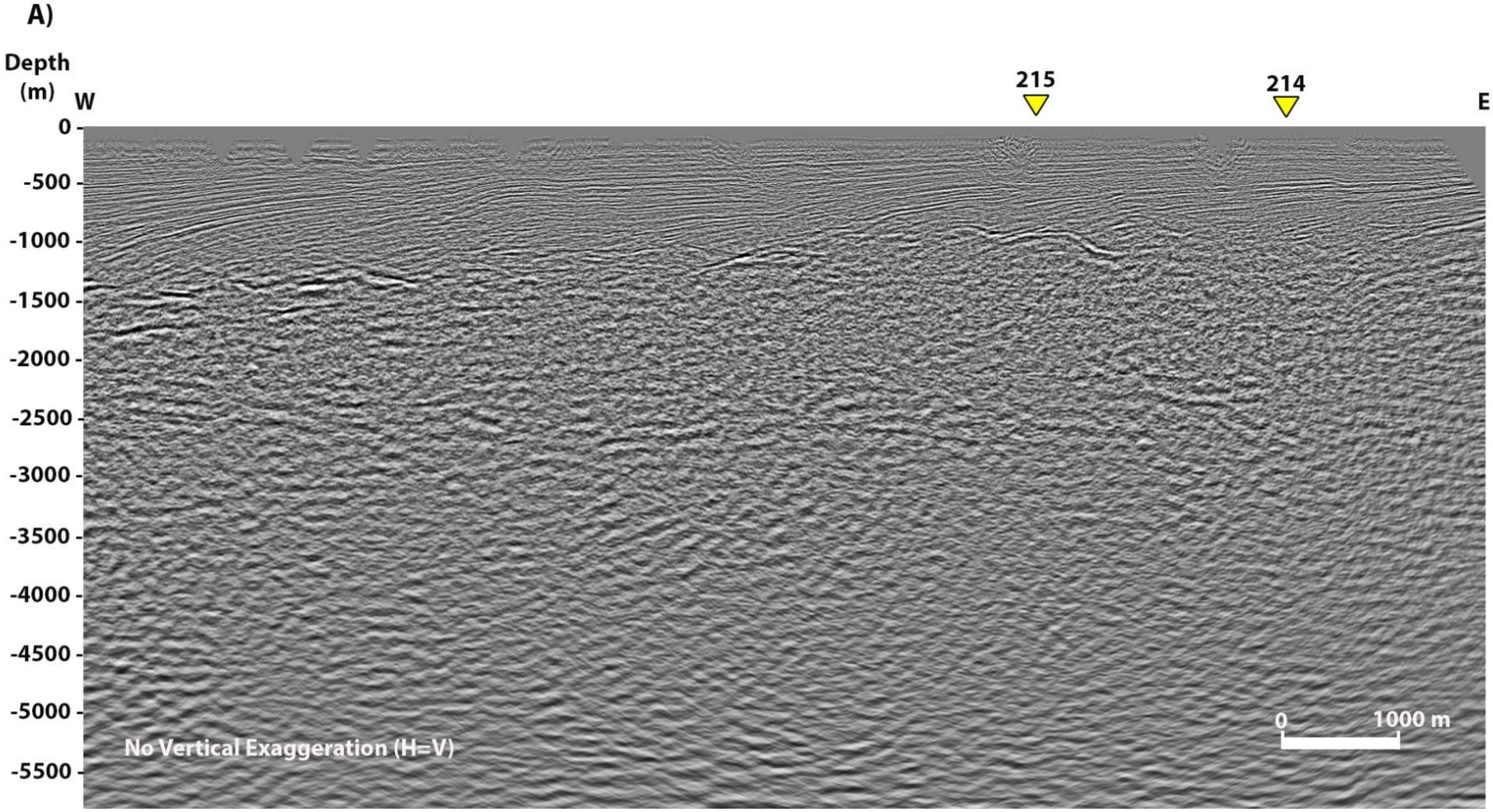
A)
Depth
(m)
W
215
214
E
0
-500
-1000
-1500
-2000
-2500
-3000
-3500
-4000
-4500
-5000
-5500
No Vertical Exaggeration (H=V)
0
1000 m

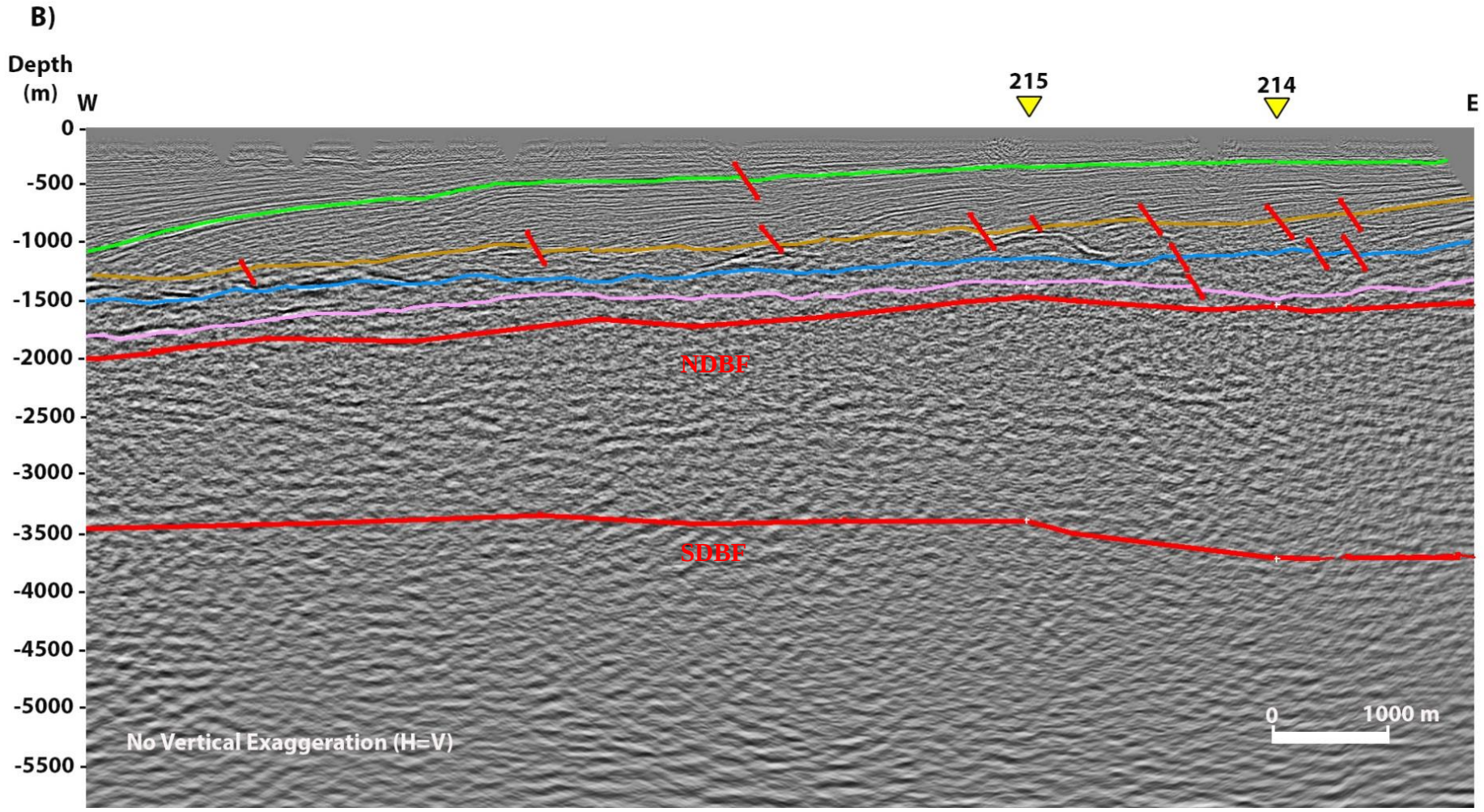

Figure 48- Depth converted uninterpreted **(A)** and interpreted **(B)** E-W trending seismic reflection profile, MUD-99-212. The yellow triangles represent cross lines MUD-99-215 and 214. Color codes indicates formation tops (Surface = Hamzali Formation, green = Huseyinciler Formation, orange = Aydin Formation, blue=Bascayir Formation, pink = Basement, red = Normal faults, NDBF: North Dipping Boundary Fault, SDBF: South Dipping Boundary Fault).

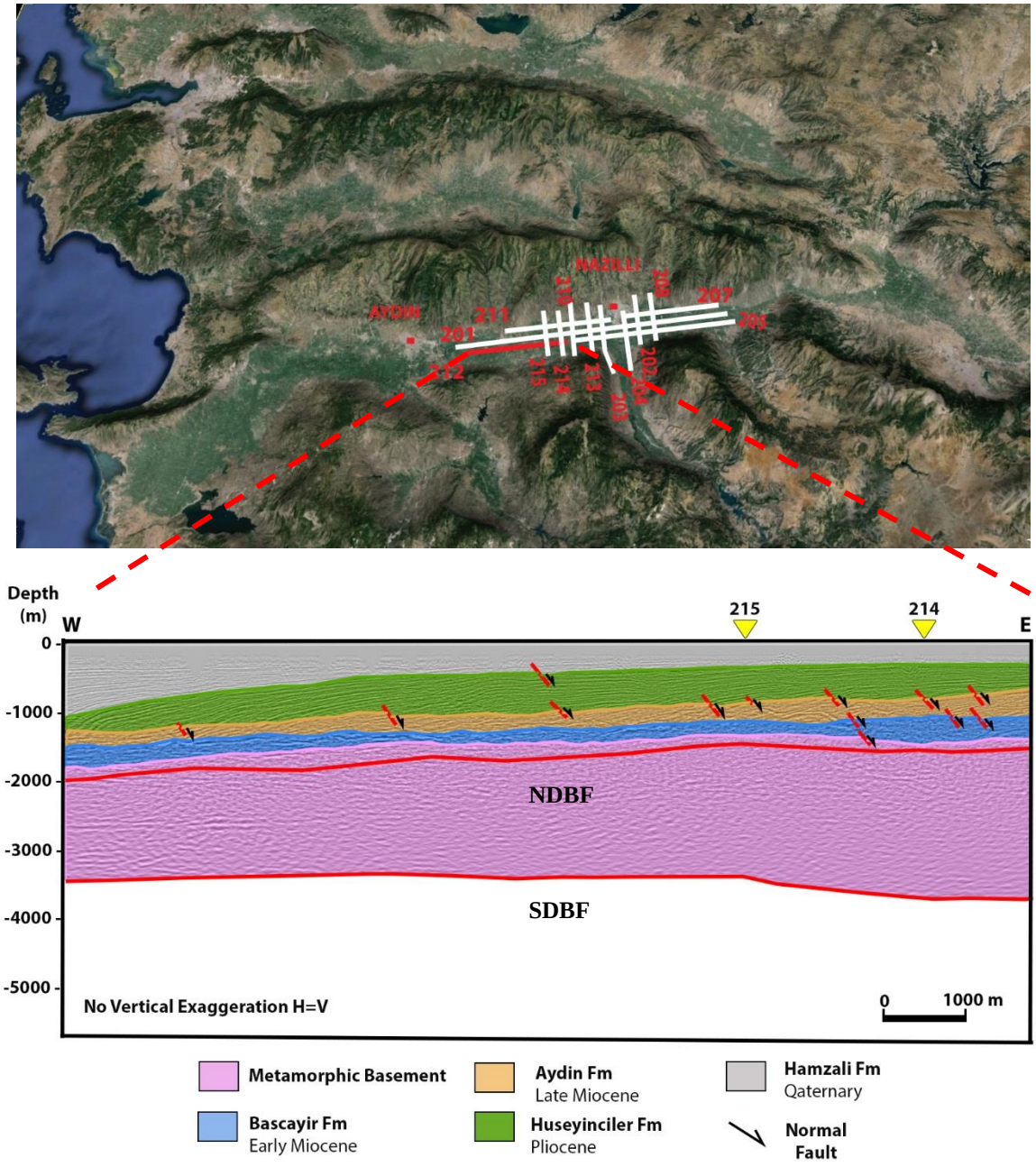

Figure 49- Structural cross-section along E-W oriented MUD-99-212 seismic reflection profile. The yellow triangles represent cross lines MUD-99-215 and 214 (NDBF: North Dipping Boundary Fault, SDBF: South Dipping Boundary Fault).

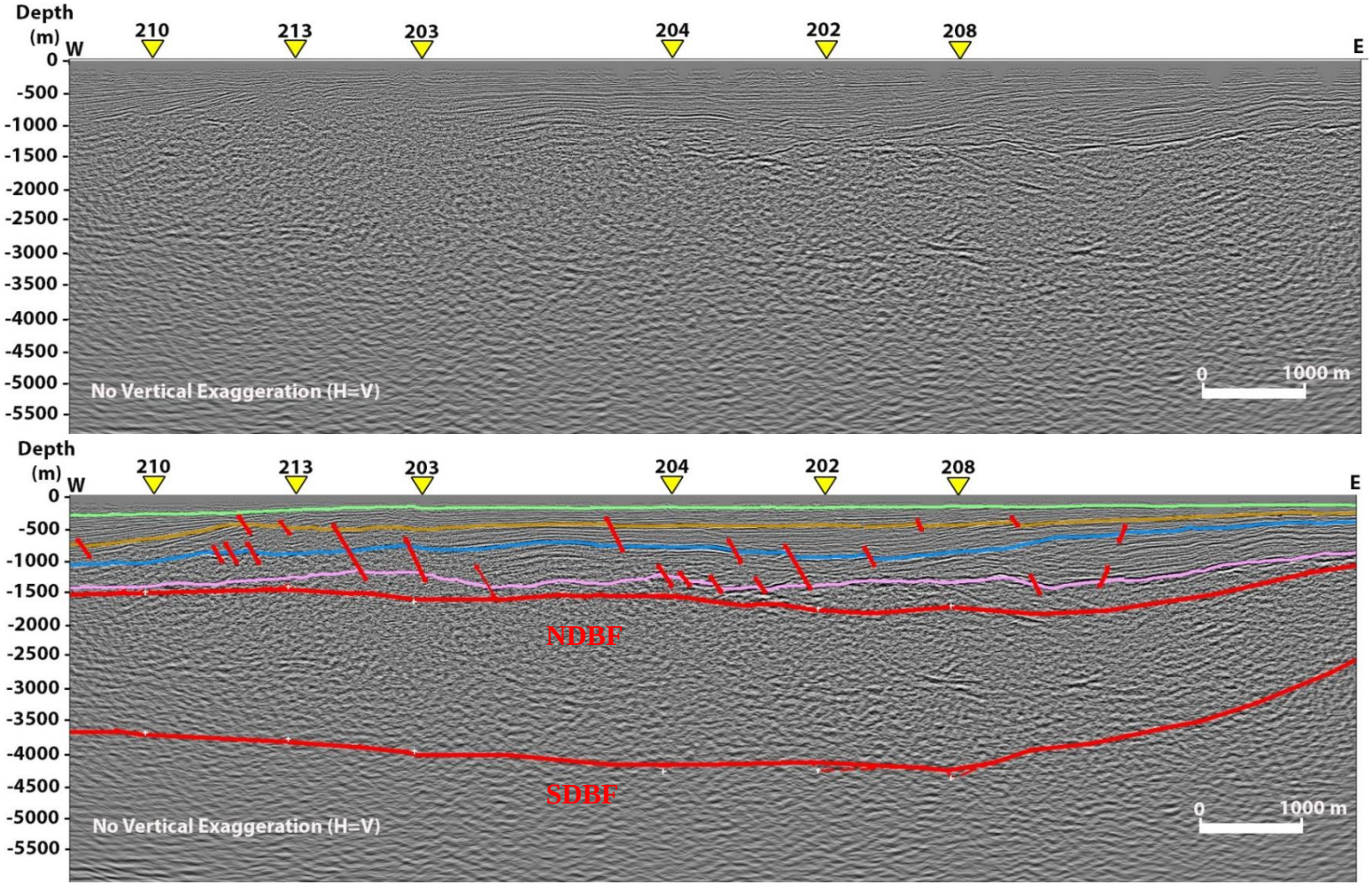

Figure 50- Depth converted uninterpreted and interpreted E-W trending seismic reflection profile, MUD-99-205. The yellow triangles represent cross lines MUD-99-210,213,203,204,202 and 208. Color codes indicates formation tops (Surface = Hamzali Formation, green = Huseyinciler Formation, orange = Aydin Formation, blue =Bascayir Formation, pink = Basement, red = Normal faults, NDBF: North Dipping Boundary Fault, SDBF: South Dipping Boundary Fault).

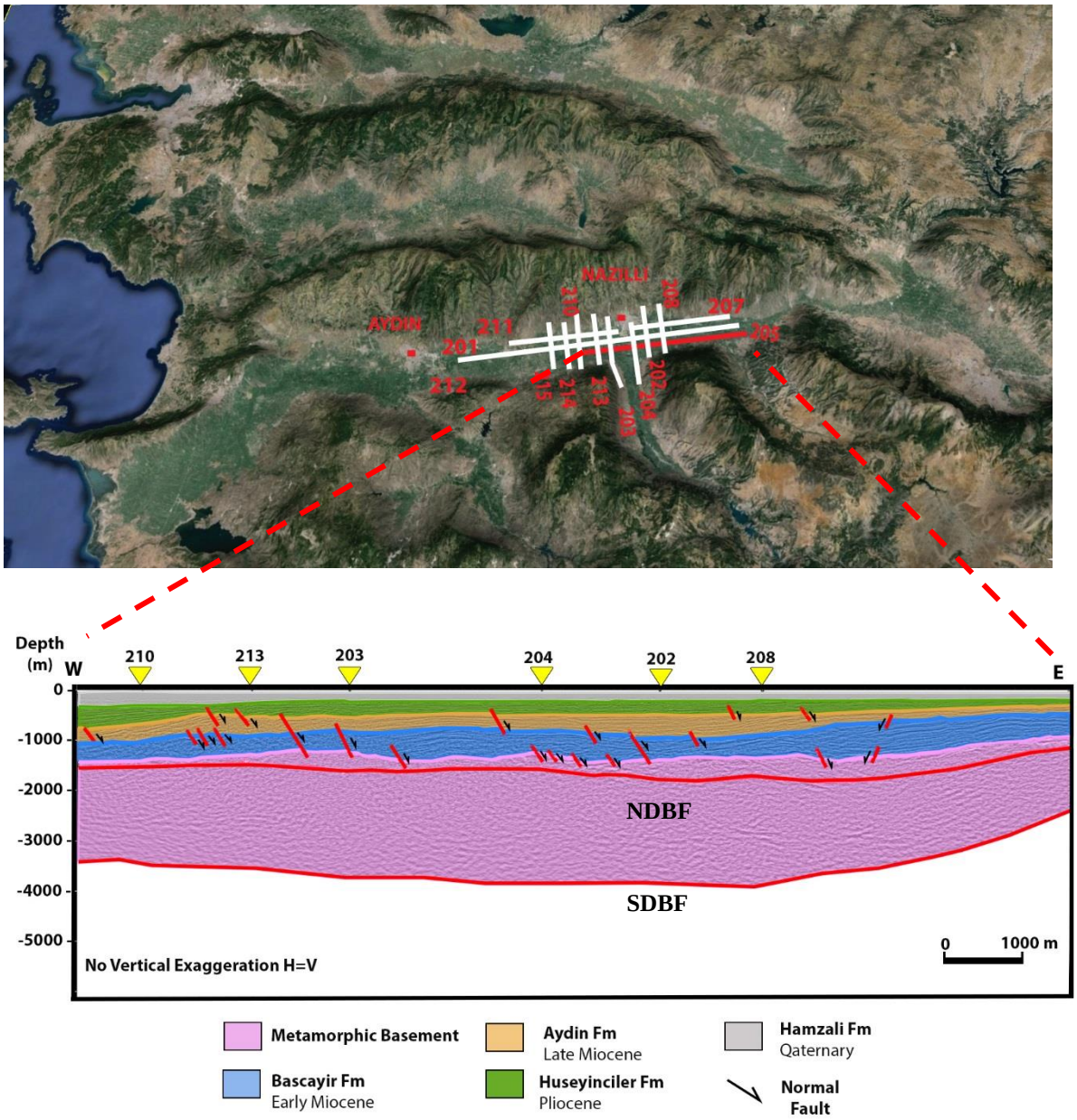

Figure 51- Structural cross-section along E-W oriented MUD-99-205 seismic reflection profile. The yellow triangles represent cross lines MUD-99-210,213,203,204,202 and 208, (NDBF: North Dipping Boundary Fault, SDBF: South Dipping Boundary Fault).

5. KINEMATIC EVOLUTION AND SUBSIDENCE HISTORY

5.1 Kinematic Evolution

A kinematic model, constructed using the 2D Move software based on the depth converted seismic reflection profiles, provides an insight for the evolution of the Büyük Menderes Graben. In this chapter, the evolution of the graben is discussed from its initiation during the Cenozoic extension to its current geometry based on balanced cross-sections and backstripping techniques to delineate the development of the extensional architecture in the graben.

The model reveals that in the early Miocene, the Büyük Menderes Graben initially started to open along its northern margin with a normal fault dipping ~70° to the south during the early Miocene (Figure 52). Continued N-S extension caused downward warping along the south dipping normal fault and formed the north dipping boundary fault (~62°) as an antithetic fault of the south dipping fault in the early Miocene (Figure 52).

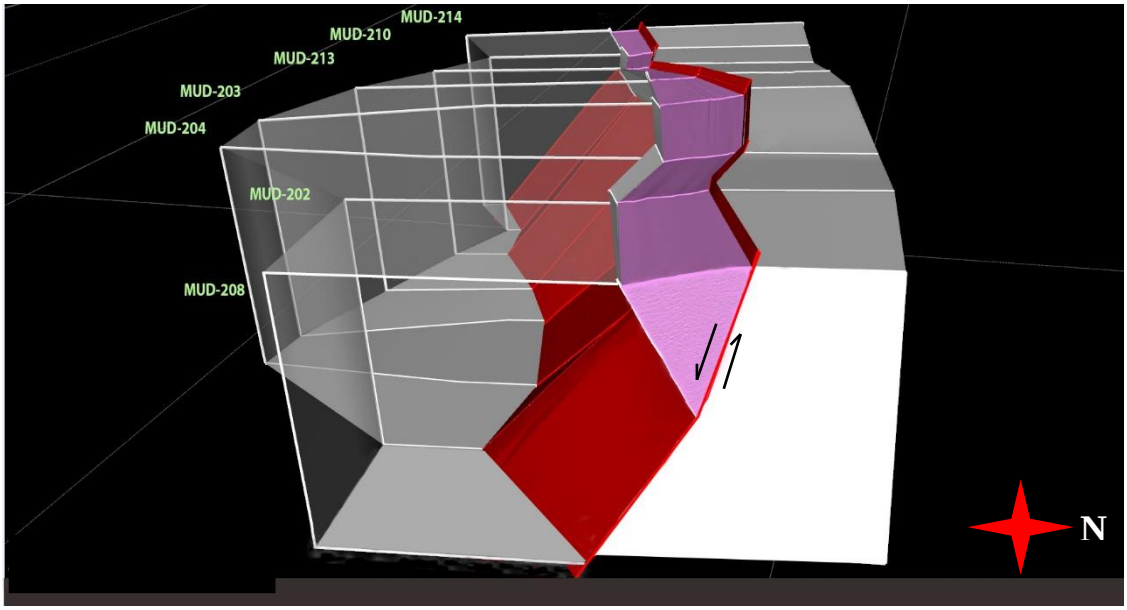

Figure 52- Initiation of the south dipping boundary fault and its antithetic, the north dipping fault. The pink unit represents the metamorphic basement rocks.

As the extension continued and the graben enlarged, the south dipping fault rotated to ~54° as a result of footwall uplift. This process caused the metamorphic basement to deform and form steeper, high angle synthetic growth faults (Figure 53a). The lowest part of the Bascayir Formation may have started to deposit as a clastic unit soon after the south dipping normal fault and its antithetic are formed. Continued rotation of the northern margin triggered rotation of the southern margin to ~50°, which resulted in developing synthetic faults of the north dipping boundary fault (Figure 53b). Consequently, this deformation on the both side created more accommodation space for the Bascayir Formation deposition in the early Miocene (Figure 53b). Footwall uplift and associated rotation of the south and north dipping faults on both margins of the graben and differential loading due to the Bascayir Formation sediments enabled growth faulting along the synthetic faults and their subsequent rotation. This caused sedimentary units of the graben thicken basinward on the hangingwall of the boundary faults and get thinner towards the basin margins (Figure 54a).

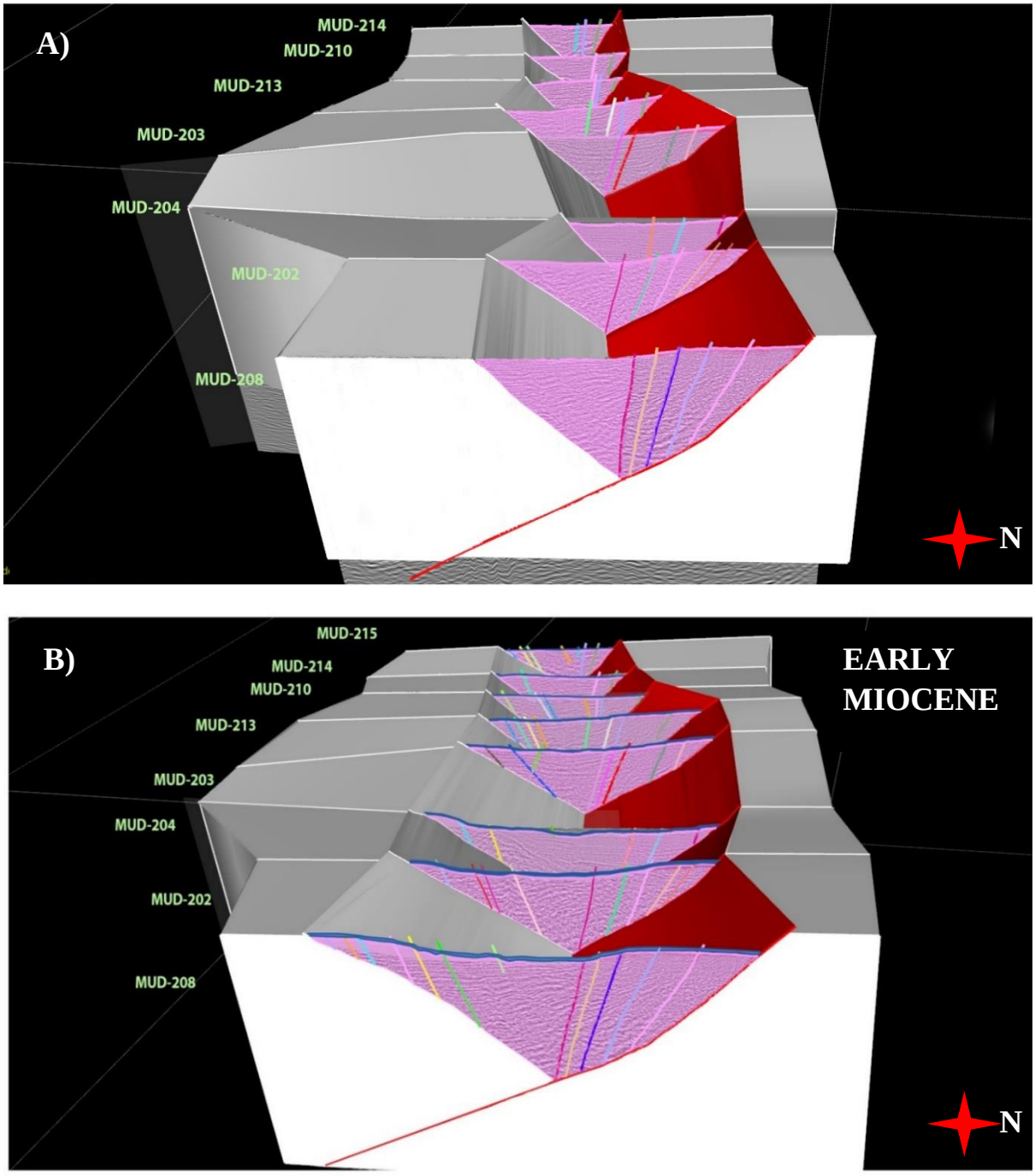

Figure 53- A) Formation of the high angle synthetic faults that superimposed onto the south dipping boundary fault as a result of footwall uplift during the extension; **B)** Rotation of the north dipping boundary fault caused the formation of the synthetic fault along the southern margin, creating accommodation space for the Bascayir formation deposition at the beginning of the early Miocene.

By the end of the early Miocene, sedimentary rocks of the Bascayir formation continued to be deposited almost symmetrically as a result of continued N-S extension and associated rotation of the boundary faults on the northern and southern margins (Figure 54a). At the eastern part of the study area, the south dipping fault rotated to a dip angle of ~46 ° which gradually decreased at depth to ~38°. The rotation lessened towards the west, and the width of the graben floor became narrower. During this time, the south dipping boundary fault and its synthetic splays are formed allowing more sediment accumulations on the northern margin of the graben due to creation of more accommodation space (Figure 54a). Synextensioanal growth faulting also provided the formation of new accommodation space on the downthrown side of the growth faults which caused the Bascayir Formation to thicken towards the center of the graben and gradually thin towards the edges of the graben (Figure 54a). This extensional geometry caused the graben to start to display its wedge shape geometry at the end of the middle Miocene.

During the middle Miocene to late Miocene, the north dipping boundary fault rotated more than (~4°) the south dipping boundary fault. Therefore, the synthetic growth faults located on the southern margin of the graben during this time created more accommodation space for the late Miocene Aydin Formation deposition. Hence, the graben has experienced a depocentre shift to the north dipping boundary fault along its southern margin (Figure 54b).

Finally, during the Pliocene to recent time, the post Miocene (Huseyinciler and Hamzali formations) sediments were deposited slightly symmetrical along the graben, preserving its wedge shape geometry. During this time, the amount of subsidence rates decreased due to the graben margins having experienced less rotation than during the Miocene deposition (Figures 55 a and b).

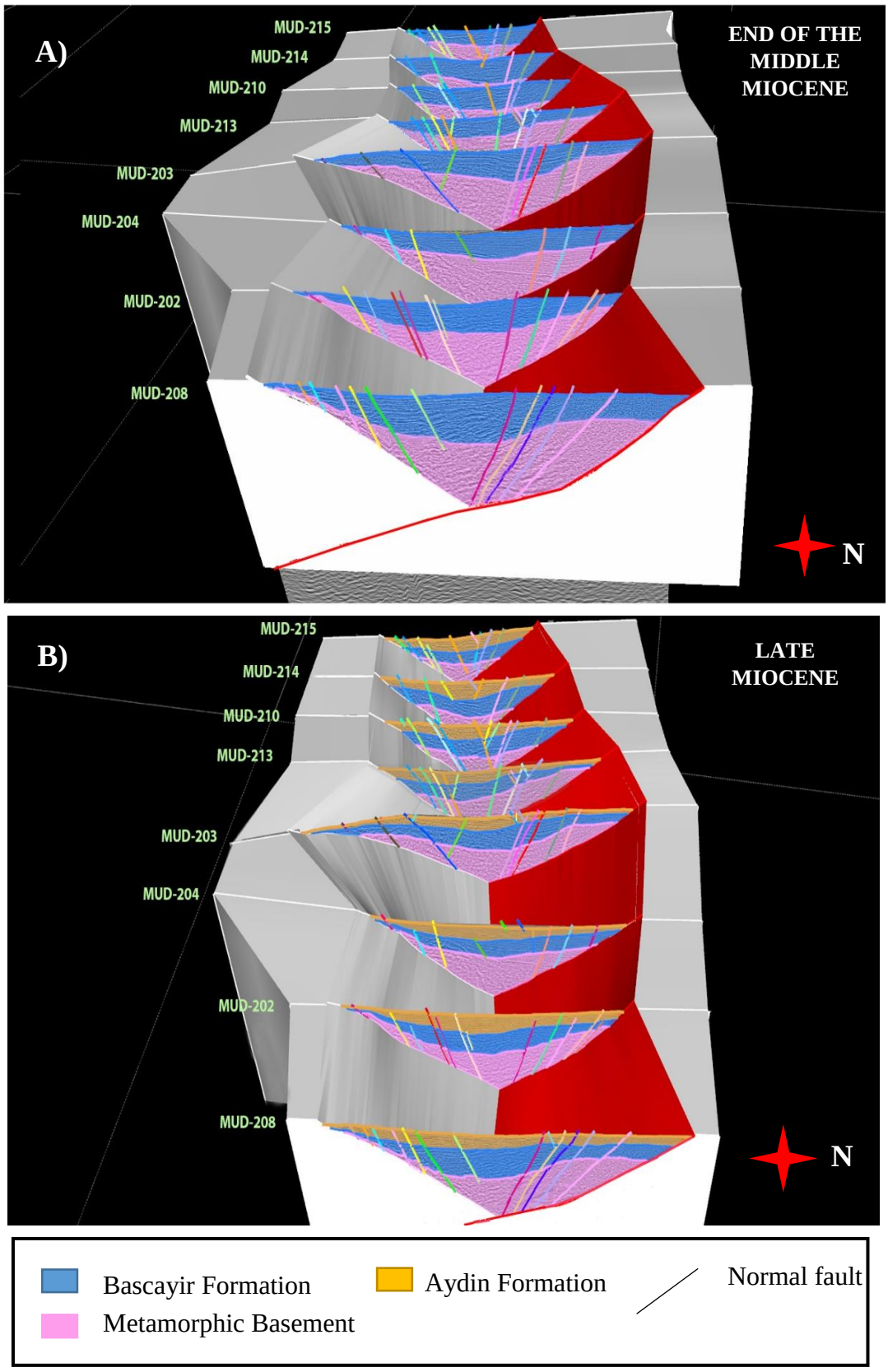

Figure 54- A) Deposition of the Bascayir formation, thickening toward to the south dipping boundary fault at the end of the middle Miocene; **B)** Deposition of the Aydin formation, showing the depocentre shift towards the south as a result of the rotation of the north dipping boundary fault.

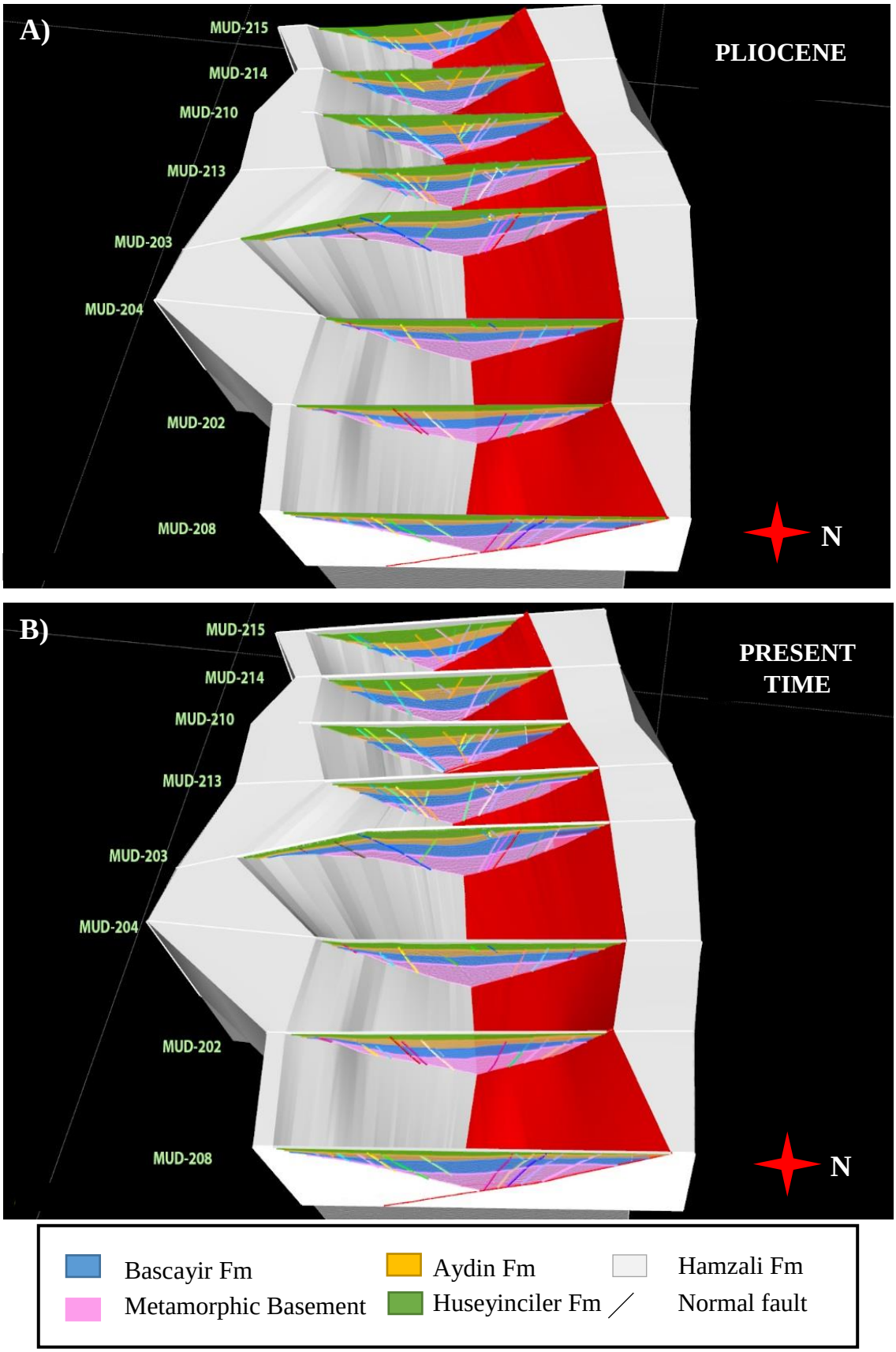

Figure 55- A) Deposition of the Huseyinciler Formation in the Pliocene; and **B)** the present time geometry of the graben.

5.2 Tectonic Subsidence

Tectonic subsidence analyses calculated from the backstripped cross sections along the Büyük Menderes Graben is used to delineate rates of sedimentation in the early Miocene, middle Miocene, and Plio-Pliostecene. The plot diagram in Figure 56 shows the tectonic subsidence rates calculated within the study area from east to the west and from the northern margin to the southern margin.

The backstripping curves of tectonic subsidence (Figure 56) indicate that the graben has more subsidence in the central part and the subsidence decreases towards the edges, which also contributed to wedge shape geometry together with growth faulting associated with the Cenozoic extension. Towards the western part of the study area, the general trend of subsidence curves for the central part of the graben show a decrease towards an intrabasinal high which is located between the seismic profiles MUD-99- 203-213 and an increase towards the profile MUD-99- 215. This indicates that graben kinematics have varied from the east to the west within the study area. The subsidence at the northern and southern flanks increases due to narrowing of the width of the graben floor towards the seismic reflection profile, MUD-99-215.

The subsidence curves, representing sediment accumulation at the center of the graben at the end of the early and late Miocene (~23 Ma and ~12 Ma), show a general decrease towards the western part of the study area, except between profiles MUD-99- 203 and MUD-99-213 where an intrabasinal high is located. This indicates that extension might have initiated from eastern part of the study area and continued to the west. The diagram also shows that the northern flank experienced more sediment deposition during the early Miocene. This shows a relationship with the balanced structural cross-sections, indicating that the south dipping boundary fault along the northern margin rotated more than the north dipping boundary fault along the southern margin of the graben. Therefore, this agrees with

the statement that the development of the graben was controlled by the south dipping boundary fault on the northern flank during the deposition of the Bascayir Formation in the early Miocene.

The transition to the Aydin Formation deposition in the late Miocene (~12 Ma) is characterized with almost the same amount of increase in the subsidence rates of the Bascayir Formation deposition. However, during this time, more sediment accumulation occurred in the southern flank compared to the northern flank indicating that the north dipping boundary fault became more dominant compared to the south dipping fault (Figure 56).

After the late Miocene, the graben experienced a slow subsidence rate at the end of the Pliocene, specifically at both margins compared to the center of the graben and the subsidence rates gradually decreased to present time. This suggests that the extension rate of the graben associated with boundary fault rotation decreased after the Miocene (Figure 56).

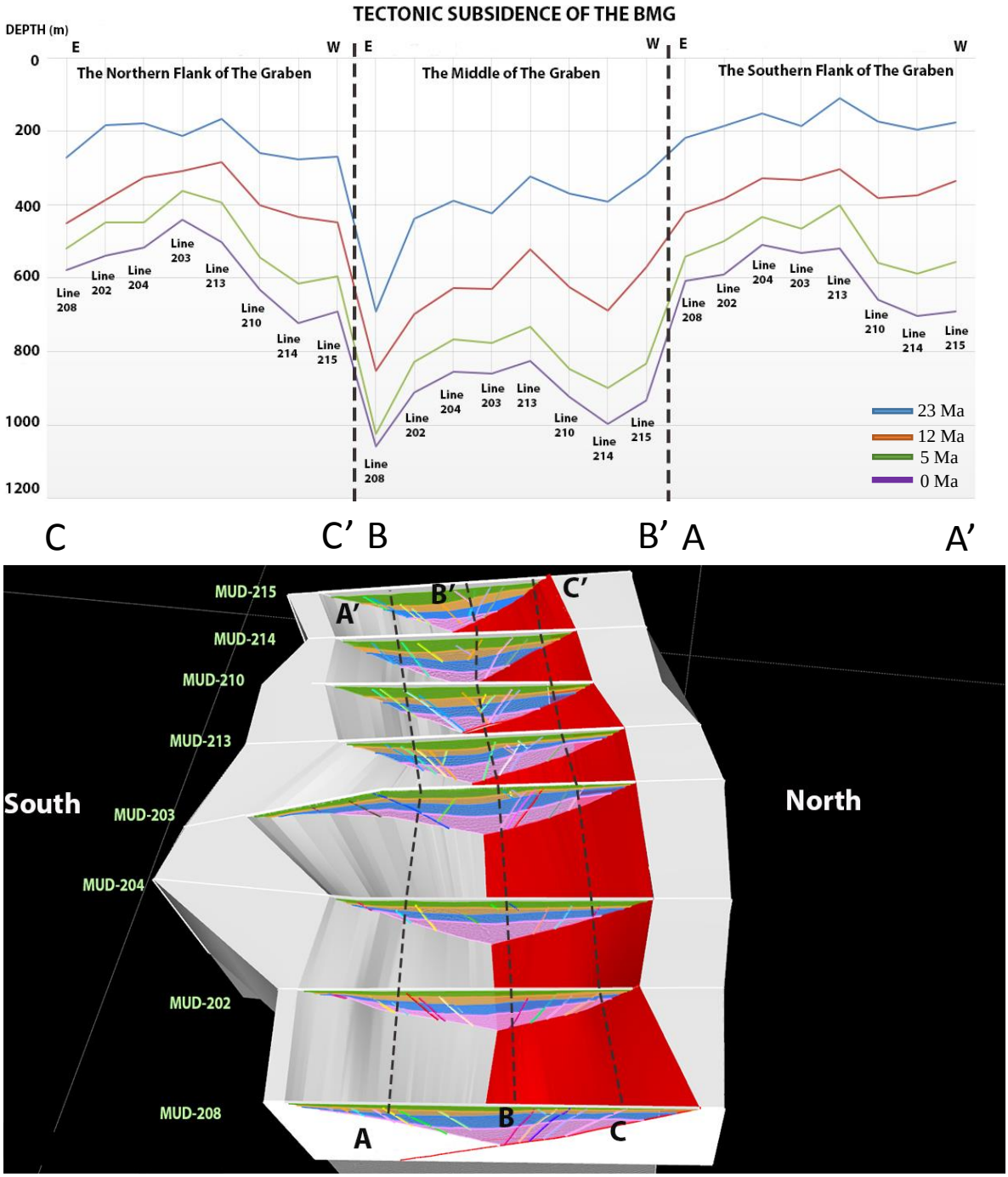

Figure 56- A) Tectonic subssidence rates during the deposition of each formation. The colored lines show the deposition time for each formation. Blue: the middle Miocene, the Bascayir Formation; Orange: the late Miocene, the Aydin Formation; green: the Plionce, Huseyinciler Formation and purple: present time, Hamzali Formation. **B)** Cross sections constructed from northern ,the central, and southern parts of the Buyuk Menderes Graben in the study area.

6. DISCUSSION

Previous studies concerning evolution of the two major E-W trending grabens, the Alaşehir and Büyük Menderes grabens, proposed several different models to explain extensional deformation of the Menderes Metamorphic Core Complex (MMCC) in western Turkey. These models came to the conclusion that both grabens are structurally symmetrical and developed under the control of opposite dipping detachment faults (Gessner et. al., 2001; Seyitoğlu et. al., 2000 and 2002; Çemen et al., 2006; Çiftçi and Bozkurt 2009 and 2010; Gessner et. al., 2013). However, the initial geometry of the detachment faults remained controversial. Some researchers suggested that the detachment faults of the E-W trending grabens were formed initially as low angle listric faults (Hetzel et al., 1995b; Kocyiğit, 1999; Sözbilir, 2001). Others, however, suggested based on their field and subsurface evidence that the detachment faults were initially formed as high angle normal faults and rotated to their low dip angle as a result of isostatic rebound and associated rolling-hinge process in their footwall blocks (Gessner et. al., 2001; Seyitoğlu et. al., 2000 and 2002; Çemen et al., 2006; Çiftçi and Bozkurt 2009 and 2010; Gessner et. al., 2013; Ersoy et al., 2014).

Based on field oriented geological work, Seyitoğlu et al., (2000, 2002 and 2004) and Çemen et al., (2006) suggested that the Alaşehir Graben was developed along its southern margin by a north dipping detachment fault, which was initially formed as a high angle normal fault which rotated to a low angle due to the rolling hinge process which caused a large rollover structure on the hanging wall of the detachment surface. Çiftci and Bozkurt (2010) interpreted 2-

D seismic reflection profiles in the Alaşehir Graben and determined that the flat-ramp geometry of the detachment fault caused the formation of the large rollover structure on the southern margin of the graben (Figure 57). Both surface and subsurface studies conclude that the interpreted structural geometry of the Alaşehir Graben agrees with the supradetachment basin development in the region regardless of the initial dip angle of the detachment faults.

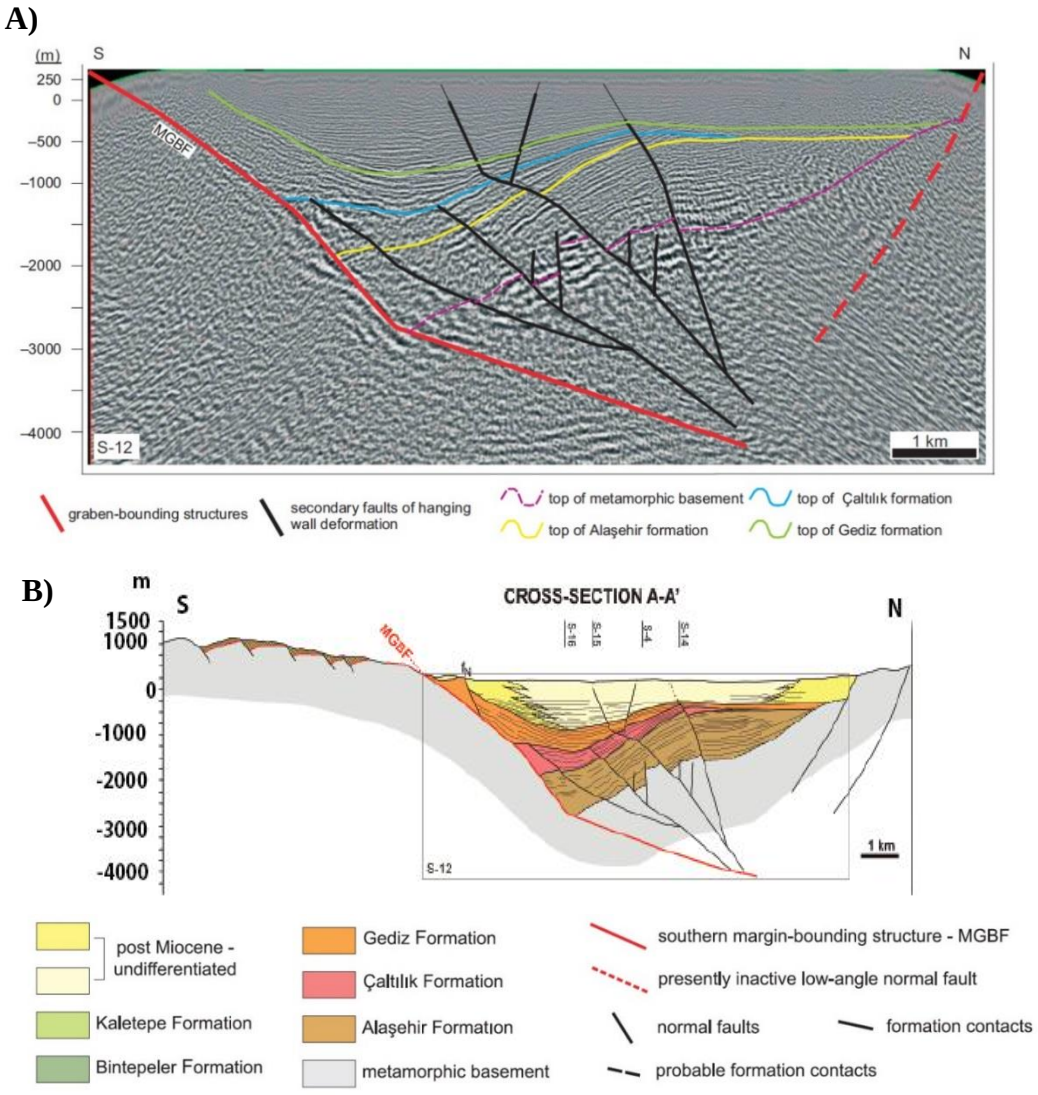

Figure 57- A) Interpreted seismic profile, S-12 from Çiftçi and Bozkurt (2010) showing fault-bend and roll over relationship on the main graben boundary fault (in solid red line); **B)** Structural cross section along the seismic profile S-12 (from Çiftçi and Bozkurt, 2010).

A similar structural geometry was proposed by Seyitoğlu et al., (2004), Göğüş et al., (2004) and Çemen et al., (2006) for the development of the Büyük Menderes Graben based on field mapping along the northern margin of the graben. These studies suggested that the Neogene sedimentary rock accumulation in the Büyük Menderes Graben is controlled by a south dipping, low angle detachment fault along the northern margin of the graben. In addition, based on seismic interpretations, Çiftçi et al., (2010) proposed that the south dipping detachment fault of the Büyük Menders Graben has a listric geometry at ~2.5 km and becomes horizontal about 10 km at depth.

Balanced structural cross sections constructed during this study do not support the previous interpretation for the following reasons. First, the cross sections reveal that the south dipping fault shows nearly planar geometry, proceeding to a dip of ~38° to 45° along the graben from east to the west within the study area (Figures 24 to 39). Second, the cross-sections clearly demonstrate that the Büyük Menderes Graben does not have a rollover structure related to the proposed listric geometry on the hanging wall of the south dipping boundary fault surface along the northern margin of the graben. Third, kinematic modeling suggests that after the initial accumulation of sedimentary rocks in the early to middle Miocene (Bascayir Formation), there was a depocenter shift towards the southern side of the graben, which is seen in the available seismic reflection profiles in the study area (Figures 24 to 39). In addition, the Neogene sedimentary units thicken towards the center of the graben, and thins towards the edges of the graben on its northern and southern margins, suggesting that the graben evolution was controlled by two boundary faults on both margins. Hence, the previously proposed listric geometry of south dipping fault controlled structural evolution of the Büyük Menderes Graben can not

explain the subsurface structural geometry and the pattern of deposition of sedimentary rocks within the graben in the study area.

The lines of evidence explained above suggest that the Büyük Menderes Graben has experienced a rifting, controlled by two oppositely dipping planar boundary faults. The kinematic model constructed during this study suggests that depocenter shift to the southern side of the graben is related to the north-dipping boundary fault along the southern margin of the graben being more active during the deposition of the late Miocene Aydin Formation. Also, the trajectory of the south dipping fault may flatten out at the deeper part of the graben in upper crust and join a deeper structure as a result of the domal rise related to isostatic rebound along the South Anatolian shear (SWASZ).

6.1 Proposed Model for the Extensional Geometry of the Central Menderes Metamorphic Core Complex

Previous structural models of the central part of the Menderes Metamorphic Core Complex (CMMCC) suggest that the E-W trending Büyük Menderes and Alaşehir grabens were formed symmetrically along oppositely dipping detachment surfaces and therefore subsurface geometry of the grabens are similar. (Hetzel et al., 1995b ; Kocyiğit, 1999; Sözbilir, 2001; Gessner et. al., 2001; Seyitoğlu et. al., 2000,2002 and 2004; Çemen et al., 2006; Çiftçi and Bozkurt 2009 and 2010; Gessner et. al., 2013; Ersoy et al., 2014; Seyitoğlu and Işık., 2015).

The difference in subsurface geometry of the E-W trending grabens bordering the central part of the Menderes Metamorphic Core Complex (CMMCC) discussed in this study illuminates that the previously proposed extensional mechanism for the CMMCC needs to be updated based

on the results of this study. Therefore, a new model was developed for extensional evolution of CMMCC and E-W trending graben formation in the region.

The model suggests that the Cenozoic extension in the Menderes Metamorphic Core Complex may have been initiated asymmetrically in the late Oligocene following the Eocene Alpine collision and formation of the Izmir- Ankara suture zone, which brought the Lycian nappes over the Menderes Massif (Figure 58 a and b) (Şengor et al., 1984; Çemen et al., 2006; Seyitoğlu et al., 2004; Seyitoğlu and Işık., 2015). This extension was generated along the Southwest Anatolian Shear Zone (SWASZ) as a main breakaway and resulted in a domal uplift beneath the region. (Figure 58 b) (Seyitoğlu et al., 2004; Çemen et al., 2006).

The domal uplift caused the reactivation of the Lycian nappes as an extension structure in opposite directional movement and the first exhumation of the high grade metamorphic rocks of the Menderes massif in the late Oligocene (Seyitoğlu et al., 2004; Çemen et al., 2006) (Figure 58 b). Three lines of evidence support this interpretation: 1) the presence of the Lycian nappes on the footwall of the SWASZ, containing the Taurids Marbles and Ophiolites (Seyitoğlu et al., 2004; Çemen et. al., 2006); and 2) the presence of conglomerate fragments of the Taurids Marbles and Ophiolites in the Oligocene sedimentary rocks of the Ören and Kale-Tavas basins in the southern Menderes Massif formed along the hanging wall of the SWASZ (Seyitoğlu et al., 2004; Çemen et. al., 2006) (Figure 58 b). These fragments were probably eroded from the upper plate (cover rocks) of the Menderes Massif during the Oligocene extension (Seyitoğlu et al., 2004; Çemen et. al., 2006; Ersoy et al., 2014); 3) The extension on the SWASZ can be also seen from the seismic reflection profile interpreted by Kurt et al., 1999. The seismic profile shows the listric geometry of the southern segment of the SWASZ related to formation of a roll over

structure and the late Oligocene basin fill over the basement (Kurt et al., 1999; Çemen et al., 2006).

The domal uplift of the Menderes massif on the hanging wall of the SWASZ has probably experienced a second stage of extension in the early Miocene, which was distributed none-uniformly along the central part of the Menderes Massif (Figure 58 c). This extension may be related to the slab tear of the African plate between the Hellenic and Cyprus arcs that causes hot asthenospheric flow beneath the Menderes Metamorphic Core Complex (Çemen et al., 2006; Biryol et al., 2011; Gessner et al., 2013; Ersoy et al., 2014; Mahatsente et al., in press).

During the Miocene extension the initially high angled Alaşehir detachment surface was probably formed in the lower end of the SWASZ as a secondary breakaway zone (Figure 58 c). This may have caused the Alaşehir Graben to evolve on the limb of the dome as a supradetachment basin. Meanwhile, the Büyük Menderes Graben has experienced a rift type deformation at the top of the dome during the formation of the secondary breakaway (Figure 58 c). The Büyük Menderes Graben initiated as a bowl-shaped depression along the south dipping, high angle normal fault with its synthetic splays as a result of footwall uplift of the northern margin. This geometry together with continued extension, formed the north dipping fault as the antithetic of the primary fault most probably as a result of rapid thinning of the lithosphere due to hot material beneath western Turkey during the N-S Cenozoic extension (Lavier and Buck 2002; Göğüş, 2014; Mahatsente et al., in press). As the footwall was uplifted by isostatic rebound during extension, the north and south dipping boundary faults formed the current wedge shape geometry in the Büyük Menderes Graben. This rift type extension is evidenced by the Miocene sediments filling the basin center almost symmetrically and gradually thinning to the

edges and rotation of the both boundary faults as interpreted in available seismic lines (Figures 24 to 39).

During the early Pliocene, extension in western Turkey was triggered by westward lateral extrusion of the Anatolian plate related to the formation of the North Anatolian fault zone about 5 Myr ago (Şengör, 1979; Şengör and Yılmaz, 1981 Şengor et al., 1984; Çemen et al., 1993,1999; Çemen et al., 2006). This together with ongoing the retreat of the African slab produced more extension along the Central Menderes Metamorphic core complex and most probably caused the formation of the Küçük Menderes Graben (Figure 58 c).

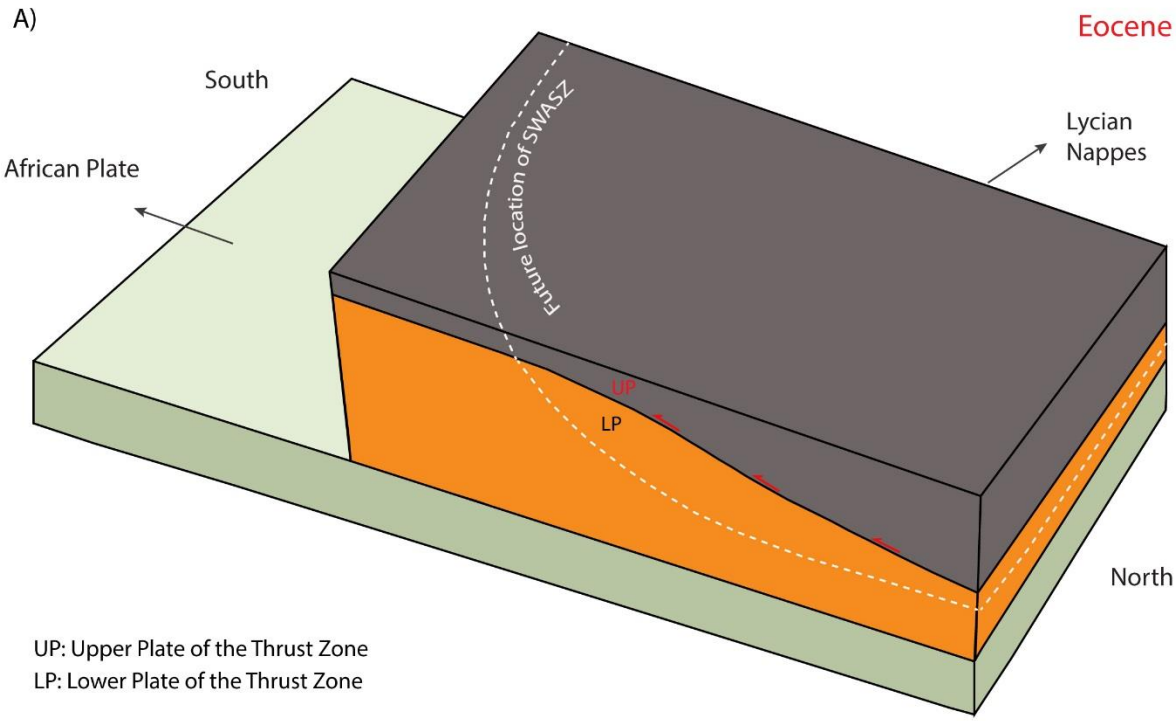
A)
Eocene
South
African Plate
Future location of SWASZ
Lycian
Nappes
UP
LP
North
UP: Upper Plate of the Thrust Zone
LP: Lower Plate of the Thrust Zone

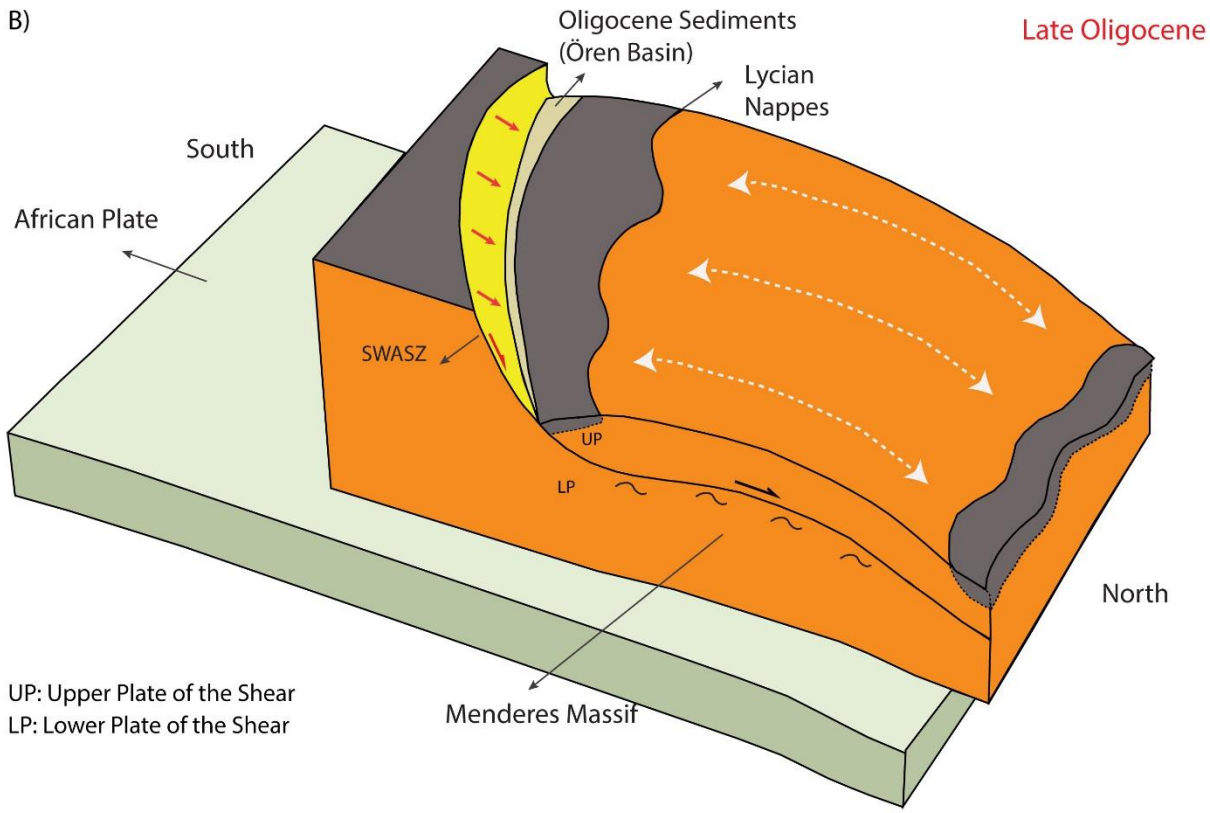
B)
Oligocene Sediments
(Ören Basin)
Late Oligocene
Lycian
Nappes
South
African Plate
SWASZ
UP
LP
North
UP: Upper Plate of the Shear
LP: Lower Plate of the Shear
Menderes Massif

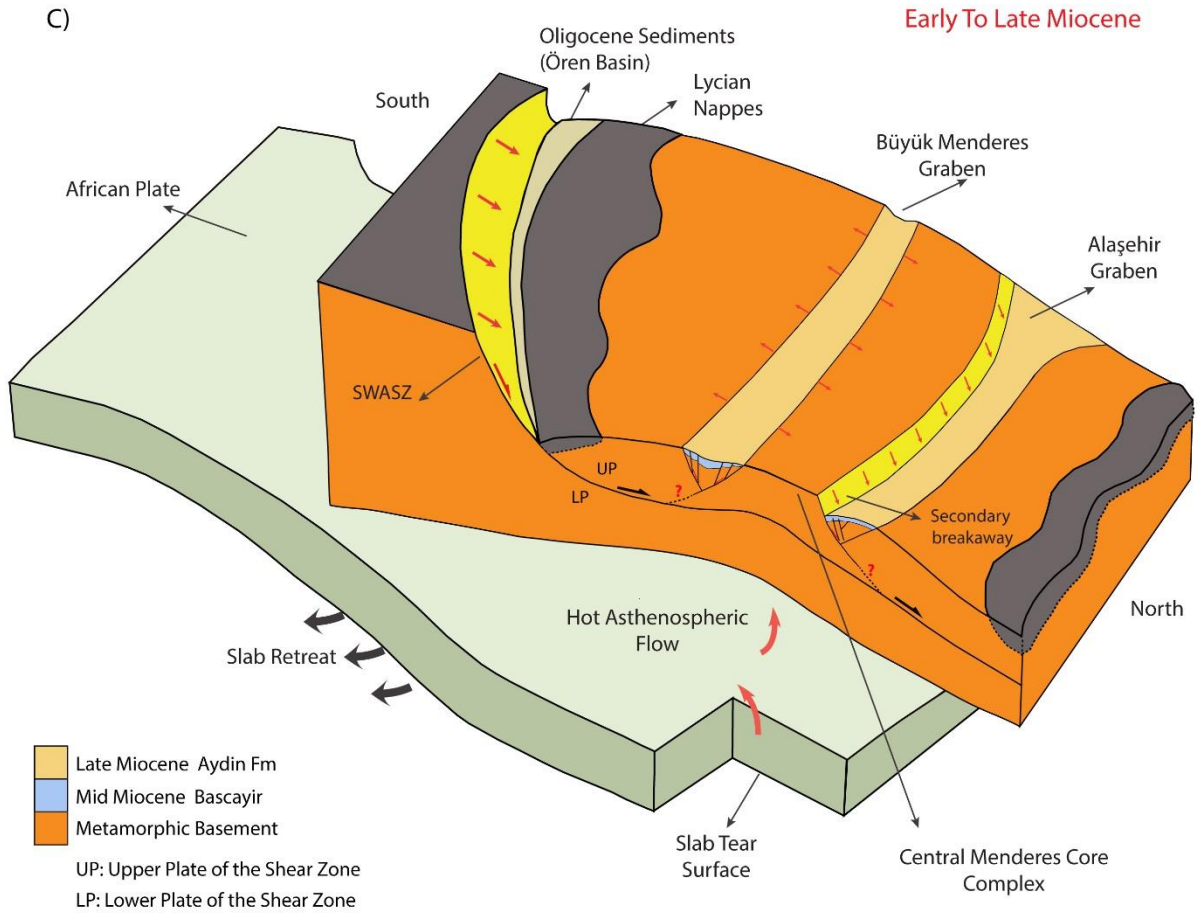
C)
Early To Late Miocene
Oligocene Sediments
(Ören Basin)
South
Lycian
Nappes
Büyük Menderes
Graben
African Plate
Alaşehir
Graben
SWASZ
UP
LP
?
Secondary
breakaway
?
North
Hot Asthenospheric
Flow
Slab Retreat
Late Miocene Aydin Fm
Mid Miocene Bascayir
Metamorphic Basement
UP: Upper Plate of the Shear Zone
LP: Lower Plate of the Shear Zone
Slab Tear
Surface
Central Menderes Core
Complex

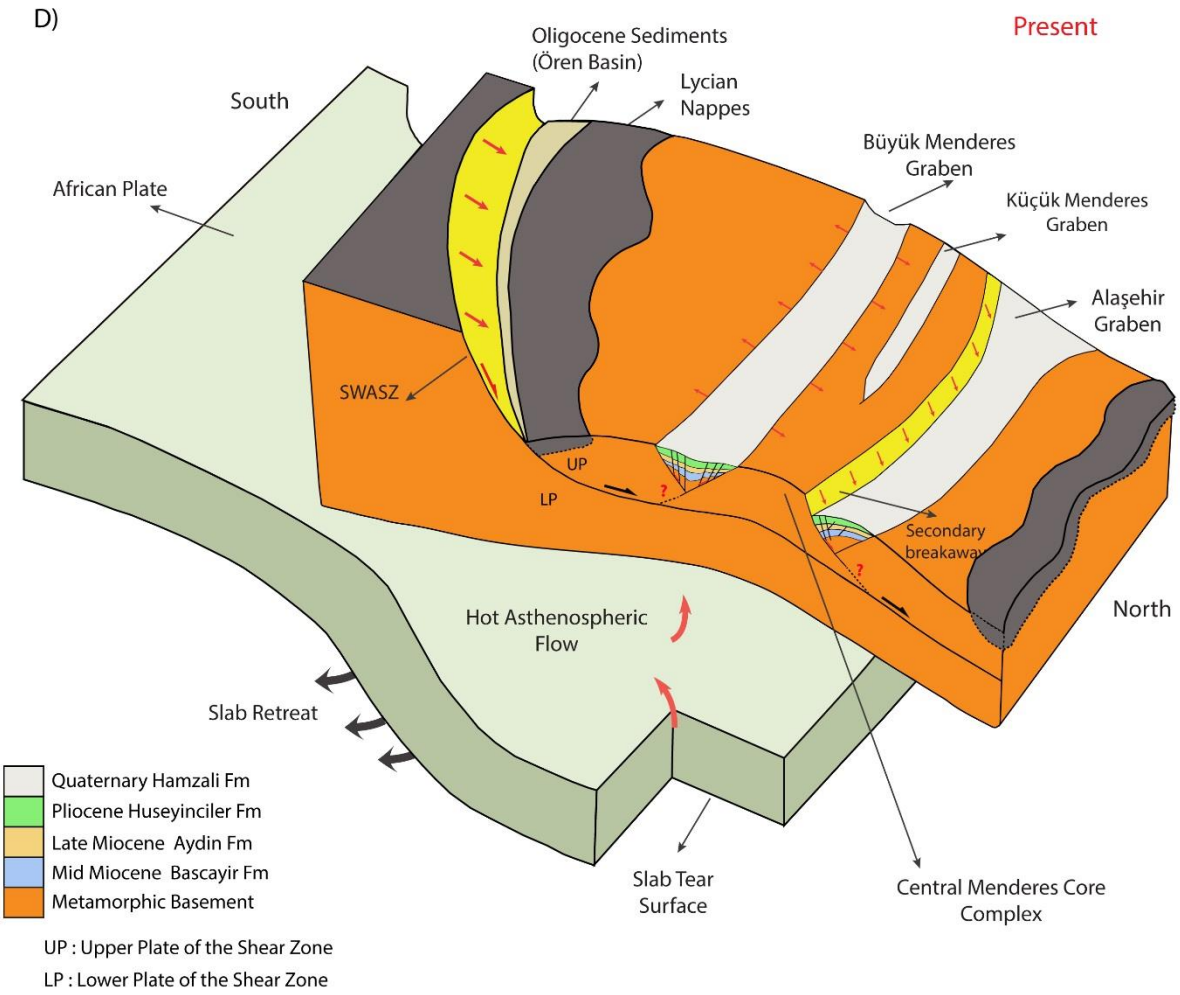

Figure 58- 3D cartoons showing the extensional model of the Central Menderes Metamorphic Core Complex (CMMCC) and the formation of the E-W trending grabens. **A)** Eocene; formation of the Izmir-Ankara suture zone and the Lycian Nappes. **B)** Initiation of the Cenozoic extension in western Turkey in the late Oligocene and asymmetric exhumation of the Menderes core complex along the SWASZ (Çemen et al., 2006; Seyitoglu et al., 2004). **C)** Development of the Alaşehir Graben along a secondary breakaway as a supradetachment basin and the Büyük Menderes Graben as a small rift basin in the early Miocene. **D)** Present time position of the CMMCC, development of the Küçük Menderes Graben, most likely due to the westward escape of the Anatolian plate in the early Pliocene (Modified from Çemen et al., 2006 and Seyitoglu et al., 2004 and 2015).

7. CONCLUSIONS

The major conclusions of this study can be summarized as below:

- The Büyük Menderes Graben has experienced a rift type extension under the control of two main boundary faults that were active during the Miocene extension along the northern and southern margins of the graben.
- The Neogene sedimentary units thicken towards the central part of the graben and become thinner towards the northern and southern margins. This indicates that the Büyük Menderes Graben has experienced synextensioanal deformation related to growth faulting.
- Tectonic subsidence rates and the kinematic model constructed during this study show that the depocenter shift to the southern margin is related to the normal movement along the north-dipping boundary fault, which was also active along the southern margin of the during the deposition of the Aydin Formation in the late Miocene.
- The kinematic model constructed during this study proposes that the graben initiation started along the high angle south dipping boundary fault on the northern margin of the Büyük Menderes Graben. Due to rapid uplift during ongoing N-S extension, the north dipping boundary fault was formed as antithetic of the south dipping boundary fault. Afterwards, the two boundary faults were active and rotated to create accommodation space for the sedimentation.

- The rotation of the boundary faults and their splays vary along the graben from east to the west within the study area. The southern flank shows more rotation than the northern flank towards the west after the intrabasinal high, which indicates that the tectonic activity of the southern flank after the early Miocene might have changed the polarity of extension and depocenter of sedimentary rocks deposition from east to the west.
- The isochore maps constructed during this study show that the Miocene sedimentary thickness of the graben (the Bascayir and Aydin formations) decreases towards the west, which might indicate that the graben opening initiated from eastern side and propagated westward. However, the present time isochore map shows that the graben has had almost a uniform thickness of sedimentary rocks from east to the west. This indicated that the graben has experienced more post-Miocene sedimentary rocks deposition towards the west.
- The fault orientation of the synthetic and antithetic normal faults of the boundary faults indicates that the normal faults on the edges of the margin have shallower dip angles than those located at the central part of the graben. This indicates that the faults located on both flanks developed first and experienced footwall uplift and fault rotation due to continuous extension.

REFERENCES

Allen, A.P., Allen, R.J., 2013, Basin Analysis, Principles and application to petroleum play Assessment, third edition book.

Arca, S. M, 2009, Investigation of Cenozoic crustal extension inferred from seismic reflection profiles and field relations, SE Arizona [P.H.D dissertation] : The university of Arizona.

Biryol, C.B., Beck, S.L., Zandt, G., Ozacar, A.A., 2011, Segmented African lithosphere beneath The Anatolian region inferred from teleseismic P- wave tomography, Geophysical Journal International, v: 184, issue: 3, p: 1037-1057, doi: 10.1111/j.1365-246X.2010.04910.x.

Bland, S., Griffiths, P., Hodge, D., Ravaglia, A., 2006, Restoring the Seismic Image, Geohorizons.

Bond, G. C., & Kominz, M. A. 1984. Construction of tectonic subsidence curves for the early Paleozoic miogeocline, southern Canadian Rocky Mountains: Implications for subsidence mechanisms, age of break-up, and crustal thinning. Geological Society of America Bulletin, 95, 155-173.

Bozkurt, E., and Park, R.G., 1994, Southern Menderes Massif: An incipient metamorphic core complex in western Anatolia, Turkey: Journal of the Geological Society, v. 151, no. 2, p. 213–216.

Bozkurt, E., 2000, Timing of extension on the Büyük Menderes Graben, western Turkey, and its tectonic implications. Geological Society, London, Special Publications, v. 173, no.1, p.385-403.

Bozkurt, E., 2003, Origin of the NE-trending basins in western Turkey: Geodinamica Acta, v. 16, no. 2, p.61-81.

Bozkurt, E., Sözbilir, H., 2004, tectonic evolution of the Gediz Graben: field evidence for an episodic, two-stage extension in western Turkey. Geological Magazine, v. 141, p.63-74.

Buck, W.R., 1988, Flexural rotation of normal faults. Tectonics, v.7, p. 959-973.

Buck, W.R., 1991, Modes of continental lithospheric extension. F. Geophys, Res, v.96, p. 20161-20178.

Catlos, E.J., Çemen, İ., 2005, Monazite ages and rapid exhumation of the Menderes Massif, Western Turkey. International Journal of Earth Sciences 94, 204–217.

Candan, O., Koralay, E., Akal, C., Kaya, O., Oberhansli, R., Dora, O.O., Konak, N., Chen, F., 2011, Supra-Pan- African unconformity between core and cover series of the Menderes Massif / Turkey and its geological implications. Precambrian Research, 184, 1-23.

Chery, J., 2001, Core complex mechanics: From the Gulf of Corinth to the Snake Range: GSA, v. 29, no: 5, p. 439-442.

Cohen, H.A., Dart, C.J., Akyüz, H.S., Barka, A.A., 1995, Syn-rift sedimentation and structural development of Gediz and Büyük Menderes graben, western Turkey. Journal of the Geological Society London, 152, 629-638.

Cunha, T., 2008, Gravity Anomalies, Flexure and the Thermo-Mechanical Evolution of the West Iberia Margin and its Conjugate of Newfoundland, University of Oxford Wolfson College & Department of Earth Sciences.

Cunningham, A.D, Droxler, A.W., 2000, Synthetic seismogram generation and seismic facies to core lithology correlation for sites 998, 1000, and 1001. Proceedings of the Ocean Program Scientific Results, Vol.165.

Çemen, I., Göncüoğlu, M.C., Erler, A., Kozlu, H., and Perinçek, D., 1993, Indentation tectonics and associated lateral extrusion in east, southeast and central Anatolia: Geological Society of America Abstracts with Programs, v. 25, no. 7, p. A116.

Çemen, I., Göncüoğlu, M.C., and Dirik, K., 1999, Structural Evolution of the Tuzgölu Basin in Central Anatolia, Turkey: Journal of Geology, v. 107, p. 693– 706, doi: 10.1086/314379.

Çemen, I., Catlos, E. J., Gogus, O., Özerdem C., 2006, Postcollisional extensional tectonics an exhumation of the Menderes Massif in the western Anatolia extended terrane, Turkey, GSA, Special paper 409.

Çemen, I., 2010, Extensional tectonics in the basin and range, the Aegean, and western Anatolia: Introduction: Tectonophysics, v. 488, no. 1, p. 1-6.

Çiftci, G., Pamukçu, O., Çoruh, C., Çopur, S., Sözbilir, H., 2011, Shallow and deep structure of a supradetachment basin based on geological, conventional deep seismic reflection sections and gravity data in the Büyük Menderes Graben, Western Anatolia. Geophysics 32, 271-290.

Çiftci, N.B., Bozkurt, E., 2009, Pattern of normal faulting in the Gediz Graben, SW Turkey. Tectonophysics 473 234–260,

Çiftci, N.B., Bozkurt, E., 2010, Structural evolution of the Gediz Graben, SW Turkey: temporal and spatial variation of the graben basin. Basin Research 22, 846–873.

Dewey, J.F., 1988, Extensional collapse of orogens: Tectonics, v. 7, p. 1123-1139.

Dewey, J.F., and Şengor, A.M.C., 1979, Aegean and surrounding regions: Complex multiplate and Continuum tectonics in a convergent zone: GSA, v.90, p. 84-92.

Emre, T., Sözbilir, H., 1997, Field evidence for metamorphic core complex, detachment faulting and accommodation faults in the Alaşehir and Büyük Menderes grabens (western Anatolia). In International Earth Science Colloquium: Aegean Region, Izmir, v.1, p. 73-93.

Ersoy, E.Y., Helvacı, C., Sözbilir, H., 2010, Tectono-stratigraphic evolution of the NE-SW-trending superimposed Selendi basin: implications for Late Cenozoic crustal extension in western Anatolia, Turkey. Tectonophysics 488, 210–232.

Ersoy, E.Y., Çemen, I., Helvacı, C., Billor, Z., 2014, Tectono- stratigraphy of the Neogene basins in Western Turkey: Implications for tectonic evolution of the Aegean Extended Region, Tectonophysics.

Gawthorpe,R.L., Leedert, M.R., 2000, Tectono-sedimentary evolution of active extensional basins : Basin Research, v.12, p.195-218.

Gessner, K., Ring, U., Johnson, C., Hetzel, R., Passchier, C.W., and Güngör, T., 2001, an active bi-vergent rolling-hinge detachment system: Central Menderes metamorphic core complex in Western Turkey: Geology, v. 29, p. 611–614.

Gessner, K., Gallardo, L, A., Markowitz, V., Ring, U., Thomson, S, N., 2013, What caused the denudation of the Menderes Massif: Review of crustal evolution, lithosphere structure, and dynamic topography in southwest Turkey: Gondwana Research ,243-274.

Göğüş, O.H., 2004, Geometry and tectonic significance of the Büyük Menderes Detachment in the Bascayir area, Büyük Menderes Graben, western Turkey [M.S.thesis]: Oklahoma State University, Stillwater, Oklahoma.

Göğüş, O.H., 2014, Rifting and subsidence following lithospheric removal in continental. back arcs, geology society of America, v.43, no.1, p.3-6.

Gürer, O.F., Sarica-Filoreai, N., Özburan, M., Sangu, E., and Doğan, B., 2009, Progressive development of the Büyük Menderes Graben based on new data, western Turkey: Geological Magazine, v.146, no.5,p. 652-673.

Hakyemez, Y.H., Erkal, T., and Göktaş, F., 1999, Late Quaternary evolution of the Gediz and Büyük Menderes grabens, western Anatolia, Turkey: Quaternary Science Reviews, v. 18, no. 4, p. 549-554.

Hetzel, R., Ring, U., Akal, C., Troesch, M., 1995b, Miocene NNE-directed extensional. unroofing in the Menderes massif, southwestern Turkey. Journal of Geological Society London, 152, 639-654.

Holt, P, J., 2012, Subsidence Mechanisms of sedimentary Basins Developed over Accretionary Crust, Durham theses, Durham University, http://etheses.dur.ac.uk/3584/

Işık, V., Tekeli, O., 2001, Late orogenic crustal extension in the northern Menderes Massif (Western Turkey); evidence for metamorphic core complex formation. International Journal of Earth Science 89, 757-765.

Jolivet, L., et al., 2013, Aegean tectonics: Strain localisation, slab tearing and trench retreat. Tectonophysics 597–598, 1–33.

Kazancı, N., Dündar, S., Mehmet, C.A., Gürbüz, A., 2009, Quaternary deposits of the Büyük Menderes Graben in western Anatolia, Turkey: Implications for river capture and the longest Holocene estuary in the Aegean Sea. Marine Geology, v.264, p. 165-176.

Kocyiğit, A., Yusufo.lu, H., Bozkurt, E., 1999, Evidence from the Gediz graben for episodic two-stage extension in western Turkey. Journal of the Geological Society London, 156, 605-616.

Konak, N., Akdeniz, N., Öztürk, E.M., 1987, Geology of the south of Menderes massif, correlation of Variscan and pre-Variscan events of the Alpine Mediterranean Mountain Belt (Guide book for the field exursion along western Anatolia, Turkey) IFCP Project No. 5, 42-53.

Kurt, H., Demirbağ, E., and Kuşçu, I., 1999, Investigation of submarine active tectonism in the Gulf of Gökova, southwest Anatolia- southeast Aegean sea, by multi-channel seismic reflection data: Tectonophysics, v.305, p. 477-496, doi; 10.1016/S0040-1951999000037-2.

Lavier, L. L., and W. R. Buck (2002), Half graben versus large-offset low angle normal fault: Importance of keeping cool during normal faulting, J. Geophys. Res., 107(B6), 2122, doi:10.1029/2001JB000513.

Le Pichon, X., and Angelier, J., 1979, The Hellenic arc and trench system: A key to the neotectonic evolution of the Eastern Mediterranean area: Tectonophysics, v. 60, p. 1–42, doi: 10.1016/0040-1951(79)90131-8.

Le Pichon, X., and Angelier, J., 1981, The Aegean Sea: Philosophical Transactions of the Royal Society of London, v. A 300, p. 357–72.

Malz, A., Madritsch, H., Kley, J., 2015, Improving 2D seismic interpretation in challenging settings by integration of restoration techniques: A case study from the Jura fold-and-thrust belt (Switzerland). Society of Exploration Geophysicists and American Association of Petroleum Geologists, v. 3, no. 4 p. SAA37–SAA58, 16 FIGS.

McKenzie, D., 1978, Active tectonics of the Alpine-Himalayan belt: The Aegean Sea and surrounding regions: Geophysical Journal of Royal Astronomical Society, v. 55, p. 217–254.

Meulenkamp, J.E., Wortel, W.J.R., Van Wamel, W.A., Spakman, W., and Hoogerduyn Strating, E., 1988, On the Hellenic subduction zone and geodynamic evolution of Crete since the late Middle Miocene. Tectonophysics, v. 146, p. 203–215.

Mirabella, F., F. Brozzetti, A. Lupattelli, and M. R. Barchi., 2011, Tectonic evolution of a low-angle extensional fault system from restored cross-sections in the Northern Apennines (Italy), Tectonics, 30, TC6002, doi: 10.1029/2011TC002890.

Platt, P.J., Behr, M.W., Cooper, J.F, 2014, Metamorphic core complexes: windows into the mechanics and rheology of the crust : Journey of the Geological Society, v.172, p. 9-27, doi: 10.144/jgs2014-036.

Ring, U., Johnson, C., Hetzel, R., Gessner, K., 2003, Tectonic denudation of a Late Cretaceous-Tertiary collisional belt-regionally symmetric cooling patterns and their relation to extensional faults in the Anatolide belt of western Turkey. Geological Magazine, 140, 1-21.

Robein, E., 2003, Velocities, time-imaging and depth-imaging in refection seismics: EAGE.

Sclater, J.G., and Christie, P.A.F., 1980, Continental stretching; an explanation of the post-Mid- Cretaceous subsidence of the central North Sea basin: Journal of Geophysical Research, v. 85, p. 3711-3739.

Sert, S., 2015, Subsurface Structural Geology of the Eastern Part of the Büyük Menderes Graben, Western Turkey: Implications for Structural Evolution of the Alaşehir and Büyük Menderes Grabens, Master Thesis, the University of Alabama.

Seyitoğlu, G., and Scott, B.C., 1996, The cause of north-south extensional tectonics in western Turkey: Tectonic escape vs. back-arc spreading vs. orogenic collapse: Journal of Geodynamics, v. 22, p. 145–153, doi: 10.1016/ 0264-3707(96)00004-X.

Seyitoğlu, G., Çemen, I., Tekeli, O., 2000, Extensional folding in the Alaşehir (Gediz) graben, western Turkey: Journal of the Geological Society, v. 157, no.6, p. 1097–1100.

Seyitoğlu, G., Tekeli, O., and Çemen, I., 2002, the role of the flexural rotation /rolling hinge model in the tectonic evolution of the Alaşehir graben, western Turkey: Geological Magazine, v. 139, p. 15–26.

Seyitoğlu, G., Işık, V., and Çemen, I., 2004, Complete Tertiary exhumation history of the Menderes massif, western Turkey: An alternative working hypothesis: Terra Nova v.16, p. 358–364, doi: 10.1111/j,1365-3121.2004.00574.x.

Seyitoğlu, G., Işık, V., 2015, Late Cenozoic extensional tectonics in western Anatolia: Exhumation of the Menderes core complex and formation of related basins.

Spakman, W., Wortel, M.J.R., and Vlaar, N.J., 1988, The Hellenic subduction zone: Atomographic image and its geodynamic implications: Geophysical Research Letters, v. 15, p. 60–63.

Steckler, M. S., & Watts, A. B., 1978, Subsidence of the Atlantic-type continental margin off New York. Earth and Planetary Sci. Lett., 41, 1-13.

Şen, Ş., Seyitoğlu, G., 2009, Magnetostratigraphy of early -middle Miocene deposits from E-W trending Alaşehir and Büyük Menderes grabens in western Turkey, and its tectonic implications. Iç Geodynamics of Collision and Collapse at the Africa – Arabia-Eurasia subduction zone. (Ed: D.J.J. van Hinsbergen, M.A. Edwards, R. Govers), The Geological Society London, Special Publications 311, 321–342.

Şengör, A.M.C., 1979, The North Anatolian Transform Fault: its age, offset and tectonic significance. Journal of the Geological Society London, 13, 269-282.

Şengör, A.M.C., Yilmaz, Y., 1981, Tethyan evolution of Turkey: a plate tectonic approach. Tectonophysics, 75, 181-241.

Şengör, A.M.C., Görür, N., and Saroğlu, F., 1985, Strike-slip deformation basin formation and sedimentation: strike-slip faulting and related basin formation in zones of tectonic escape: Turkey as a case study: Society of Economic Paleontologists and Mineralogist Special Publication, v.37, p. 227-264.

Ünay, E., Göktaş, F., Hakyemez, H.Y., Avşar, M., San, O., 1995, Dating of the sediments exposed at the northern part of the Büyük Menderes graben (Turkey) on the basis of Arvicolidae (Rodentia, Mammalia). Geological Bulletin of Turkey, 38, 75- 80.

Wagner III, H.F., Johnson, A.R., 2006, Coupled basin evolution and late-stage metamorphic core complex exhumation in the southern Basin and Range Province, southeastern Arizona: Tectonophysics, v.420,p. 141-160.

Watts, A. B., 2001a, Gravity anomalies, flexure and crustal structure at the Mozambique rifted margin. Marine and Petroleum Geology, 18, 445- 455.

Whitney, L.D., Teyssier, C., Rey, P., and Buck, R.W, 2013, Continental and oceanic core Complexes: GSA Bulletin, v.125, no: 3/4, p.273-298, doi: 10.1130/B30754.1.

Withjack, O.M., Schlische, W.R., Olsen, P., 2002, Rift-basin structure and its influence on sedimentary systems: Sedimentation in Continental Rifts, Society for Sedimentary Geology Special Publication No.73, p. 57-81.

Xiao, H., Suppe, J., 1992, Origin of rollover. The American Association of Petroleum Geologists Bulletin. v.76, p. 509-529.

Yılmaz, Y., Genç, S., C, Gürer, F., Bozcu, M., Yılmaz, K., Karacik, Z., Altunkaynak, S., and Elmas, A., 2000, When did the western Anatolian grabens begin to develop? Geological Society Special Publication 173, p. 353–384.

Yılmaz, O., 2001, Seismic data analysis: Soc. Of Exploration Geophysics.

Yılmaz, Y., Genç, S.C., Gürer, F., Bozcu, M., Yilmaz, K., Karacik, Z., Altunkaynak, S., and Elmas, A., 2000, When did the western Anatolian grabens begin to develop? : Geological Society, London, Special Publications, v. 173, no.1, p. 353-384.

Zhu, L., Mitchell, J.B., Akyol, N., Çemen, I., and Kekovali, K., 2006, Crustal Thickness Variations in the Aegean Region and its Implications for the Extension of Continental Crust: Journal of Geophysical Research, v. 111, issue B1, doi: 10.1029/2005JB003770.